ABSTRACT

Title of Document: INVESTIGATING UNCERTAINTIES IN TRACE GAS EMISSIONS FROM BOREAL FOREST FIRES USING MOPITT MEASUREMENTS OF CARBON MONOXIDE AND A GLOBAL CHEMICAL TRANSPORT MODEL

Edward Joseph Hyer, Doctor of Philosophy, 2005

Directed By: Professor Eric S. Kasischke
Department of Geography

Boreal forest fires are a significant contributor to atmospheric composition in the high northern hemisphere, and are highly variable both spatially and temporally. This study uses a new emissions model [*Kasischke et al.*, 2005] to generate input to the University of Maryland Chemical Transport Model [*Allen et al.*, 1996], with the goal of examining and constraining the key uncertainties in current understanding of boreal forest fire behavior. Model outputs are compared with data from the MOPITT instrument as well as *in situ* measurements of CO. A case study of CO transport during the summer of 2000 is used to examine several key uncertainties in the emissions estimates, describing how current levels of uncertainty affect atmospheric composition and applying atmospheric measurements can be applied to constrain uncertainty. Source magnitudes

determined by inverse methods were shown to be highly sensitive to the assumed injection properties. For the boreal forest in 2000, the best agreement with observations was obtained with a pressure-weighted profile of injection throughout the tropospheric column, but detailed examination of the results makes clear that any uniform parameterization of injection will be a significant source of error when applied globally. Comparison of simulated CO distributions from daily, weekly, and monthly aggregate emissions sources demonstrated that while model data sources produced a valid representation of emissions at weekly resolution, the atmospheric distribution outside the source region has very little sensitivity to temporal variability at scales finer than 30 days. Different estimates of burned area produced large differences in simulated patterns of atmospheric CO. The GBA-2000 global product and the data sources used by Kasischke *et al.* [2005] gave better agreement with atmospheric observations compared to the GLOBSCAR product. Comparison of different estimates of fuel consumption indicated that atmospheric measurements of CO have limited sensitivity to spatial variability in fuels, but that current fuels maps can improve agreement with atmospheric measurements. These results provide a clear indication of how atmospheric measurements can be used to test hypotheses generated by emissions models.

INVESTIGATING UNCERTAINTIES IN TRACE GAS EMISSIONS FROM BOREAL FOREST FIRES USING MOPITT MEASUREMENTS OF CARBON MONOXIDE AND A GLOBAL CHEMICAL TRANSPORT MODEL

By

Edward Joseph Hyer

Dissertation submitted to the Faculty of the Graduate School of the
University of Maryland, College Park, in partial fulfillment
of the requirements for the degree of
Doctor of Philosophy
2005

Advisory Committee:

Professor Eric S. Kasischke, Chair
Dr. Dale J. Allen
Dr. Juying X. Warner
Associate Professor Ruth S. DeFries
Assistant Professor Axel Kleidon
Professor Robert D. Hudson

Acknowledgements

Like any doctoral dissertation, this document is a unique result of unique circumstances. Without the assistance, cooperation, and accidental intervention of a large number of people, this dissertation would have turned out very differently, or not at all.

I would like first to thank my advisor, Professor Eric Kasischke, for getting me into the boreal forest, first literally and then figuratively. The opportunity to be involved in field research in Alaska in the summer of 2000 sparked my interest in the science of boreal forests. Professor Kasischke's unwavering enthusiasm for this ambitious project was, on several occasions, the only thing saving this dissertation from oblivion.

Much of the theoretical underpinning of this dissertation was developed in conversations during and after field campaigns in Alaska, and my understanding of boreal forest ecology, carbon cycling, and many other things would be the poorer without my interactions with other scientists doing field research in Alaska, especially Jennifer Harden, Jim Randerson, Ted Schuur, Jill Johnstone, Kristen Manies, Teresa and Jamie Hollingsworth and Scott Goetz.

This project would have been impossible had Dr. Dale Allen not responded with exemplary generosity to a cold call from a graduate student in another department with virtually no background in atmospheric science. This research suffered from all of the common pitfalls of cross-disciplinary research, and Dr. Allen navigated these with excellent tact and patience.

I would like to thank all my friends and family for their support, patience, good humor, and patience during this long process.

Finally, I would like to thank my grandfather, Mr. J. Donald Edwards, for his unwavering conviction that the only path to a decent living in our times is through higher education.

This dissertation was completed with financial support from a NASA Earth System Science Fellowship.

Contents

List of Tables

List of Figures

Chapter 1. Introduction

1. Evaluating model estimates of biosphere-atmosphere exchanges at continental and global scales

The exchange of matter between the atmosphere, oceans, and terrestrial biosphere is at the very heart of the function of the Earth as a system. In recent decades, these fluxes have become central to the study of global climate change. The global average concentration of atmospheric carbon dioxide has increased by more than one-third since the pre-industrial era [*Houghton and Ding*, 2001], highlighting the potential for rapid, significant changes in the system. Understanding how changes in the biosphere can affect the atmosphere and other parts of the Earth system has become a scientific priority around the globe [*Falkowski et al.*, 2000; *Sarmiento and Wofsy*, 1999; *Waldrop*, 1984].

Emissions from biomass burning are a key linkage between the biosphere and the atmosphere. Emissions from biomass burning constitute a gross flux of carbon to the atmosphere equal to about 4.3 Pg C per year [*Andreae and Merlet*, 2001], roughly 65% of the estimated fossil fuel emissions source [*Watson et al.*, 1990]. Uncertainty in this estimate is still high, and quantifying the magnitude of these emissions, as well as understanding their spatial and temporal patterns, is relevant to scientific questions of both terrestrial ecology and atmospheric science, and tied into larger considerations of the causes and impacts of climate change [*Kasischke et al.*, 1995a].

Recent improvements in data sources and modeling methods have made it possible to generate spatially and temporally resolved estimates of biomass burning emissions at high resolutions. However, the data inputs and theoretical assumptions that

drive these models have only been tested at very fine scales using intensive investigation of a small subset of the data.

Broad-scale testing of emissions estimates using field investigations is logistically infeasible due to the size and remoteness of the areas involved. An alternative is to evaluate emissions estimates on the basis of their observable impact on atmospheric composition. Research into the chemical composition of the atmosphere has demonstrated the potential of atmospheric inverse modeling to constrain surface fluxes. Inverse modeling is so called because the chain of inference proceeds from the effect, patterns of atmospheric composition, to the cause, surface fluxes.

This study uses inverse modeling to explore how spatial and temporal patterns of CO emissions, and therefore patterns of atmospheric composition, are affected by emissions from boreal forest fires, and how the uncertainties in the emissions model affect these patterns. Comparisons of simulated patterns of CO with observations are used to evaluate how the range of emissions resulting from specific uncertainties affects agreement between modeled emissions and observations.

2. Goals

The goals of this study were as follows:

1. Describe the impact of boreal forest fires on atmospheric CO at scales relevant to long-range atmospheric transport;
2. Assess the effects of uncertainties in model inputs on simulated patterns of atmospheric CO;
3. Assess the effects of model assumptions about fire behavior on simulated patterns of atmospheric CO;

4. Describe the response of MOPITT data and surface sampling using existing networks to variability in boreal forest fire emissions;
5. Apply the atmospheric measurements to evaluate specific uncertainties in data inputs and model assumptions.

3. Study Design

This dissertation comprises four studies involving simulations of atmospheric CO during the summer of 2000. Each study addresses a particular parameter of the emissions model, and each includes the following components:

1. Theoretical background on the emissions model parameter and efforts to characterize this parameter;
2. Preparation of multiple emissions estimates covering the range of uncertainty in the model parameter;
3. Sensitivity analysis of simulated atmospheric measurements to determine how specific atmospheric measurements respond to this parameter;
4. Quantitative evaluation of emissions estimates by comparison of simulation results to atmospheric measurements.

Several of these studies also incorporate more detailed case studies of specific events to clarify certain points about fire and model behavior.

4. Organization of this Dissertation

This dissertation consists of a brief summary of the scientific context of this research, followed by the four studies, with conclusions presented at the end. The chapters are as follows:

In Chapter Two, a brief background for this research is given, summarizing the theoretical and experimental foundations and providing context for the work in this dissertation.

Chapter Three presents an examination of emissions injection height, showing the sensitivity of atmospheric measurements to this property and attempting to use atmospheric data to constrain it. Chapter Three also presents some fundamental results regarding the atmospheric simulation and the quality of the MOPITT data.

Chapter Four presents an investigation of atmospheric sensitivity to daily variability in the emissions source. This study describes the effects of temporal aggregation of simulated emissions on agreement with observations, and uses data from CO surface flask measurements, a high-resolution continuous CO analyzer, and the MOPITT instrument to assess the accuracy of daily data inputs to the emissions model.

Chapter Five compares several different high-resolution estimates of burned area for the boreal forest. The effects of these different estimates on atmospheric patterns of CO are described, and the agreement between model and measurements is used to assess the accuracy of spatial and temporal patterns of area burned from each estimate.

Chapter Six deals with variability in fuel consumption in current models. The effects of this variability on atmospheric patterns of CO are described, and different model assumptions are evaluated in terms of agreement with atmospheric observations.

Chapter Seven presents conclusions from this research.

Chapters 3-6 each contain separate literature review and methods sections. In cases where methods are redundant, references may be made to earlier chapters. The

following chapter presents a brief overview of the theoretical and experimental foundations of these studies, and attempts to place them in a broader research context.

Chapter 2. Scientific context of this research

1. Boreal forests, the global carbon cycle, and the global atmosphere

The boreal forest covers more than 14 million square kilometers of the Earth's surface above 47° N latitude. This ecosystem contains more than 30% of the total carbon stored in the terrestrial biosphere [*Apps et al.*, 1993]. This region is characterized by modest primary productivity and very low rates of decomposition, resulting in the accumulation of carbon in the ground layer. This carbon can be released to the atmosphere by fire, which is the dominant disturbance in most of the boreal forest.

The flux of carbon from boreal forest fires has interannual variability as large as an order of magnitude [*Amiro et al.*, 2001]. The principal trace gas product of biomass burning, as with all combustion, is carbon dioxide. However, carbon dioxide has a lifetime much longer than the characteristic mixing time of the troposphere, resulting in a very small spatial signal [*Tans et al.*, 1996]. Carbon dioxide does exhibit a strong seasonality in the troposphere, but this is dominated by the gross fluxes of photosynthesis and respiration, and net fluxes from biomass burning are very small relative to these. Spatial and temporal variability of partially reduced atmospheric constituents such as carbon monoxide and methane are much more strongly affected by biomass burning, both because of the shorter atmospheric lifetime and the absence of other large gross fluxes. Fires in boreal forest ecosystems will have a proportionally stronger effect on these constituents relative to carbon dioxide because of the prevalence of inefficient smoldering combustion in boreal forest fires [*Cofer III et al.*, 1996]. Large intense fires in the boreal forest can produce strong perturbations of the seasonal cycles of carbon

monoxide [*Novelli et al.*, 2003; *Yurganov et al.*, 2004a; *Yurganov et al.*, 2005] and methane [*Dlugokencky et al.*, 2001]. The variability in boreal forest fires is a large contributor to the interannual variability of carbon monoxide concentrations in the High Northern Hemisphere [*Kasischke et al.*, 2005]. The proportion of carbon monoxide has some uncertainty, and its variability is poorly understood, but the studies here will follow the convention of earlier work and assume that CO emissions are generally proportional to total fuel consumption, i.e. that the emissions factor of CO is generally invariable [*Hyer*, 2001].

Quantification of carbon fluxes from fire is important to Earth system science for three principal reasons:

1. Understanding the factors which control fire emissions will improve predictions of future boreal forest conditions based on climate change scenarios [*Flannigan et al.*, 1998; *Kasischke et al.*, 1995a; *Stocks et al.*, 1998].
2. Improved constraints on emissions of different carbonaceous species will improve models of atmospheric chemistry [*Holloway et al.*, 2000; *Logan et al.*, 1981].
3. The amount of carbon released by fires is the primary control on the net ecosystem productivity of the boreal forest, and thus determines its role as a net source or sink of carbon in the global carbon cycle [*Harden et al.*, 2000; *Kasischke et al.*, 1995a].

2. The challenge of estimating trace gas emissions from forest fires

The science of emissions estimation has advanced dramatically in recent years with the development of spatially explicit databases describing fuel loads and fire activity in different ecosystems around the globe. Estimates of carbon emissions from boreal forest fires have used spatially explicit approaches to generate spatially and temporally resolved estimates of emissions [*Amiro et al.*, 2001; *French et al.*, 2000; *French et al.*, 2002; *Kajii et al.*, 2002; *Soja et al.*, 2004]. While numerous differences remain between the approaches used in these studies, the improvement in data availability has led to an emerging consensus on the most important sources of uncertainty [*Kasischke and Penner*, 2004].

Kasischke et al. [2005] was a landmark for the systematic study of boreal forest fires. This study produced the first multi-year spatially and temporally resolved estimates of emissions for the entire boreal forest. Theoretical advances from field investigations and remote sensing studies were integrated to produce an internally consistent model of fire behavior in the boreal forest. The theoretical framework used in *Kasischke et al.* [2005] connected uncertainties in fire behavior to physically observable properties of forest stands, paving the way for field investigations to make significant gains in reducing these uncertainties.

This emissions model makes it possible to examine the impacts of forest fires across the entire boreal zone in an integrated fashion. This approach lends itself to broad-scale examinations of the key uncertainties in forest fire emissions. These uncertainties have been reduced previously using detailed field investigations of small cases. The results of these investigations have been applied by extrapolation to descriptions of the

global emissions source. The accuracy of the global emissions source is therefore dependent on the accuracy of this extrapolation and the extent to which field studies represent the broader properties of the boreal forest.

3. The potential of atmospheric modeling to constrain surface sources

The implementation of the GIS-based emissions model from *Kasischke et al.* [2005] allowed the generation of emissions estimates from boreal forest fires with a high degree of flexibility in terms of data inputs, model parameters, and output resolution. This emissions model, the Boreal Wildfire Emissions Model – 1 (BWEM-1), is the foundation for the studies in this dissertation. In each study, the model is used to generate emissions estimates with different data sources or different model assumptions, at a resolution suitable for input to a chemistry and transport model. With the chemistry and transport model, these emissions estimates are transformed into simulated spatial and temporal patterns of atmospheric CO that can be compared directly with atmospheric observations.

Advances in atmospheric physics and chemistry, as well as vast increases in available computing power, have made it possible to model atmospheric transport and chemistry with ever-increasing resolution and realism. Computer models have been used to study every aspect of the atmosphere, and have examined both the current state of the atmosphere and the potential of climate change to alter the chemical and radiative balance of the atmosphere. They have also been used to model the relationship between terrestrial trace gas sources and the atmosphere, both to understand the atmospheric impacts of terrestrial processes, and to use atmospheric measurements to constrain the magnitude and distribution of terrestrial fluxes. Inversion of atmospheric measurements

has emerged in recent years as a promising method for achieving further constraint of terrestrial sources [Gurney et al., 2002].

The advantage of this inverse methodology is that it is sensitive to the behavior of the source over broad scales even without extensive coverage. This makes it an excellent complement to intensive studies, because the effects of insights derived from fine-scale studies can be tested in terms of their effects on the global source.

4. The potential of MOPITT for expanding modeling capabilities

The Measurement of Air Pollution from Space (MAPS) instrument, which first flew in 1981 on board the second flight of the space shuttle, employed the technique of correlation spectroscopy to measure carbon monoxide in the middle and upper troposphere [*Reichle Jr. et al.*, 1982]. This method involves passing incoming radiance through a cell with a known concentration of the target species, and comparing the resulting attenuated radiance to radiance passed through a vacuum cell. The MAPS instrument flew on board two other space shuttle missions in 1984 and 1994, and a number of useful advances in understanding distribution and behavior of carbon monoxide resulted from the data produced by this satellite (e.g. [*Christopher et al.*, 1998; *Faluvegi et al.*, 1999]).

The potential of space-based measurements of CO for the study of biomass burning was evident from the initial MAPS missions [*Newell et al.*, 1989]. *Christopher et al.* [1998] used the MAPS data to examine CO emissions from fires in Indonesia, and found that the CO response to fires was more than double that predicted by their model (which was very simple and did not account for transport of emissions).

The Measurement of Pollutants in the Troposphere (MOPITT) instrument is the successor to the MAPS instrument. It uses a highly improved version of this retrieval method to obtain a vertically resolved profile of carbon monoxide. This instrument obtains measurements at a high spatial and temporal resolution: a 22km ground cell footprint with measurements over almost the entire globe every three days [*Drummond and Mand*, 1996]. This instrument was launched with the Terra satellite and became operational in March of 2000.

Liu et al. [2005] describe the sensitivity of the MOPITT CO measurement to fire activity as observed using the thermal channels of the AVHRR instrument. They showed the CO retrievals from MOPITT to be strongly correlated to fire activity, but with a high degree of variability in the response.

Heald et al. [2004] compared inverse results for Asian CO sources using aircraft measurements from the TRACE-P campaign to results obtained from inversion of MOPITT measurements. They found that the two measurement types produced similar results but that the MOPITT data yielded a better constraint on sources because of better spatial coverage of the study area.

The sensitivity of MOPITT data to CO emissions from a range of natural and anthropogenic sources is by now well established [*Allen et al.*, 2004; *Arellano et al.*, 2004; *Lamarque et al.*, 2003; *Petron et al.*, 2004]. The studies in this dissertation examine the sensitivity of these measurements to spatial patterns in the CO emissions related to specific properties of the boreal forest fire emissions source. This approach differs from most inverse modeling studies because the focus is on the spatial and temporal patterns of the source, rather than the absolute magnitude.

5. A process-based approach to inverse modeling

Early efforts at using inverse modeling of atmospheric measurements to constrain surface sources evaluated discrete hypothetical emissions estimates developed from theoretical considerations. *Fung et al.* [1991] constructed several different ground-up estimates of the spatial and temporal distribution of global methane emissions to evaluate hypotheses about the relative contribution of different processes, and evaluated each estimate based on its skill at reproducing the latitudinal and seasonal gradients of atmospheric methane from observations. As atmospheric modeling and measurements improved, emphasis shifted from hypothesis testing to numerical inversions of source magnitudes [*Ciais et al.*, 1995; *Fan et al.*, 1998]. This approach requires separation of fluxes into broad geographic components, because of computational challenges with high-resolution inversions, and mathematical limitations of the inversion algorithms when applied to sparse observations. The inversion results obtained by this method have been shown to be highly sensitive to the choice of geographic regions for analysis [*Kaminski et al.*, 2001].

A significant shortcoming of the numerical inversion approaches currently used is that errors in source magnitude over broad regions cannot be attributed to specific properties of the source. Process-based models of terrestrial sources have multiple uncertainties both positive and negative, and errors in source magnitude may be related to any combination of these uncertainties.

The studies presented in this dissertation use a spatially and temporally resolved model of boreal forest fires to generate estimates of CO emissions specifically tailored to examine current uncertainties in the model. The University of Maryland Chemistry and

Transport model (UM-CTM) [*Allen et al.*, 1996] is used to generate simulations of the atmospheric distribution of CO based on these estimates. The results of the atmospheric simulation are transformed to match the sampling and sensitivity characteristics of different atmospheric measurement types.

From these simulated atmospheric measurements, the sensitivity of atmospheric observations to model uncertainties can be determined. This sensitivity determines the potential of MOPITT and other atmospheric data for examination of source characteristics beyond absolute magnitude. The ability of different emissions estimates to reproduce the observed spatial and temporal patterns of atmospheric CO can be used to constrain specific uncertainties in the emissions model. This *process-based* investigation of surface sources expands the potential of atmospheric inversion for the study of land surface processes.

The next four chapters present initial results from application of this method to specific issues in model estimation of boreal forest fire emissions, using atmospheric measurements to examine the atmospheric injection of emissions (Chapter Three), the quality of daily information on fire activity (Chapter Four), different estimates of burned area (Chapter Five), and different treatments of fuel consumption (Chapter Six).

These studies are the first to use this process-based inverse methodology, but the range of investigations to which this methodology might be applied extends far beyond these studies. The hope is that these preliminary demonstrations of this method will lead to its application to a broad range of problems in the study of mass exchange between the land surface and the atmosphere.

Chapter 3. Examining injection properties of boreal forest fires using surface and satellite measurements of CO transport

1. Abstract

A chemistry and transport model (CTM) was used to evaluate injection properties of carbon monoxide (CO) emissions from boreal forest fires during June-August 2000. CO emissions calculated using a spatially and temporally resolved model of boreal fire emissions, the Boreal Wildfire Emissions Model -1 (BWEM-1) [*Kasischke et al.*, 2005], were used as input to the CTM, and several different injection scenarios were evaluated, ranging from surface injection to injection near the tropopause. Model output was transformed to match the sampling properties of surface CO measurements from flask samples, as well as satellite retrievals of CO from the MOPITT instrument. Simulation of surface measurements showed that CO enhancement from a source injected at the surface is three times the enhancement caused by a source in the upper troposphere. Simulated MOPITT retrievals were shown to be more sensitive to high-altitude sources, with upper-tropospheric injection producing on average 10% higher total column CO in the HNH compared with surface injection. Agreement between surface observations and model output was best with surface injection, but the contribution of mid- and upper-tropospheric injection was difficult to evaluate because simulated emissions injected at these altitudes produced a small signal in surface measurements. MOPITT observations agreed best with emissions distributed throughout the tropospheric column, except near the source region, where surface injection produced slightly better results. Examination of a case study in Southern Russia during early June 2000 showed that injection height from large fire events is highly variable, and can extend throughout the tropospheric

column. Use of a pressure-weighted algorithm to distribute boreal forest fire emissions vertically at the source was shown to be preferable to all single-layer injection simulations. However, variability in injection height will continue to be a source of error in transport models using any fixed parameterization.

2. Introduction

Biomass burning is the largest direct terrestrial source of CO, adding on the order of 750 Tg CO per year to the atmosphere [*Holloway et al.*, 2000]. CO emissions from boreal forest fires make up only a small fraction of this source on average. However, the interannual variability in boreal forest fires can be an order of magnitude, and in high fire years the boreal forest fire CO source can be 20% or more of global biomass burning CO [*Kasischke and Bruhwiler*, 2002; *Kasischke et al.*, 2005]. Emissions from boreal forest fires come mostly from a small fraction of the largest fires occurring each year [*Stocks et al.*, 2002]. The size and intensity of these large fires is sufficient to create the possibility of convective uplift of emissions independent of local stability [*Lavoue et al.*, 2000]. This phenomenon has been identified as the source of aerosol intrusions into the stratosphere in several case studies [*Fromm et al.*, 2000; *Livesey et al.*, 2004]. The variation in the height attained by fire emissions in the atmosphere is poorly understood, and has substantial consequences for atmospheric composition and chemistry.

The injection properties of the source will determine the transport and chemical evolution outcomes for emissions from a given event. The vertical distribution of emissions in the atmosphere will also affect the sensitivity of any atmospheric measurement to these emissions. This sensitivity has quantitative implications for inverse modeling of source magnitudes.

This chapter describes an experiment to examine the vertical distribution of boreal forest fire emissions through the atmospheric column. A chemistry and transport model (CTM) was used to simulate the atmospheric distribution of boreal forest fire CO with a range of injection properties. The sensitivity of CO measurements from flask samples as well as from the MOPITT instrument to injection height was estimated from CTM outputs, in order to demonstrate the importance of correct specification of injection height for inverse estimation of source magnitude. CTM outputs were compared to CO concentrations from surface measurements as well as retrievals from the MOPITT satellite. The goal of these comparisons was to evaluate the variability in the vertical profile of emissions during the 2000 fire season, and evaluate the results obtained from various simple uniform parameterizations of smoke injection in terms of their ability to accurately describe the spatial and temporal patterns of atmospheric CO from boreal fires.

This chapter consists of four parts. The remainder of this section is a review of theoretical and experimental work on the process of smoke injection. The Methods section describes the transport model and CO data sources, and the simulation methods used to evaluate injection hypotheses. The Results section has three main components. First, model output is analyzed to test the effects of MOPITT sampling and the MOPITT averaging kernel on estimates of total column CO as well as atmospheric CO burden. Next, the effect of injection height on source detection by both surface measurements and MOPITT is examined using the results of the CTM simulation. Finally, CTM output is compared to atmospheric observations, using both global statistical analysis and a case

study of a large complex of fires in southern Russia. The final section presents the conclusions of this experiment, and suggests further work to be done on this subject.

2.1. Theory of forest fire smoke injection

Trace gas emissions from surface sources generally enter the atmospheric circulation near the ground with low energy. They are rapidly cooled to the background air temperature, mixed through the boundary layer, and mixed into the free troposphere by turbulent mixing and convection as determined by local meteorological conditions. However, there is abundant evidence that forest fire emissions are often lofted into the free troposphere by a process both faster and more coherent than turbulent mixing. Emissions lofted in this fashion will enter the free troposphere with far less dilution and less chemical and physical alteration, compared with emissions lofted from the boundary layer under ordinary meteorological conditions. This high-energy convective lofting alters the vertical profile of emissions at the geographic source, and produces transport outcomes similar to having an emissions source located in the free troposphere. Accurate simulation of the transport pathways and chemical evolution of forest fire emissions requires that this process be correctly described.

Injection of forest fire smoke is governed by both the energy of the fire and the stability of the local atmosphere. The energy transfer from the advancing front of a forest fire can be estimated by the fire intensity $I=cmr$, where c is the heat of combustion of the fuel, m is the mass of fuel consumed, and r is the rate of fire spread [*Byram*, 1959]. The output from this calculation is kilowatts of energy per meter of the flaming front. For large forest fires, this value can exceed 50,000 kW m^{-1} [*Stocks and Kauffman*, 1997], which is sufficient to cause convective lofting of fire smoke independent of local stability

conditions. When this lofting occurs, fires are said to be "plume-dominated," indicating that the vertical mixing is dominated by the buoyancy of the hot fire emissions. *Fromm et al.* [2003] propose a positive feedback in these cases whereby a hot emissions plume lofting upwards through an unstable atmosphere might strengthen the instability, resulting in stronger winds at the surface as well as enhanced lightning. This would create conditions favorable to further burning, and enhanced convective lofting of emissions. Effects of this type are the reason that plume-dominated fires are said to "create their own weather."

Lavoué et al. [2000] derived values for I from several experimental fires, and proposed a linear relation between I and injection height. While this proposed relationship was based on very sparse data, it did highlight the significant energy difference between crown and surface fires, as well as the higher energy associated with larger fires. *Lavoué et al.*'s [2000] empirical relationship between I and injection height implies that the range of burning conditions commonly observed in the boreal zone could result in effective injection heights ranging from 2500m for surface fires to above 7500m for large crown fires. However, local meteorological conditions can suppress or promote lofting, resulting in a broader range of outcomes. This theoretical range of effective injection heights has been verified by studies of wild and experimental fires, as discussed below.

2.2. Direct evidence for forest fire injection height

Direct observations of emissions plumes from wildfires and experimental forest fires demonstrate the range of effective emission heights. They do not provide a

generalized picture of the properties of the boreal forest fire source, but are illustrative of the range of possible injection heights.

Fromm and Servranckx [2003] performed a detailed satellite analysis of a large forest fire in NW Canada, using satellite measurements to identify smoke-polluted air masses and calculate height and temperature of the plume top. The case that they examined, in May 2001, combined energetic burning with extremely active convection to loft smoke emissions up to the tropopause, where a small fraction of the plume entered into the stratosphere. *Jost et al.*[2004] analyzed observations from aircraft measurements off the coast of Florida, and found enhanced aerosol and CO in the middle stratosphere between 14.7 and 15.8 kilometers above sea level. These enhancements were shown by trajectory calculations and satellite data analysis to have originated from fire activity in Saskatchewan. This type of extreme event appears to be uncommon. *Livesey et al.* [2004] examined more than a decade of satellite data from the Microwave Limb Sounder, and found only one episode of forest fire smoke intrusion into the stratosphere.

Goode et al. [2000] flew aircraft over active wildfires in Alaska, and report plume heights generally in the range of 1500-2500m for fires in forested areas. They sampled a range of fire sizes and fuel densities. The observations they made give a reasonable idea of how injection might function in a high fire danger condition, but the sample is too small to indicate the distribution of conditions or the frequency of outliers.

Detailed observations were made of the smoke plume from the Smoke, Clouds and Radiation-C (SCAR-C) experimental fire in the Pacific Northwest [*Hobbs et al.*, 1996]. This was a small prescribed fire of logging debris. Measurements of the smoke plume from this fire showed that in the center of the fire, smoke was lofted to 600m,

while smoke outside the hottest part of the fire was held below 300m by a strong inversion [*Trentmann et al.*, 2002].

These observations are indicative of the range of injection conditions for temperate and boreal forest fires. Process-based modeling of the complex interaction between fire energy and local meteorology requires data that are not available for most fires. Modeling experiments simulating atmospheric transport of fire emissions have relied on simple parameterizations of the injection process, and the results of these experiments sometimes shed light on the injection process. The next section is a brief review of how injection height has been treated in transport simulation experiments of boreal and temperate forest fires.

2.3. Treatment of smoke injection in transport modeling experiments

Forster et al. [2001] modeled the transport of emissions from North America to Europe in August 1998. They concluded that large forest fires in northwest Canada were responsible for aerosol enhancements observed over the European continent as well as enhanced CO measured at Mace Head, Ireland. Their transport simulations distributed the forest fire emissions evenly between the surface and 2500m at the source. Another study of the same fire events, however, used an injection height range of 3000-5000m to produce the best match with observations of NO2 from the Global Ozone Monitoring Experiment (GOME) and the TOMS aerosol index [*Spichtinger et al.*, 2001].

In some cases, local instability may accomplish the same effect as convective lifting caused by energetic burning. *Lamarque et al.* [2003] modeled the CO emissions from a group of fires in the northwestern US in 2000, using the MOZART-2 chemical transport model. They released the forest fire CO at the surface, and found it was

immediately lofted into the mid-troposphere. *Colarco et al.* [2004] modeled a plume from forest fires in Quebec in July 2002, examining which injection scenarios most effectively reproduced measurements taken over Washington, DC. They found that good results could be obtained by releasing the emissions at the surface, where local convection would immediately lift them into the free troposphere, or by releasing emissions at altitude. However, they found that the approach of distributing the initial emissions release in the lower troposphere above the boundary layer (500-~3000m) produced results inconsistent with their observations, because the bulk of the emissions subsided rapidly to the surface and did not arrive at the measurement location.

Effective injection height of emissions over a fire event is the result of both the energy of the fire itself and the local meteorological conditions. The variability in these factors makes modeling of injection height for specific fire events a daunting task. However, for global modeling purposes, a simple uniform parameterization of the injection process may produce adequate results.

A global parameterization of this process would consist of a vertical distribution describing the mass fraction of emissions that are convectively lofted to each layer of the atmospheric column above the emissions source. This vertical distribution would give the best agreement with observations for global studies, and could be used as a base for more detailed models of the process.

The bulk injection properties of the boreal forest fire source are not necessarily as variable as the properties of individual events, for two reasons. First, the total emissions from this source are dominated by a small fraction of the largest events. Second, the large forest fires that contribute the most to the total emissions have some covariance with

meteorological conditions [*Skinner et al.*, 1999]. Thus, the forest fire events producing the largest atmospheric signal are likely to be concentrated in a small range of the possible conditions, and it may be possible to effectively describe the bulk injection properties of this source with a relatively simple parameterization.

3. Methods

3.1. Study Period

CO emissions from boreal forest fires were simulated for the 2000 fire season. The 2000 season was chosen because of a change in the retrieval used for the MOPITT data resulting from a cooler failure on board the instrument in May 2001, and also because of the availability of other data sources related to fire activity and atmospheric composition. Subsequent validation results have shown that MOPITT retrievals before and after the change in instrument configuration have comparable accuracy and precision [*Emmons et al.*, 2004]. The CTM simulation was run from 1 January 2000, with a 12-month spin-up for non-boreal sources. Spin-up of the model was done using assimilated winds for 2000. March 2000 was the earliest month including any CO from the boreal source. Output from the CTM simulation was analyzed and compared with observations for the period from 1 June – 31 August 2000. A large CO source from fires in the Mongolian steppe in close proximity to the Russian fires was found to cause substantial interference with the signal from boreal fires in observations before 1 June. This study therefore uses observations from 1 June – 31 August, because the Mongolian source is poorly constrained by the input data and is not the subject of this investigation.

3.2. Boreal forest fire emissions model

CO emissions from boreal forest fires were estimated using the data inputs described in *Kasischke et al.* [2005]. Estimates of fire size, location and timing from satellite observations and fire management agencies were combined with spatially explicit maps of above-ground and ground-layer biomass to estimate fuel consumption and trace gas emissions. The source estimate used here is an older version than that described by *Kasischke et al.*, with several important differences. The estimate used here does not include a seasonal parameterization of fire severity. CO emissions from Russian fires are calculated based on an estimated fraction of biomass consumed in aboveground and ground-layer fuels, similar to the approach used by *French et al.* [2000]. North American CO emissions are estimated using regionally averaged levels of fuel consumption, following the method of *Amiro et al.* [2001]. Other chapters in this dissertation include detailed evaluation of this CO source, including comparative evaluations of temporal resolution (Chapter 4), burned area estimates (Chapter 5), and model assumptions about fuel consumption (Chapter 6). The source used for this study is directly compared with the source from *Kasischke et al.* [2005] in Chapter 6.

Boreal fires in 2000 produced an estimated 87.6 Tg CO, near the average annual total for 1995-2003 reported by *Kasischke et al.* [2005]. This estimate exceeds the value for the year 2000 estimated by *Kasischke et al.* [2005] because of differences in the model treatment of fuel consumption (see Chapter 6). Of the total boreal fire CO emissions, 83.5 Tg was from 9.3 Mha of fire in Russia, of which 63% occurred before 1 June. The remaining CO was from fires during June-August in Canada and Alaska. The year 2000 was a moderate to large fire year compared with other recent years in Russia,

and a low fire year in Canada and Alaska, compared to both recent and long-term inventories [*Stocks et al.*, 2002; *Sukhinin et al.*, 2004].

3.3. Other CO sources

Figure 3-1 shows the annual time series of all CO sources used in this study. All the principal sources of CO to the atmosphere were included in the CTM simulation, with the exception of CO from soils, which are expected to be a minor contributor to overall CO emissions, and for which no comprehensive data source is available [*Kuhlbusch et al.*, 1998; *Zepp et al.*, 1997]. Fossil fuel CO was estimated with the inventory described by *Bey et al.* [2001], with Asian emissions from the recent inventory of *Streets et al.* [2003a] superimposed. CO emissions estimates from biomass burning outside the boreal zone were taken from the Global Fire Emissions Database product (http://www.ess.uci.edu/~jranders/readme1.txt). This database estimates emissions using fire size, location, and timing inputs from the Tropical Rainfall Monitoring Mission (TRMM) satellite instrument [*Giglio et al.*, 2003], and estimates fuel consumption using a dynamic vegetation model, the Carnegie-Ames-Stanford Approach (CASA) [*Potter et al.*, 1993]. Details of this emissions dataset can be found in *van der Werf et al.* [2003]. Production of CO from biofuel combustion including agricultural burning and fuelwood use was estimated based on the inventory of *Yevich and Logan* [2003].

In addition to surface sources, the model includes photochemical production of CO from methane oxidation as well as isoprene and terpene oxidation. Methane oxidation was calculated online using fixed methane fields from *Dlugokencky et al.* [1994] and OH fields from *Spivakovsky et al.* [2000]. Production of CO from oxidation of isoprene and terpene was calculated offline using the method of *Allen et al.* [1996].

The principal atmospheric sink of CO is oxidation by hydroxyl, and this mechanism is calculated online in the CTM. Fixed OH fields from *Spivakovsky et al.* [2000] were used.

3.4. Transport simulation

Transport and chemistry of CO were simulated with the University of Maryland CTM (UMD-CTM) [*Allen et al.*, 1996; *Allen et al.*, 1997], using assimilated meteorological data from version 3 of the GEOS DAS [*Hou et al.*, 2003]. The UMD-CTM was run at a resolution of 2° latitude by 2.5° longitude, with 17 sigma layers and 18 pressure layers, a sigma-pressure interface of ~242 hPa, and a model top pressure of 0.01 hPa. Layers in the troposphere and lower stratosphere match those in the GEOS DAS. Turbulent mixing in the UMD-CTM is confined to the planetary boundary layer (PBL). CO is mixed uniformly through the depth of the PBL at each model time step (15 minutes). A detailed description of the UMD-CTM is given by *Park et al.* [2004].

3.5. CO surface measurements

Surface measurements of CO concentration were obtained from the NOAA CMDL Cooperative Air Sampling Network (http://www.cmdl.noaa.gov/ccgg/flask.html). For this study, flask measurements from all fixed stations were used. The flask samples are intended to represent regional background conditions, and so are generally collected in remote areas. A quality control process is used to flag measurements that are contaminated by local trace gas sources, and flagged measurements were excluded from this study. More information on the measurement, calibration, and quality control of these data can be found in *Novelli et al.* [2003] (see also *Novelli et al.* 1991; 1998; 1992).

CTM outputs for comparison to surface observations were sampled in the grid cell containing the measurement location, at the time step nearest the collection date and time for each flask measurement.

3.6. MOPITT measurements

The MOPITT Level 2 CO product consists of retrieved profiles of CO at up to seven nominal pressure levels, as well as total column CO (TC CO). The MOPITT CO retrieval uses a maximum *a posteriori* method, which incorporates a contribution from a fixed *a priori* profile [*Deeter et al.*, 2003]. The instrument takes data over the entire globe every three days, with a spatial footprint for each retrieval of 22 km by 22 km. The instrument was operational throughout the study period except for a calibration activity during 4-14 July [D. Ziskin, personal communication, 2004]. The MOPITT CO retrieval is sensitive to cloud cover. Cloud detection at latitudes below 65° is done using MOPITT radiance data, and the MODIS cloud cover product is used at higher latitudes [*Warner et al.*, 2001]. Only retrievals in the High Northern Hemisphere (latitude > 30° N) with surface pressures above 850 hPa are included in this study.

A number of quality indicators are included with each retrieval, including estimates of the radiometric error and the contribution of the *a priori* profile to the retrieved profile. The "percent *a priori*" is reported only for the seven layers of the MOPITT CO profile and not for the total column, so the value for the 700mb layer was used to exclude data with greater than 40% contribution of the *a priori* profile (<1% of data). Retrievals with a radiometric error greater than 25% of the total column CO were also excluded (~7% of retrievals). A more rigorous filtering of the data produced better agreement with model simulations, but reduced the coverage of the data, especially at

high latitudes. These selection criteria resulted in roughly 40,000 usable retrievals in the HNH per full day of instrument operation.

3.7. Simulation of MOPITT retrievals from transport model outputs

CO concentrations were output by the CTM on a 2° latitude by 2.5° longitude grid at six hour intervals. Each MOPITT retrieval was matched to its corresponding location on the output grid, and a vertical profile was extracted from CTM output by temporal interpolation of the two time steps nearest the time of the retrieval. This profile was then interpolated to the nominal MOPITT pressure levels. The interpolated profile was then convolved with the *a priori* profile and the averaging kernel according to the method described by *Deeter* [2000]. The result of this calculation is a simulated MOPITT retrieval based on the CTM model output. Total column CO amounts were calculated using the hydrostatic relation, as described by *Emmons et al.* [2004]. Spatial interpolation of these column amounts was used to calculate the total HNH CO burden. The biases and errors associated with each of these processing steps are analyzed in detail in section 4.1.

3.8. Injection height scenarios

Five simulations of boreal forest fire smoke injection were performed, each testing an idealized depiction of the injection process. Four of these simulations injected emissions at a single layer in the model, and the fifth distributed emissions in a pressure-weighted scheme throughout the tropospheric column, equivalent to a constant mixing ratio through the column at the emissions source.

In the first case, emissions were inserted at the lowest model layer (BORSFC). They were then mixed instantaneously within the planetary boundary layer by the CTM, and entrained into the free troposphere as dictated by the CTM. This scenario enables us

to test how well the PBL mixing in the CTM can simulate transfer of forest fire emissions into the free troposphere, without any additional convective uplift.

In the second and third cases, emissions were injected into a layer between 650 and 700 hPa (BOR700), or between 450 and 500 hPa (BOR500). These simulations should depict how emissions are transported that do not spend any time in the PBL prior to entering the free troposphere. In a small fraction of cases the BOR700 injection layer fell within the PBL.

The fourth case represents rapid uplifting of forest fire emissions through the entire troposphere to near the tropopause (BOR250). Emissions were injected at the top layer in the sigma portion of the model.

The final simulation was run using a pressure-weighted distribution of emissions through the tropospheric column (BORMIX), and served as a baseline for attempts to model injection height using a single uniform vertical distribution of emissions at the source. The correlation between this source and the single-layer injection scenarios is indicative of the amount of information available to test each specific injection height scenario (see Section 4.3.2).

3.9. Nomenclature used in this chapter

Non-boreal sources of CO used in this study are not generally analyzed separately. The total CO from all non-boreal sources is referred to as the BACKGROUND in this paper. The five model runs of the boreal forest fire CO source are designated BORSFC, BOR700, BOR500, BOR250 and BORMIX, and are described above. Simulated CO values combining the BACKGROUND and boreal CO are referred to as ALLSFC, ALL700, etc., depending on which boreal source run is used.

Because the boreal source contributes only a fraction of the total CO in most measurements, the correlation between observed CO and the simulated boreal source will generally be driven by the correlation between the simulated boreal source and the major sources of variability in the observations, which are sometimes not related to the boreal source. To obtain more meaningful comparisons between observations and simulated boreal CO, the residuals obtained by subtracting the BACKGROUND simulation from the observations were used. Derived values referred to as "residuals" in the remainder of this paper were calculated using this method.

4. Results

4.1. Effect of MOPITT sensor properties on detection of CO

Output from the CTM was transformed into a set of simulated MOPITT retrievals by a process that altered all of the sampling characteristics of the CTM output. To examine the effect of this transformation, total column CO was calculated from the CO concentration profiles obtained from each processing step. These total column amounts were resampled back onto the CTM output grid and interpolated to calculate total CO burden for each model time step. Figure 3-2 shows time series of HNH CO burden from each processing stage for the BACKGROUND simulation. The nominal sampling repeat rate for MOPITT is 3 days, so 3-day averages are shown for each of the resampled time series. Table 3-1 shows the effect of each processing stage on the total column CO values, compared with the TC CO from the raw CTM output. Mean and standard deviation of error in total column values are shown for each stage.

The first processing step involves resampling the gridded CTM output to the spatial and temporal coordinates of the MOPITT retrievals. Results of this processing

step are labeled as MOPITT XYT in Figure 3-2. A map of MOPITT retrieval density (Figure 3-3) reflects mostly the influence of cloud cover. The highest sampling density is over the Mediterranean Sea and the Middle East, and the sparsest coverage is over the subpolar Atlantic and northern Scandinavia. The period from 6-17 August does not include retrievals north of 65°N because the MODIS cloud mask required to process high-latitude retrievals was unavailable for those dates [D. Ziskin, personal communication]. The absence of data from polar and subpolar latitudes results in a positive bias in the interpolated HNH CO burden, which is readily visible in Figure 3-2. When this time period is removed from the sample, the bias in 3-day average CO burden is +0.68 Tg CO (+/- 0.39 Tg CO, 1-σ), or +0.76% (+/- 0.4%) of the total BACKGROUND CO burden. The sampling density of MOPITT in the HNH is therefore adequate to obtain reasonably accurate estimates of total HNH CO with 3 days of data, provided data from high latitudes are available.

In the second processing step, vertical profiles in the CTM coordinate system are resampled to the seven nominal MOPITT levels (MOPITT Z in Figure 3-2 and Table 3-1). This processing step results in a positive bias in the total column CO amounts, averaging +1.9% (+/- 2%). The resulting bias in the HNH CO burden averages +2.5% (+/- 0.6%). Much of this bias is caused by a relative increase in the column depth represented by the surface layer output. The vertical coordinate system in the CTM has several layers in and near the boundary layer, which show a gradient of CO in areas affected by surface sources. The lowest retrieval level in the MOPITT data generally includes the entire boundary layer and more, and concentration at this level is estimated as the interpolated concentration at the retrieval bottom pressure (close to the surface

pressure). This results in a positive bias in estimated total column CO, which is greatest in areas near surface CO sources. Some additional bias and error at this step results from differences between the surface pressure from the GEOS-DAS and the retrieval bottom pressure from the MOPITT data, which is derived from the NCEP reanalysis data set [*Deeter et al.*, 2003]. The retrieval bottom pressure from the MOPITT data averages 1.9 +/- 14 hPa higher than the CTM surface pressure. This discrepancy increases the relative contribution of the surface layer to the TC CO, which results in a slight positive bias in simulated TC CO.

The final step in preparing simulated MOPITT retrievals is application of the averaging kernels to the simulated profiles (MOPITT AVGKER in Figure 3-2 and Table 3-1). This stage causes the most drastic changes to the simulated CO values, because the CO concentration data from the CTM output is combined with the *a priori* profile used in the MOPITT CO retrieval. The bias in TC CO resulting from this processing step is negative, because the weight of the surface layers is reduced by the averaging kernel. This acts to partially offset the positive bias resulting from vertical interpolation. The final simulated TC CO has a mean bias of +1.7% (+/- 6%) relative to the total column CO calculated from the raw CTM output. This bias varies with the influence of surface sources of CO: application of the averaging kernel reduces TC CO estimates in areas with strong surface sources, and increases TC CO in regions relatively distant from surface sources. Averaged over the HNH, this bias has a mean of +2.0% (+/- 0.9%) for estimated 3-day average HNH CO burden during the study period.

The overall biases are relatively small, but errors in individual simulated retrievals can be large, and variations in the spatial coverage of the satellite can artificially affect

calculated spatial and temporal averages. Especially at finer scales, resampling is required for quantitative comparison of model output to MOPITT data, or for comparison of MOPITT data to CO concentration data from other sources. Interpretation of TC CO values from MOPITT should also take into account the tendency of MOPITT to underestimate CO near strong surface sources.

4.2. Effect of injection height on forest fire CO signal in observations

CO concentration output from the CTM was used to generated simulated data sets with the same horizontal, vertical, and temporal sampling characteristics as the CO measurements from surface flask data as well as from MOPITT. The comparison of injection height scenarios in these simulated data sets shows the theoretical effect of injection height on signal strength from boreal forest fires in the measurement data. The differences in signal strength have important implications for inverse modeling studies where the measurements are used to determine the magnitude of the CO emissions source.

4.2.1. Boreal source strength in model output

Figure 3-4 shows the fractional contribution of simulated non-boreal sources to total CO burden, as well as the contribution of the boreal fire CO scenarios BORSFC, BOR700, BOR500, and BOR250. All figures are proportional to the total CO burden from all non-boreal (BACKGROUND) sources. The bottom portion of Figure 3-4 shows the relative contribution of the different non-boreal CO sources, and the top portion shows the contribution of boreal CO relative to the total non-boreal CO source. Monthly average data are shown for the entire globe, as well as the HNH and the eastern quadrant of the HNH, which includes the strongest boreal CO sources.

In the global average, differences between injection scenarios for the entire globe are caused by differences in photochemical removal of CO at different altitudes in the model. Figure 3-4 shows that these differences are very small. In the HNH average, CO burden from boreal CO will also vary because of differences in meridional transport at different levels in the troposphere. These differences are much larger than differences due to chemistry, but still relatively small for this simulation. When only the eastern quadrant of the HNH is considered, differences in zonal transport become apparent, as emissions injected at higher altitudes are advected more efficiently away from the source region.

Figure 3-5 shows the time series of CO burden estimated from the raw CTM output for the HNH and the eastern quadrant of the HNH, for the BACKGROUND, ALLSFC, ALL700, ALL500, ALL250 and ALLMIX scenarios. The differences among injection scenarios are similar to what is observed in Figure 3-4: meridional transport and chemistry cause small differences compared to zonal transport, which controls the persistence of emissions near the source region. The ALL250 source is removed from the eastern quadrant of the HNH much more quickly than the other scenarios. The ALLMIX scenario produces results similar to ALL700.

Based on Figure 3-4 and Figure 3-5, it is clear that zonal average CO concentrations should not be very sensitive to injection height. However, vertical sampling bias creates significant differences in the boreal fire CO signal detected by both surface measurements and MOPITT retrievals, as discussed below.

4.2.2. Simulated CO surface measurements

A total of 504 measurements from 52 sites in the NOAA/CMDL network were used in this study, including 283 measurements from 23 sites in the HNH. Figure 3-6

shows the relative contribution of non-boreal and boreal CO sources to these measurements. When Figure 3-4 and Figure 3-6 are compared, two different kinds of bias are evident. One is the spatial sampling bias: the density of surface measurements in the HNH is far greater than over the rest of the globe. The consequence of this for boreal forest fire CO is that the fraction of the total CO attributable to these fires in the global average is biased high. This is a consequence of the sparse network of measurement sites, and indicates that averages over multiple measurement sites should be interpreted with caution.

The other bias that can be seen in Figure 3-6 is the enhanced detection of CO from surface sources compared with sources in the free troposphere. The contribution of the photochemical source of CO is reduced in the simulated surface measurements, and the influence of surface sources such as fossil fuel combustion is enhanced. For the boreal source, this results in a slightly greater sensitivity to the BORSFC source compared with the BOR700 source, but the more dramatic difference is in the relative influence of the BOR500 and BOR250 sources. Globally, the burden of CO from the BOR250 simulation is nearly identical to the BORSFC and BOR700 simulations, but the amount of boreal CO detected at the surface is only one-third. In the context of inverse modeling experiments, where the atmospheric observations are used to estimate the source magnitude, the accuracy of the derived source magnitude will be dependent on correct specification of the injection profile of the source.

4.2.3. Simulated MOPITT measurements

Figure 3-7 shows the time series of CO burden in the HNH and its eastern quadrant as calculated from the simulated MOPITT data set. The time series calculated

from the MOPITT observations is also shown. The MOPITT instrument samples the entire Earth with a 3-day repeat rate: therefore, a 3-day moving window has been applied to the time series. The MOPITT time series for the HNH has very little variability, and does not appear to be strongly sensitive to boreal forest fire activity. However, the trend of MOPITT data matches that of the BACKGROUND simulation, showing the influence of increased photochemical removal of CO during the NH summer. When only the eastern quadrant of the HNH is considered, the broad feature in the MOPITT data from 15-30 June corresponds to the peak of boreal fire activity in June.

Comparison of Figure 3-5 and Figure 3-7 shows that the sensitivity of the MOPITT instrument has a strong interaction with injection height. The emissions injected at the surface produce a much smaller signal in the MOPITT data, because of MOPITT's lack of sensitivity in the lower troposphere. The vertical distribution of the BOR250 source corresponds well with the peak of the MOPITT averaging kernels, and so these emissions produce a strong signal. The implication for inverse modeling is that if the injection process is not modeled correctly, the influence functions will have a bias, due to biased vertical sampling of the atmosphere.

4.3. Comparison of model output to observations

Analysis of simulated measurements from model output shows that the sampling properties of various atmospheric measurements have interactions with injection height that can change the magnitude of the signal. Uncertainty in the magnitude of non-boreal sources affects the capacity of these measurements to constrain the absolute magnitude of the boreal source. To learn more about the distribution of injection heights, the

differences in the spatial and temporal patterns of CO concentration that result from different injection scenarios will be compared to observations.

In this section, model output is compared to observations of CO concentration from surface measurements as well as MOPITT retrievals. For each of these data sets, the model simulation is first evaluated with the boreal source excluded (BACKGROUND). The boreal source will then be evaluated by comparison with the residuals obtained by subtracting the BACKGROUND simulation from the atmospheric measurements.

4.3.1. Comparison to surface CO measurements

Figure 3-8 compares the surface CO observations to model outputs from the BACKGROUND simulation for each month of the study period. The model captures effectively the contrast between clear air masses in the Southern Hemisphere and more polluted air masses in the HNH, but is less effective at capturing the variability within the HNH. At concentrations higher than about 150 ppbv, the agreement between model and measurements appears to break down, with many episodes of elevated CO in the observations not captured in the model results, and many high simulated CO concentrations failing to appear in the observations.

Many different sources of error affect the match between model and measurement. Some error can be attributed to incorrect specification of surface source magnitudes: an inverse model experiment by *Palmer et al.* [2003] using data from the TRACE-P campaign found that Asian anthropogenic sources of CO used in this model were potentially underestimated by more than 50%. *Allen et al.* [2004], also using TRACE-P data, showed similar results, finding that the best match to observations was

obtained by reducing Asian biomass burning CO by 50% and increasing Asian fossil fuel and biofuel CO by 59%.

Error in simulated atmospheric transport is a large source of error, estimated by *Palmer et al.* [2003] to be about 20-30% of total error. The method used by *Palmer et al.* to estimate transport error also includes some other error sources, such as incorrect description of the spatial and temporal pattern of sources in model inputs, so the error attributable to incorrect transport is probably smaller.

Representation error caused by the coarse model resolution could cause the model to overestimate CO in measurements near CO sources. This error results from the fact that most CO sources, especially from fossil fuels and biomass burning, have a fine spatial pattern relative to the CTM resolution. This results in artificial spreading of concentrated emissions in CTM simulations, which can be a large source of error in comparison with measurements taken near point CO sources. This error produces both under- and over-estimates of CO concentration, in a proportion determined by the relative scale of the transport simulation and measurements. For the comparison in this section, overestimation by the model is likely to account for the majority of cases where this error is significant.

In addition to all of these sources of error, CO from boreal fires is likely responsible for some high CO events in the observations.

Figure 3-9 compares the CO contribution from the modeled boreal source to the residuals obtained by subtracting the BACKGROUND simulation from the surface CO observations. It is qualitatively clear from the BORSFC comparison that model simulation of boreal sources is successful at capturing some of the variability in surface

CO measurements not captured by the BACKGROUND sources, though other sources of variability remain. The magnitude of the surface signal decreases with higher injection height: the average CO enhancement from the boreal source is 23ppbv for the BORSFC simulation, and only 8ppbv for the BOR250 source. The BOR700 simulation (results not shown) looks only slightly flatter than the BORSFC simulation, and is similarly correlated, indicating that the transport model readily mixes CO from that elevation down to the surface. The BOR500 and BOR250 CO appear to be only rarely mixed to the surface level, and so the CO enhancement from these sources is small and less variable. The CO enhancement from the BOR250 source is less than 10% of the observed CO in over 95% of the data.

From the data shown in Figure 3-9, it is evident that a substantial fraction of the emissions from boreal fires are transported from the surface layer or the lower troposphere. Since surface measurements have very low sensitivity to the BOR500 and BOR250 injection scenarios, the results of this comparison do not indicate what fraction of boreal CO in the free troposphere is injected in the middle and upper troposphere. In order to accurately evaluate whether mid- and upper-tropospheric injection of boreal forest fire smoke contributes to the distribution of CO in the HNH, measurements of CO in the free troposphere must be examined. In the next section, data from the MOPITT instrument are applied to the problem of comparative evaluation of different injection scenarios.

4.3.2. Comparison of non-boreal CO sources to MOPITT observations

MOPITT retrievals in the HNH during the study period were processed according to the method discussed in Section 2.6.1. Spatial autocorrelation in the MOPITT data,

and sampling error caused by the variations in MOPITT sampling density, reduce the independence of the sample, and may lead to bias in statistical comparisons. To compare simulated data from model outputs to MOPITT observations, both simulation and measurement data sets were resampled back onto the 2° latitude by 2.5° longitude CTM output grid, with a six-hour sampling interval. This reduced the sample size, but also reduced the sampling bias associated with MOPITT spatial coverage, and reduced autocorrelation in the data sets. This also has the effect of partially suppressing the representation error caused by the scale mismatch between MOPITT observations and CTM output.

Figure 3-10 shows monthly average total column CO for the HNH during June, July, and August 2000 for the MOPITT data, the BACKGROUND simulation, and the residuals obtained by subtracting the BACKGROUND simulation from the MOPITT data. The model performs reasonably well at reproducing the broad-scale features of the CO distribution observed by MOPITT, including large anthropogenic plumes extending into the Pacific from China and into the Atlantic from the eastern United States. The model underestimates CO concentrations around the globe. The BACKGROUND simulation shows a large feature of very low CO concentrations over western Canada and southern Alaska that is only slightly evident in the MOPITT data. The residual images show clearly that the CO emissions originating in eastern Asia and eastern North America are underestimated by the model. The residual images also show features of elevated CO, such as over the central Pacific and off the west coast of North America, which are absent in the BACKGROUND model simulation.

The causes of the discrepancies between the model and observations are similar to those for surface measurements. One difference is that representation error should be somewhat smaller, since the spatial coverage of MOPITT is better, and the scale of the MOPITT data is closer to that of the model. Table 3-2 shows statistical estimators of model performance relative to MOPITT, calculated for the entire HNH and several geographic subsets. All statistics were calculated by comparing the MOPITT total column CO with simulated values from the BACKGROUND simulation.

Table 3-2 shows the mean bias of the model, excluding the boreal source, compared to the MOPITT observations. In all regions, the model underestimates CO. The overall bias of the BACKGROUND simulation tracks the contribution of the boreal CO source, with the largest discrepancy in June, averaging 6e17 molecules cm^{-2} over the entire HNH, which is about 30% of the mean MOPITT total column CO during June. The discrepancy between the model and MOPITT data is mostly consistent across geographic regions, with greater differences over the Pacific.

Palmer et al. [2003] propose that the mean bias of simulated values is indicative of errors in the magnitude of the source, and that the scatter of errors is indicative of other types of error, including transport error and errors in the spatial and temporal pattern of the model source. The standard deviation of model errors was used as an estimate of the scatter of model errors (Table 3-2). Since all CO sources in the BACKGROUND simulation are monthly or annual means, the monthly errors are indicative of how well the model is capturing spatial dynamics and transport of emissions, while the values for the entire study period also indicate the model's ability to replicate the seasonal dynamics of CO.

Finally, Table 3-2 shows the correlation between model output from the BACKGROUND simulation and MOPITT total column CO. Correlations in all regions are best for August, and model performance is generally weakest in June and July, which is the opposite of how the model performed relative to the surface observations (see Figure 3-8). Low correlation for July over the Atlantic is attributable to high CO values in the north Atlantic, likely originating in Canada or the northeastern US (see Figure 3-10). Some of the discrepancies between the BACKGROUND simulation and MOPITT data are clearly the result of CO from boreal fires, but other sources of error are also evident from this comparison.

4.3.3. Boreal source signal in MOPITT retrievals

The contribution of the boreal source to simulated CO concentrations in the HNH is between 15-25% over the study period, with some variability between regions. Many of the differences between injection height simulations can be attributed to the effect of the MOPITT averaging kernel. Figure 3-11 shows the vertical profiles of each model run calculated from both the raw CTM output and after application of the MOPITT averaging kernels. Two effects of the application of averaging kernels to the model output can be seen in the comparison between the original CTM output profiles and the simulated MOPITT profiles. First, all of the single-layer injection simulations show a sharp peak in the mean vertical profile caused by a few profiles close to the emissions source with extremely high CO in the injection layer. Once the averaging kernel is applied, these sharp peaks disappear, despite being close to the nominal MOPITT pressure levels. The other effect is the heightened sensitivity of the MOPITT averaging kernel to the upper troposphere, and very low sensitivity to the surface. An indication of the sensitivity of the

MOPITT instrument is the difference between the ALLSFC and ALL700 simulations in the lower troposphere. In the CTM output, the ALLSFC simulation has much higher CO at the surface. However, once the MOPITT averaging kernel is applied, the ALLSFC CO in the lowest layer of the MOPITT retrieval is actually lower than the ALL700 CO. This lack of sensitivity at the surface also masks the sharp features in the model output caused by high concentrations in the boundary layer over surface CO sources.

Table 3-3 shows the correlations among total column CO values from the CTM simulations. The negative correlations between the BACKGROUND and BOR sources indicate that the regions with the greatest amount of boreal fire CO are in otherwise relatively clean air, which reflects the geographic separation of the boreal forest fire source. Correlations among different BOR simulations reflect similar patterns of horizontal transport between model runs. The BORMIX model output is strongly correlated to all of the other BOR simulations.

4.4. Agreement between boreal source and MOPITT data

Simulated TC CO from CTM output was compared with MOPITT data to determine which injection scenario correspond best to the spatial and temporal patterns of CO elevation not captured by the simulated non-boreal sources. The application of the averaging kernel, and specifically the inclusion of *a priori* data, mean that the simulated MOPITT CO values are not a simple linear sum of the constituent sources. *Arellano et al.* [2004] describe a method to remove the *a priori* component of each MOPITT retrieval so that the MOPITT data can be compared to a linear sum of the influence of each constituent in the simulation. This comparison incorporates the averaging kernels and therefore reflects the MOPITT vertical sensitivity, but does not include a contribution

from the *a priori* profile. The disadvantage of this approach is that the values thus obtained do not correspond directly to any observable physical quantity, i.e. they are not physically meaningful. However, this method permits construction of simulated observations as a linear sum of constituent sources, which can be directly compared to MOPITT observations. For the purposes of this paper, *Arellano et al.*'s [2004] method was used to construct estimates of the boreal CO contribution to simulated MOPITT total column CO, which were compared with the residuals obtained by subtracting the BACKGROUND simulation from the MOPITT data.

Figure 3-12 shows bias, error variance, and model-measurement correlation statistics, comparable to what is shown in Table 3-2. The model bias (Figure 3-12a) simply reflects the level of observed CO enhancement in each simulation, because the simulation underestimates the observed CO in all cases.

The standard deviation of model errors (Figure 3-12b), is higher over land compared to water, due to the influence of high simulated CO values near source regions. Simulated MOPITT retrievals from any grid cell containing fire emissions will be elevated, which is a source of representation error because the fire and smoke plume actually occupy only a small fraction of the grid cell, which does not necessarily overlap with any MOPITT retrievals. Thus, even when the model is capturing the spatial and temporal variability of the fire source, the scatter of model errors over source regions will be high due to the model's coarse resolution relative to the observations. The strength of the boreal signal in simulated MOPITT total column CO drives the error statistics near the source because of this effect. Thus, the scatter in the error is much higher for BOR250

vs. BORSFC over Asia and the Pacific, near the source of most of the boreal CO, compared to over North America and the Atlantic.

In regions far from the source, the error scatter is driven by the degree to which spatial and temporal patterns of elevated CO in the observations are captured by the model. The correlation values for the Atlantic (Figure 3-12c) show the same pattern as the scatter in model errors, with lower scatter corresponding to better correlation. The BORMIX simulation shows the best correlation with observations, except over Asia, where the BORSFC simulation performs slightly better.

The performance of the BORMIX simulation indicates the likelihood that, if the horizontal and vertical transport in the model are unbiased, the overall vertical distribution of forest fire smoke does include some contribution throughout the tropospheric column. The correlation of each of the single-layer injection simulations to the observations supports this. However, because there are significant covariances among injection simulations, strong conclusions cannot be drawn based on the individual performance of the single-layer scenarios. The resolution of this experiment is not sufficient to specify quantitatively the proportion of emissions injected at the different levels. In the next section, a case study of large fire events in southern Russia during early June is used to better illuminate the relationship between injection scenarios and observations.

4.5. Case study examination of southern Russia fires

Between 30 May and 7 June 2000, roughly 250,000 hectares burned in the Russian boreal forest near the Chinese and Mongolian borders. The emissions from those fires show up prominently in the MOPITT data from this region, and present evidence of

a complex pattern of smoke injection. Figure 3-13 shows the MOPITT total column CO for two 2-day periods, 3-4 and 5-6 June, along with the results of the BACKGROUND simulation, and the residuals obtained by subtracting the BACKGROUND simulation from the observations. Many of the areas of enhanced CO in the MOPITT data are consistent with the pattern of enhancement from the boreal forest fires. The region of active forest fires during this period is marked on the MOPITT CO map (Figure 3-13) with an asterisk. Figure 3-14 shows the simulated pattern of CO enhancement from boreal forest fires for each of 4 injection scenarios. From Figure 3-14, it is evident that the prevailing winds at the surface and aloft are different. Near the surface, advection is slower, resulting in less spreading of the forest fire plume. At higher levels, the emissions move southeast more rapidly, and then tend to move clockwise back toward China. In the case of the BOR250 simulation, the peak of the emissions plume appears to have moved around to a position directly south of the fire origins by 6 June.

The MOPITT data shows a spatial and temporal pattern of CO enhancement that suggests the influence of the fire events in southern Russia. However, all of the single-layer injection scenarios miss some parts of the enhancement pattern. For instance, the CO enhancement in the Yellow Sea during 5-6 June is captured only with high-altitude injection of forest fire emissions (BOR500 or BOR250), while the elevated CO east of Hokkaido during the same period is more consistent with the BOR700 simulation.

To solidify attribution of MOPITT features to smoke from different injection altitudes, the difference between the 850 and 350mb layers in the MOPITT retrieval was used as an indicator of the relative weighting of the upper and lower troposphere in the total column CO [*Kim et al.*, 2004]. This difference generally decreases with distance

from surface sources; it is therefore correlated with total column CO in regions where surface sources dominate. As an indicator of local high-altitude CO sources, the retrievals were filtered to identify "top-heavy" retrievals, where total column CO is more than 20% above the mean, and the 350mb CO is greater than the 850mb CO by at least 10 ppb. These retrievals make up about 1% of the 32,700 usable retrievals in the region shown in Figure 3-13 during 3-6 June.

Figure 3-15 shows locations of "top-heavy" retrievals, marked with "x", superimposed on the gridded MOPITT TC CO, as well as the simulated CO enhancement from the BORMIX scenario. On 3-4 June, there are no "top-heavy" retrievals in the immediate vicinity of the fires, where the BORSFC simulation indicates high CO. Immediately to the south, however, where the BOR500 and BOR250 simulations indicate high-altitude emissions are transported, a trail of "top-heavy" retrievals can be seen extending down to the border of North Korea. The "top-heavy" retrievals are also present in a region of elevated CO extending south-southwest from the fires, which is not replicated in any of the BOR simulations. During 5-6 June, the "top-heavy" retrievals are co-located with the simulated plumes from the BOR500 and BOR250 simulations. Over the Kuril Islands, where observations of elevated CO correspond to the general pattern from the BOR700 simulation, there are no "top-heavy" retrievals. This analysis shows that it is possible to distinguish elevated plumes from near-surface plumes in MOPITT data. The pattern of these plumes indicates that the real plume behaves as if forest fire emissions are injected at a range of altitudes throughout the tropospheric column.

The ALLMIX scenario spread boreal fire CO throughout the tropospheric column. This approach produced results globally that were better than any of the single-

layer injection scenarios. Examination of the case study indicates that this is because boreal fires inject CO at a range of altitudes. However, the distribution of emissions observed by MOPITT does not match the BORMIX scenario, and indicates that injection properties vary even within this case study. Emissions transported near the surface result in a substantial overestimate of CO in the immediate vicinity of the source during 3-4 June, but the emissions plume over the Kuril Islands on 5-6 June, also associated with lower-level transport, is underestimated by the BORMIX scenario. This suggests that any fixed parameterization of the vertical distribution of emissions will still produce errors in simulated transport.

5. Conclusions

A high-resolution model of the CO source from boreal forest fires was used as input to a CTM to evaluate how atmospheric observations might respond to variations in injection height, and to test whether observed patterns of atmospheric CO could better constrain the injection properties of the boreal forest fire source.

Examination of simulated atmospheric measurements derived from CTM output showed that both surface and MOPITT measurements of atmospheric CO are quite sensitive to injection height of the CO source. Surface measurements have very little sensitivity to high-altitude injection sources, showing only one-third the enhancement seen from a source of identical magnitude injected at the surface. MOPITT measurements, on the other hand, have more sensitivity to higher-altitude sources. A CO source injected in the upper troposphere produced total column CO values from MOPITT about 10% larger over the entire HNH compared to surface injection of an identical quantity of CO.

Examination of the effects of the MOPITT sampling and averaging kernel on simulated CO gave a mean bias in total column CO resulting from the MOPITT sampling and averaging kernel of +2.4%. However, this overall result was not reproduced in source regions: in 5% of retrievals, mostly in areas with large influence of surface sources, calculated total column CO differed by more than 14%. Simulated total column CO was extrapolated to estimate the CO burden in the HNH, and the 3-day average CO burden was found to have a bias associated with the MOPITT sampling properties averaging only 1.3%. This shows that the nominal 3-day sampling rate of the MOPITT instrument, even when reduced by cloud cover, is sufficient for measurement of CO variation over the HNH, provided overly strict filters are not applied to the data.

The best agreement between model output and surface measurements of CO was obtained with surface injection. However, the lack of sensitivity to CO sources in the middle and upper troposphere made it difficult to evaluate those scenarios using surface measurements.

Agreement between CTM simulations with different injection properties and MOPITT observations was similar. The differences in model errors between injection scenarios were often dominated by the vertical sensitivity of the MOPITT instrument, especially in the source region. In all regions except over the forest fire source, the best agreement was obtained by a simulation in which forest fire CO injection was parameterized by a pressure-weighted distribution throughout the tropospheric column.

A case study of a forest fire smoke plume from fires in Southern Russia during 3-6 June was used to examine the relationship of different injection simulations to MOPITT data in more detail. Comparison of model results with observations from this area

showed that injection height was highly variable in this event. The MOPITT observations showed a pattern of elevated CO that was consistent in some places with low-altitude injection and in others with high-altitude injection. This pattern was confirmed by examination of the vertical information in the MOPITT retrievals.

This study shows that for global studies of the forest fire source, an empirical parameterization of injection height should distribute the CO source through the tropospheric column. This approach will still produce significant errors, which will be greater at finer scales. Accurate description of the long-range transport of forest fire emissions requires an accurate description of injection height, but data to support an explicit model of injection is sparse. Pressure-weighted distribution of emissions through the tropospheric column is a good first-order approximation to describe the bulk properties of the source at a global scale. However, variability in injection height will be a substantial source of error in modeled transport of forest fire emissions until a more complete model of emissions injection can be developed.

6. Tables

	Abs. TC error vs. CTM output profiles		TC error as fraction of TC from CTM output	
	Mean	**σ**	**Mean**	**σ**
MOPITT Z	+5.24e16	9.2e16	3.70%	5%
MOPITT AVGKER	+2.74e16	1.04e17	2.44%	7%

Table 3-1. Error in estimated total column CO (TC CO) resulting from vertical resampling of CTM output and application of MOPITT averaging kernel. Positive errors indicate an overestimate of TC CO relative to TC CO calculated from 35-layer CTM output profiles. The designation MOPITT Z refers to the processing step where the CTM output profiles are resampled to the 7-layer nominal vertical profile of the MOPITT instrument, and MOPITT AVGKER refers to the processing step where the MOPITT averaging kernel is applied. See text for details.

		HNH	WATER	LAND	PACIFIC	ATLANTIC	N. AMERICA	EURASIA
Model Error (mol. Cm-2)	ALL	5.29E+17	5.62E+17	4.95E+17	6.41E+17	4.94E+17	5.07E+17	4.89E+17
	June	5.99E+17	6.18E+17	5.76E+17	7.08E+17	5.54E+17	6.03E+17	5.61E+17
	July	5.14E+17	5.45E+17	4.78E+17	6.14E+17	4.76E+17	4.94E+17	4.70E+17
	August	4.60E+17	5.03E+17	4.26E+17	5.84E+17	4.29E+17	4.09E+17	4.34E+17
SD of Error (mol. Cm-2)	ALL	2.73E+17	2.78E+17	2.71E+17	2.80E+17	2.59E+17	3.01E+17	3.05E+17
	June	2.61E+17	2.67E+17	2.58E+17	3.00E+17	2.16E+17	2.36E+17	3.00E+17
	July	2.55E+17	2.67E+17	2.45E+17	2.51E+17	2.62E+17	2.71E+17	2.50E+17
	August	2.57E+17	2.58E+17	2.61E+17	2.30E+17	2.59E+17	3.33E+17	2.28E+17
Correlation (r)	ALL	0.56	0.51	0.58	0.61	0.44	0.50	0.63
	June	0.56	0.47	0.60	0.50	0.46	0.59	0.61
	July	0.53	0.43	0.60	0.57	0.30	0.52	0.63
	August	0.61	0.61	0.61	0.75	0.53	0.51	0.70

Table 3-2. Model error statistics from BACKGROUND simulation, by geographic region. All statistics were calculated by comparison of TC CO values resampled to the 2.5° by 2° model output grid.

	BORSFC	BOR700	BOR500	BOR250	BORMIX
BACKGROUND	-0.09	-0.07	-0.05	-0.05	-0.07
BORSFC	-	0.80	0.65	0.51	0.83
BOR700		-	0.79	0.55	0.85
BOR500			-	0.78	0.91
BOR250				-	0.82

Table 3-3. Correlations among simulated MOPITT TC CO for BACKGROUND model run and BOR model runs.

7. Figures

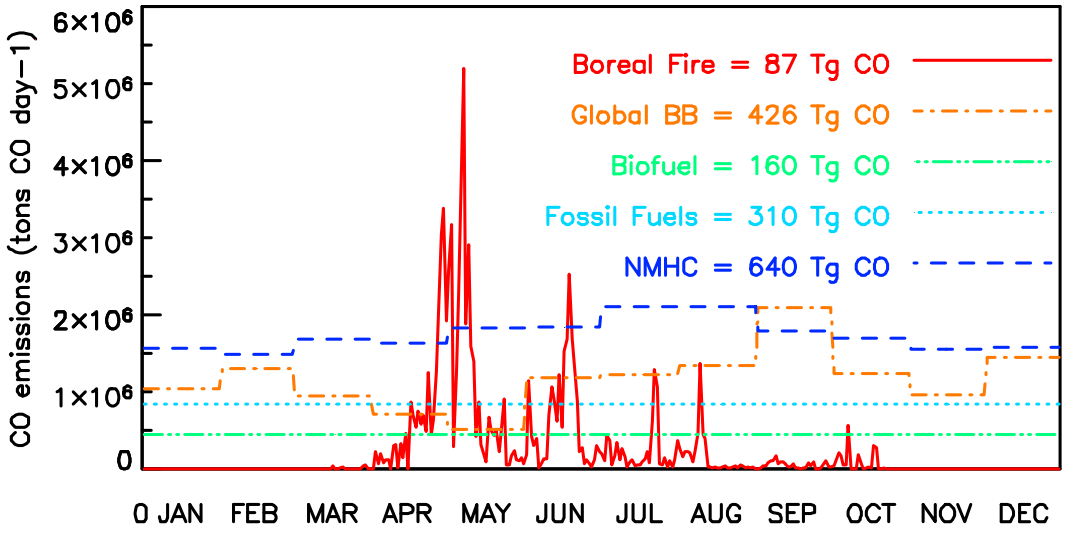

Figure 3-1. CO sources used in the CTM simulation. Sources are described, with citations, in Section 3.3.

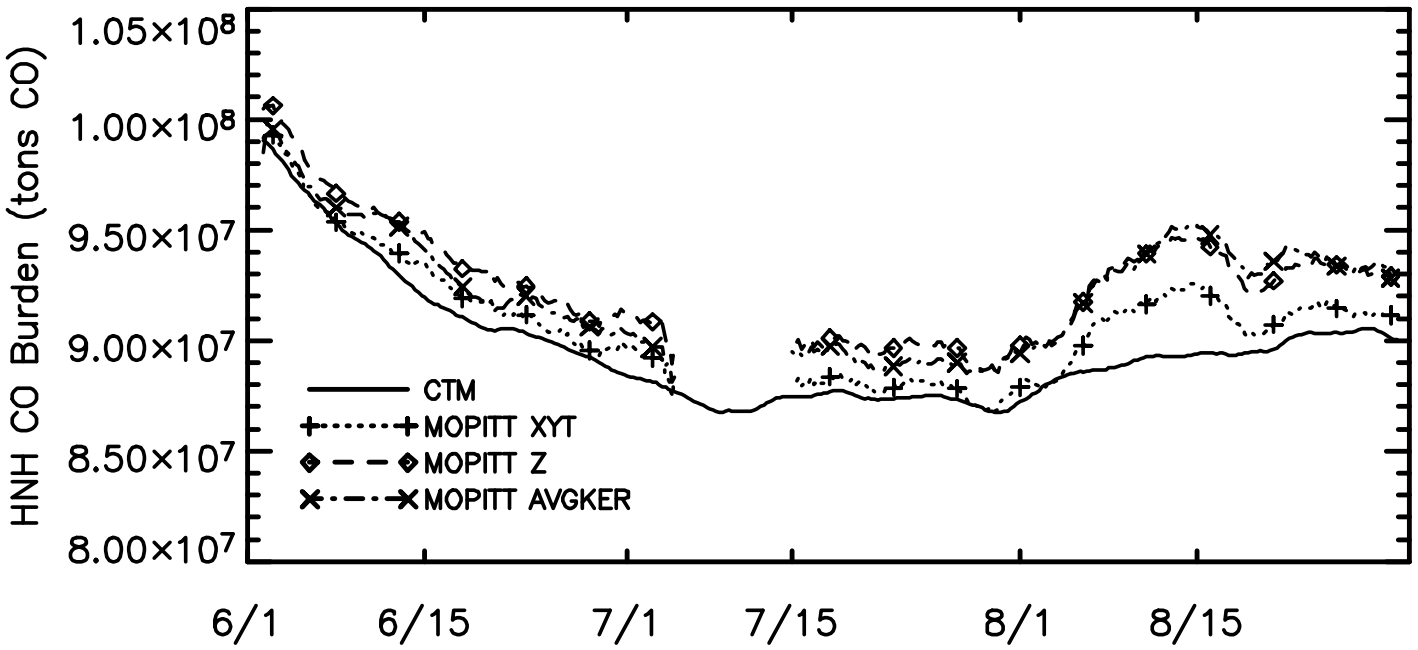

Figure 3-2. Time series of HNH CO burden calculated at different stages of MOPITT simulation procedure. Processing algorithm is discussed in detail in Section 3.1. Elevated CO during 6-17 August is a caused by the absence of MOPITT data north of 65°N.

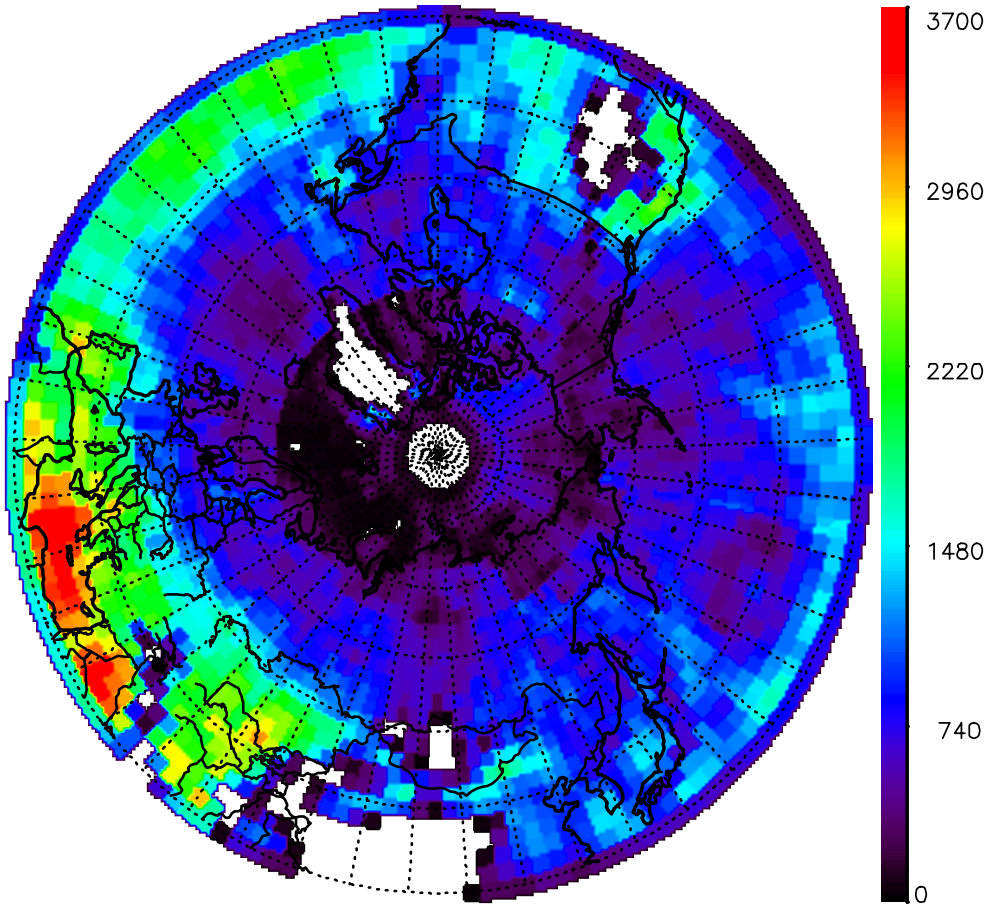

Figure 3-3. Number of MOPITT retrievals in the HNH during June-August 2000, aggregated to a 2.5° by 2° grid. The total number of retrievals, after filtering, was 3.2 million, for an average of about 250 per grid cell during the study period. White areas have no retrievals.

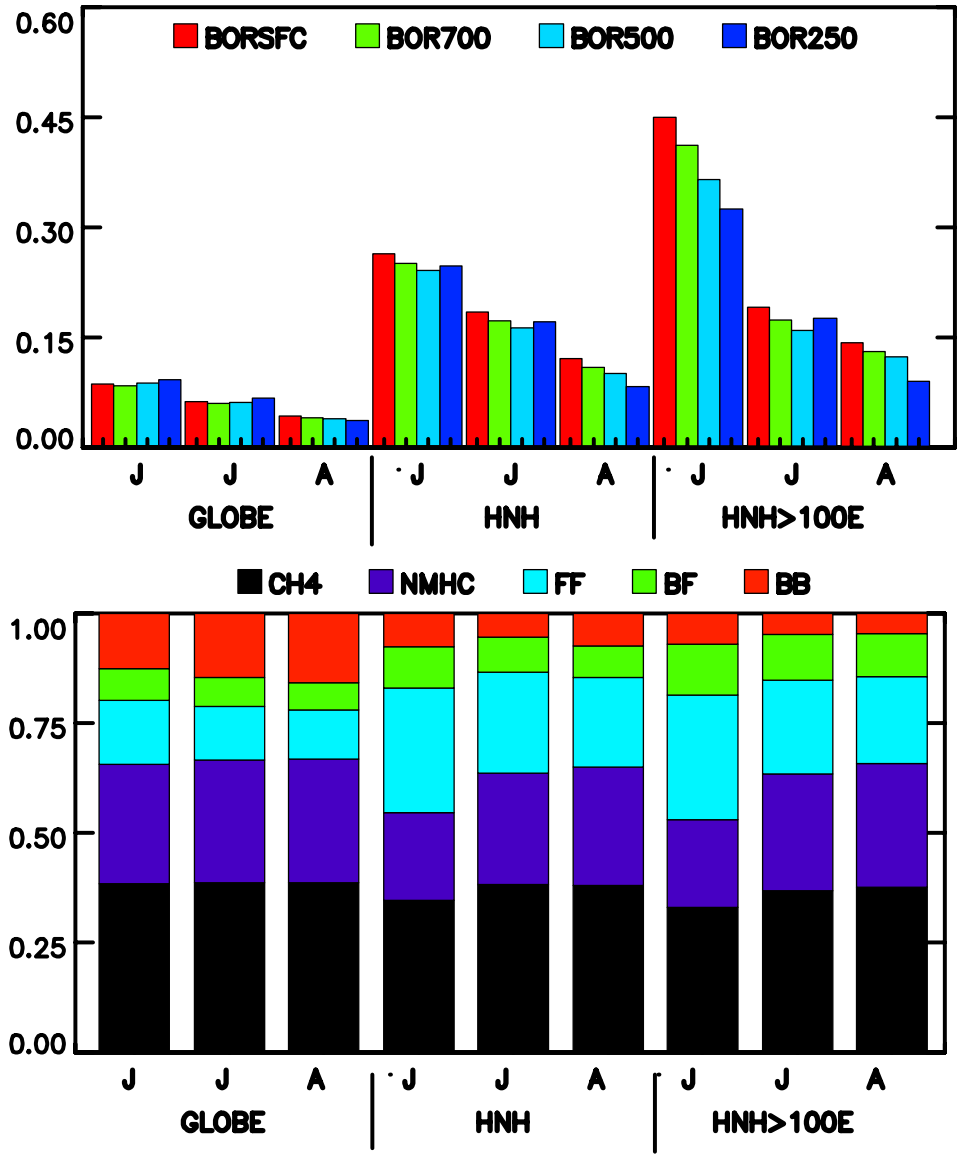

Figure 3-4. Fraction of HNH CO burden from each constituent, calculated from model output. All fractions are percentages of total CO from non-boreal sources. The top portion shows the percentage enhancement of simulated CO burden from inclusion of the boreal source. The bottom shows the fraction makeup of the CO burden from non-boreal sources. Non-boreal sources are as follows: CH4= methane oxidation, NMHC= oxidation of isoprenes and terpenes, FF= fossil fuels, BF= biofuel combustion and BB= biomass burning (outside the boreal zone).

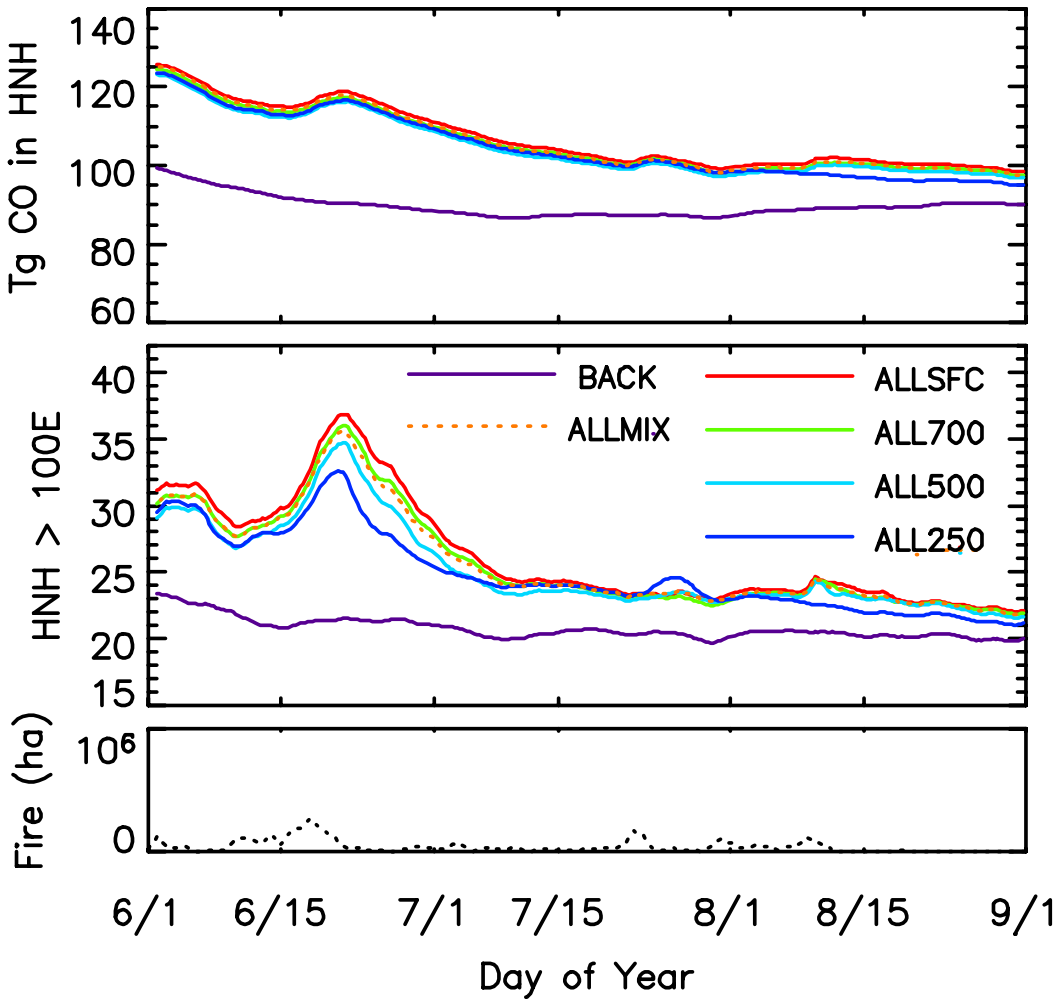

Figure 3-5. Time series of CO burden in the HNH calculated from model simulations of non-boreal sources (BACK, purple line), and different injection scenarios for the boreal source (ALL). Time series are shown for the entire HNH, as well as the eastern quadrant of the HNH, which includes the most intense fire activity during the study period. The bottom panel shows the time series of area burned in the boreal forest.

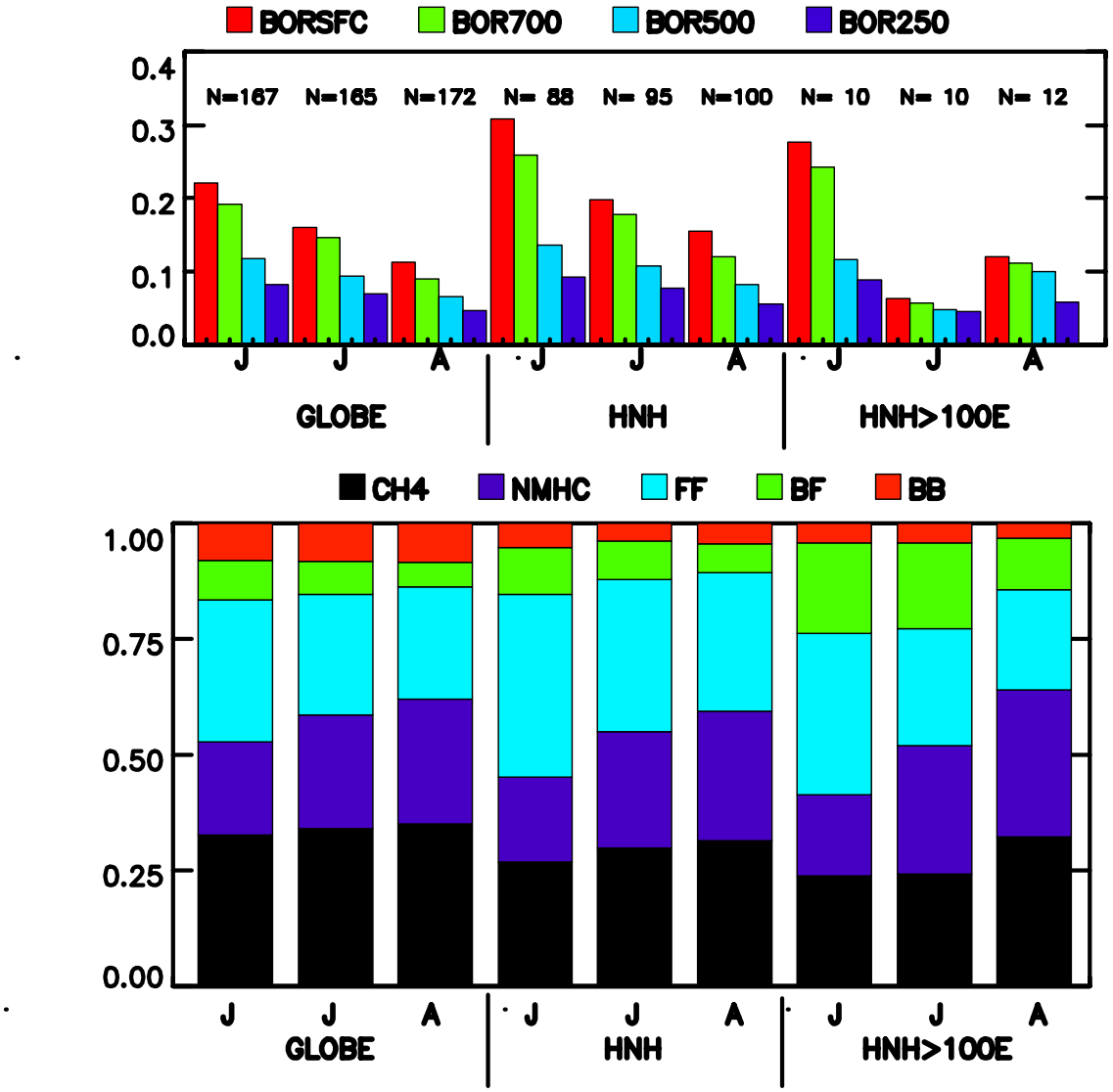

Figure 3-6. Fraction of HNH CO burden from each constituent, calculated from model output resampled to match CO surface measurements from the CMDL network. All fractions are normalized to total CO from non-boreal sources. For legend key, see Figure 3-4.

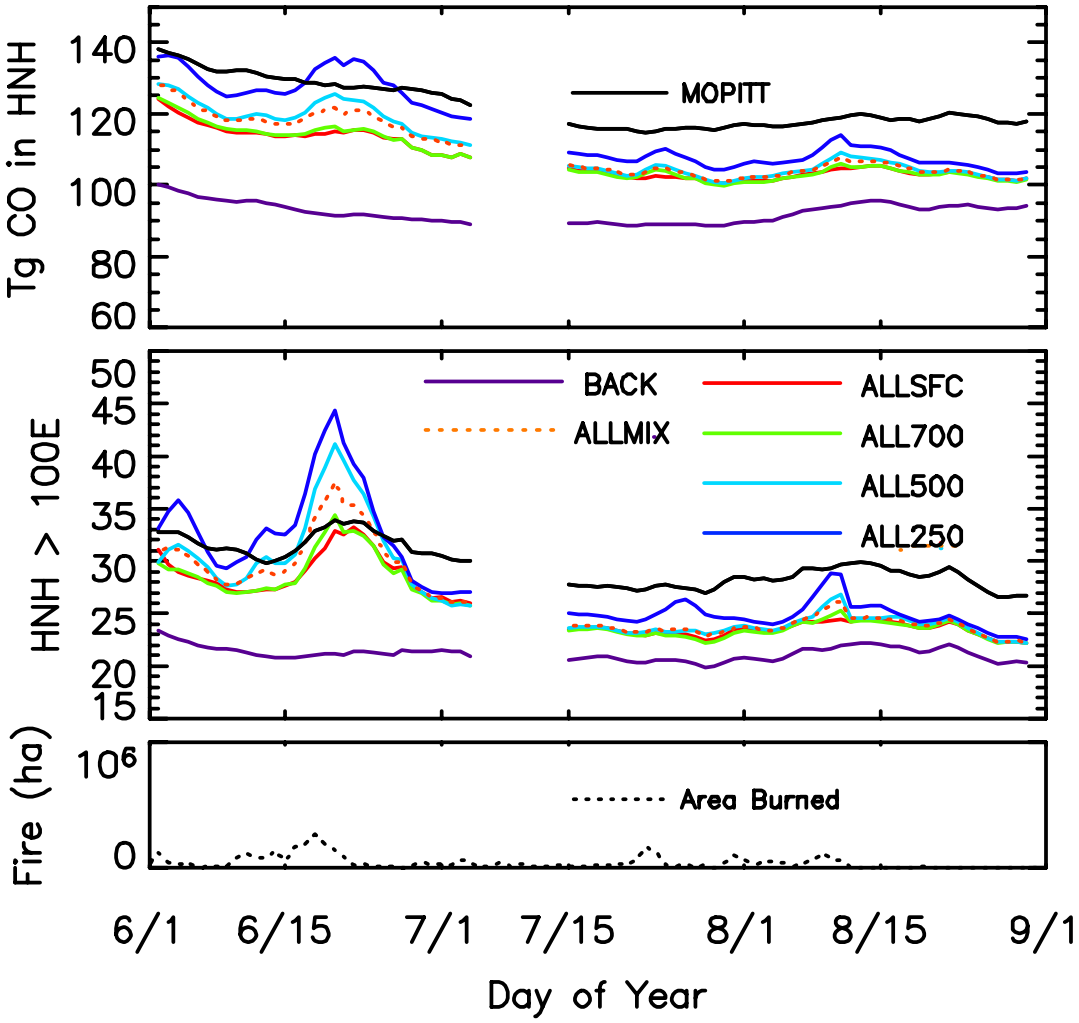

Figure 3-7. Time series of CO burden in the HNH calculated from simulated MOPITT data, as well as from real MOPITT observations (black).

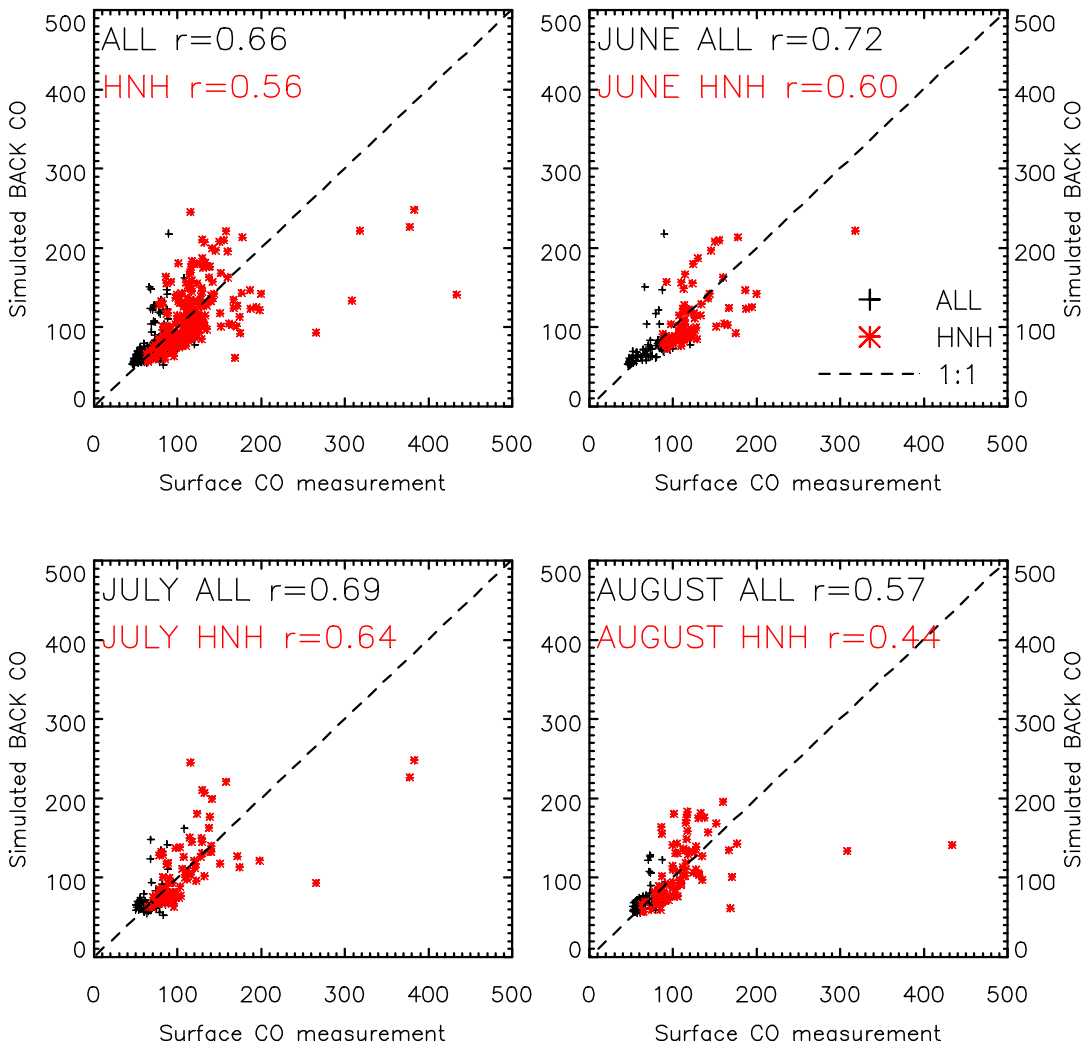

Figure 3-8. Monthly and overall comparison of model outputs from simulation of non-boreal sources (BACK) to surface CO observations from the CMDL network. Measurements from stations north of 30°N are shown as red asterisks, the remaining measurements are shown as black "+" signs. Correlations shown are for the entire global data set (N=504) and the HNH only (N=283). Months in the study period had a nearly equal number of measurements.

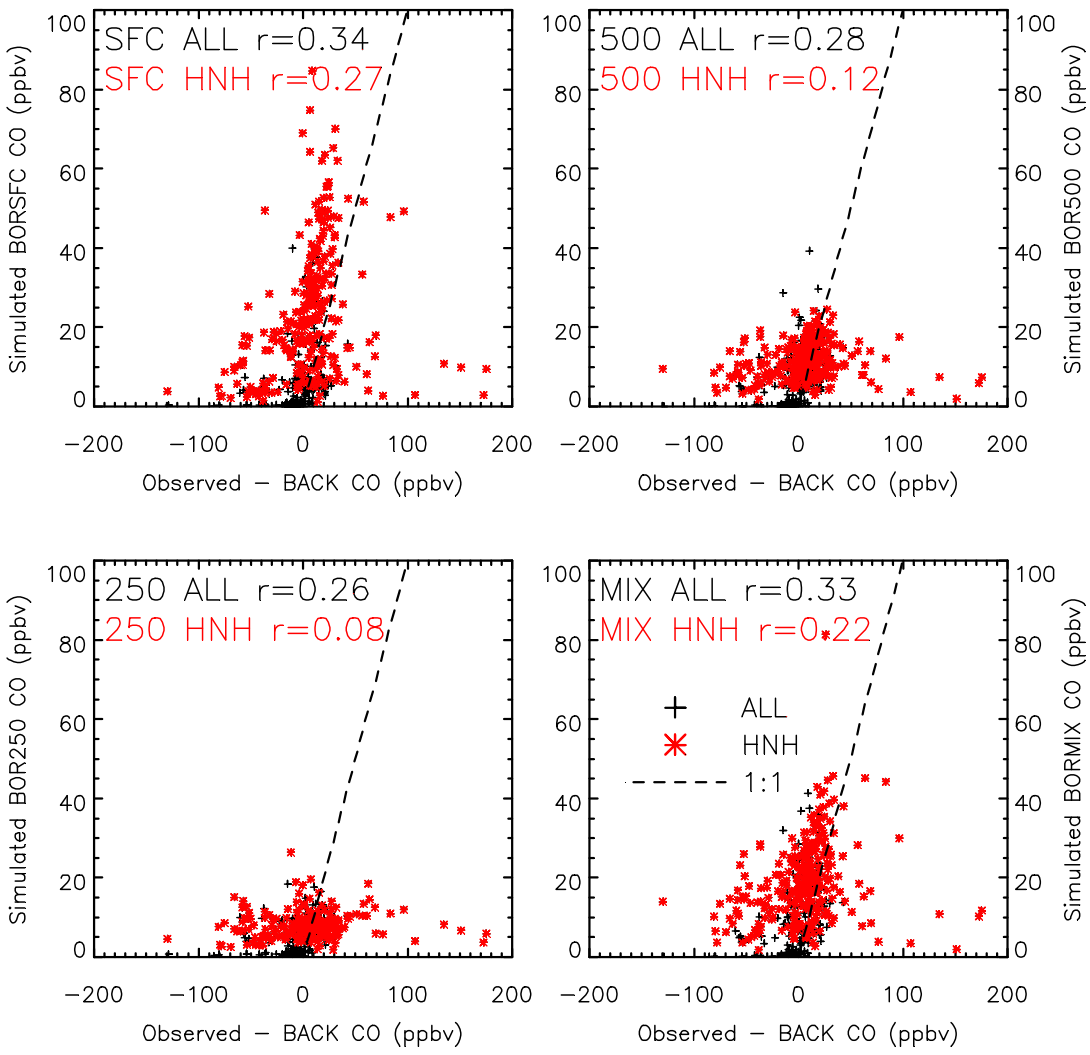

Figure 3-9. Comparison of model simulations of CO from boreal fires to residuals obtained by subtracting the BACKGROUND simulation from the surface CO measurements. Shown here are comparisons for the BORSFC, BOR500, BOR250, and BORMIX simulations. The BOR700 simulation (not shown) produced results similar to the BORSFC simulation.

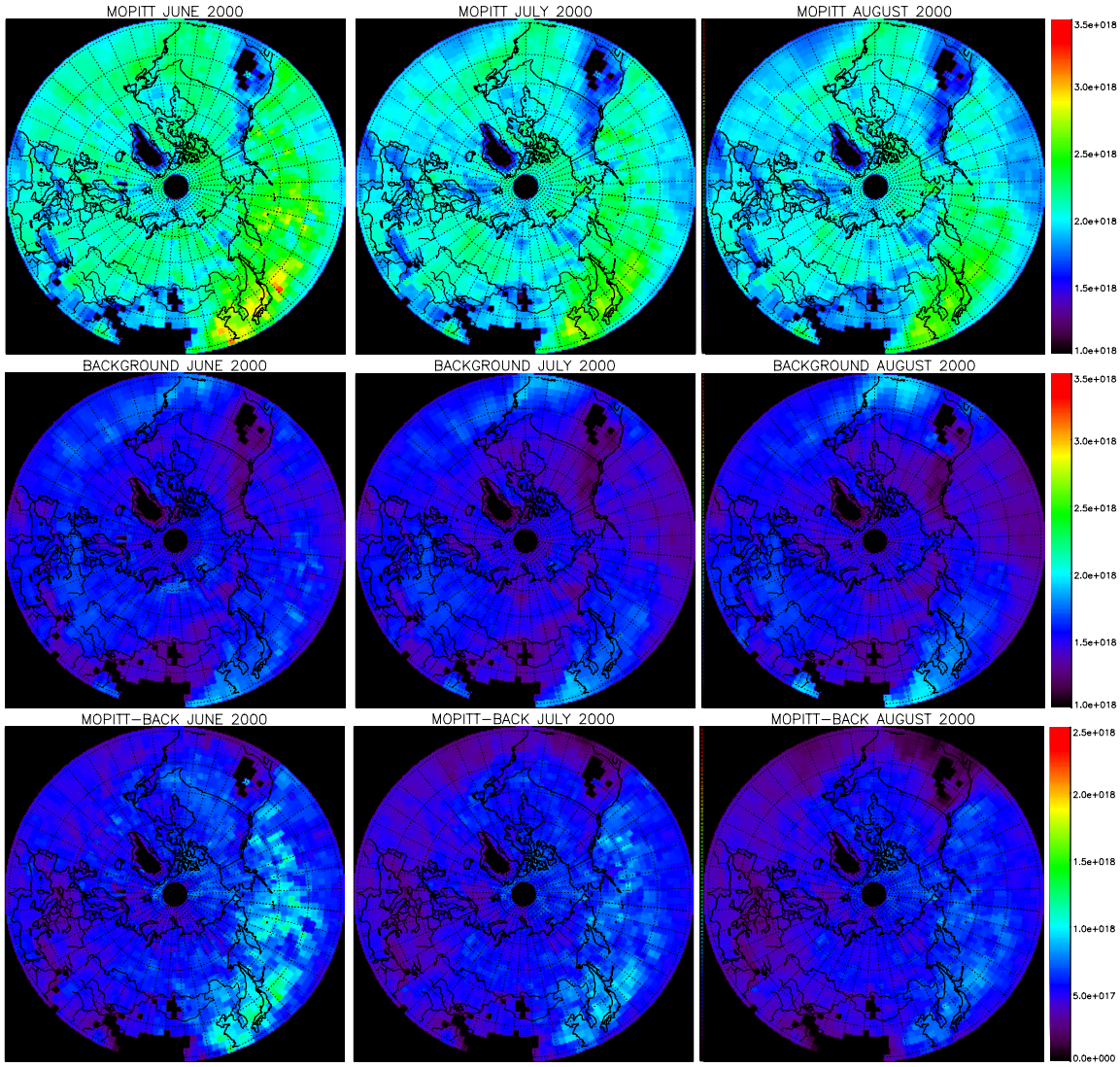

Figure 3-10. ROW 1: Monthly mean total column CO from MOPITT, resampled to a 2.5° by 2° grid. ROW 2: Monthly mean total column CO from the BACKGROUND simulation. Model outputs were processed to simulate the sampling properties of MOPITT, then resampled for display. ROW 3: Residuals obtained by subtracting BACKGROUND simulated TC CO from MOPITT TC CO. Note that the scale is different for Row 3.

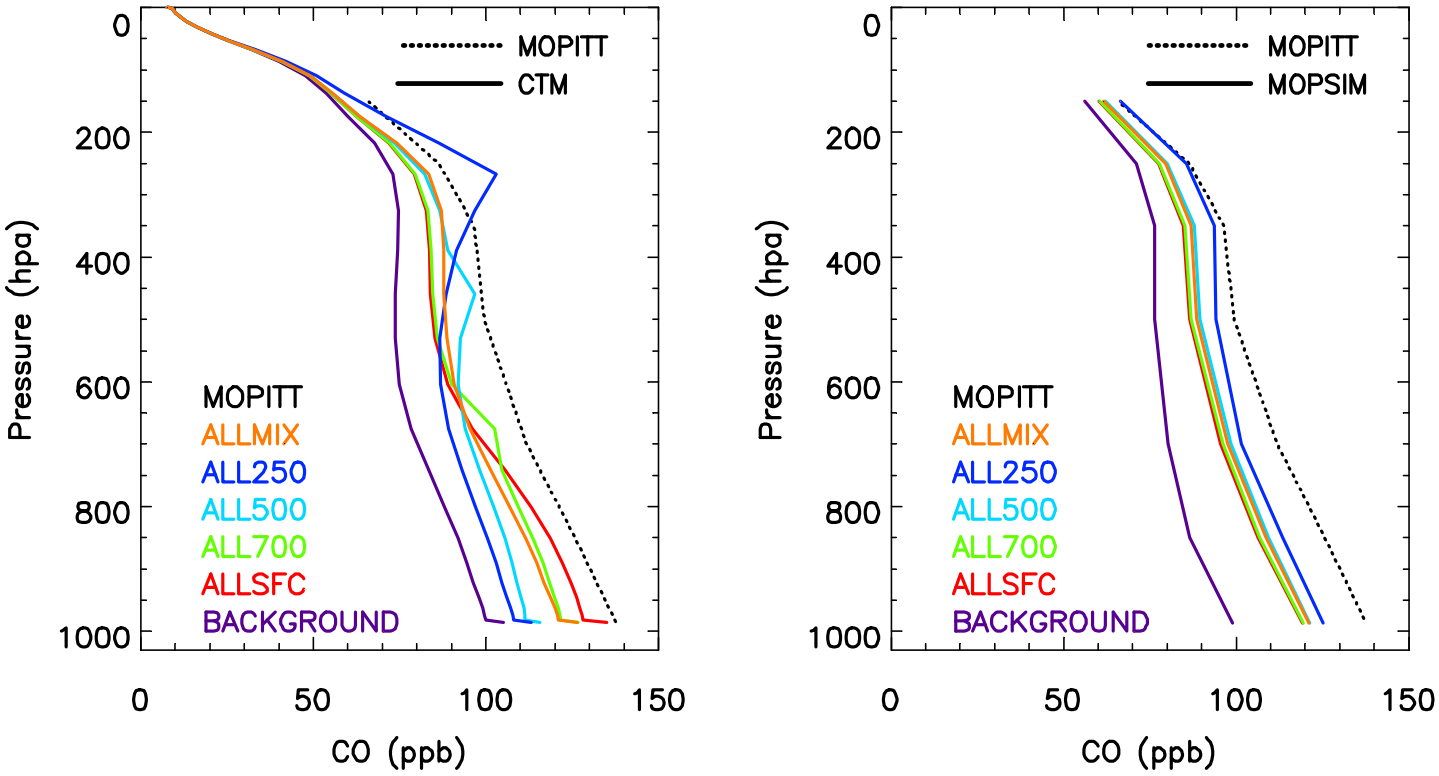

Figure 3-11. Mean vertical profiles from MOPITT (dotted line) and for each of the simulations in this experiment. For model outputs, profiles are shown from both the raw 35-layer output of the CTM (solid lines), as well as from the simulated MOPITT values (dashed lines).

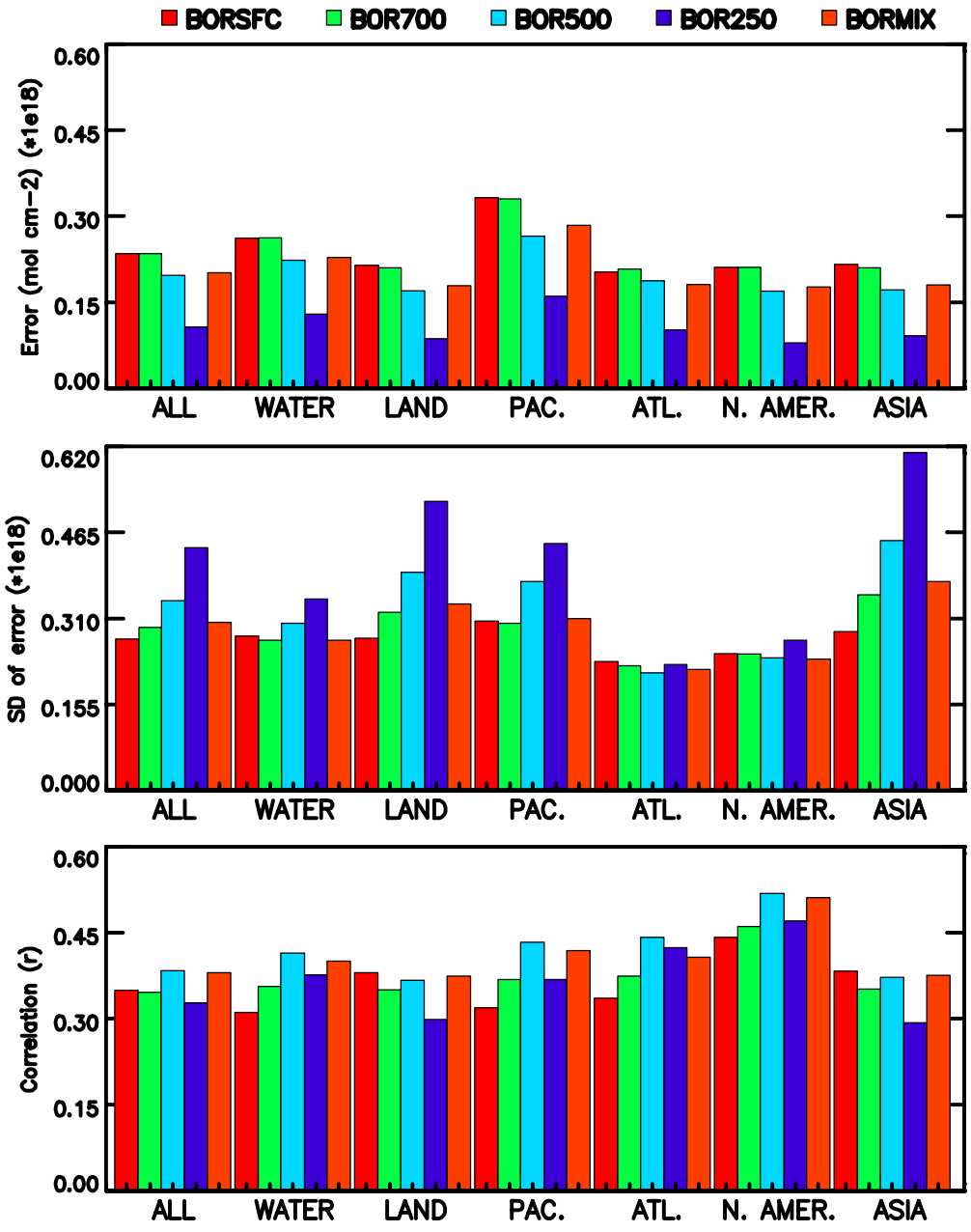

Figure 3-12. Error statistics from comparison of the simulated boreal source CO to the MOPITT TC CO measurements with the simulated BACKGROUND sources removed. A) Absolute error in TC CO, positive values indicate CO is underestimated by the model. B) Scatter of errors, calculated as the standard deviation of model errors. C) Correlation of model values to MOPITT residuals.

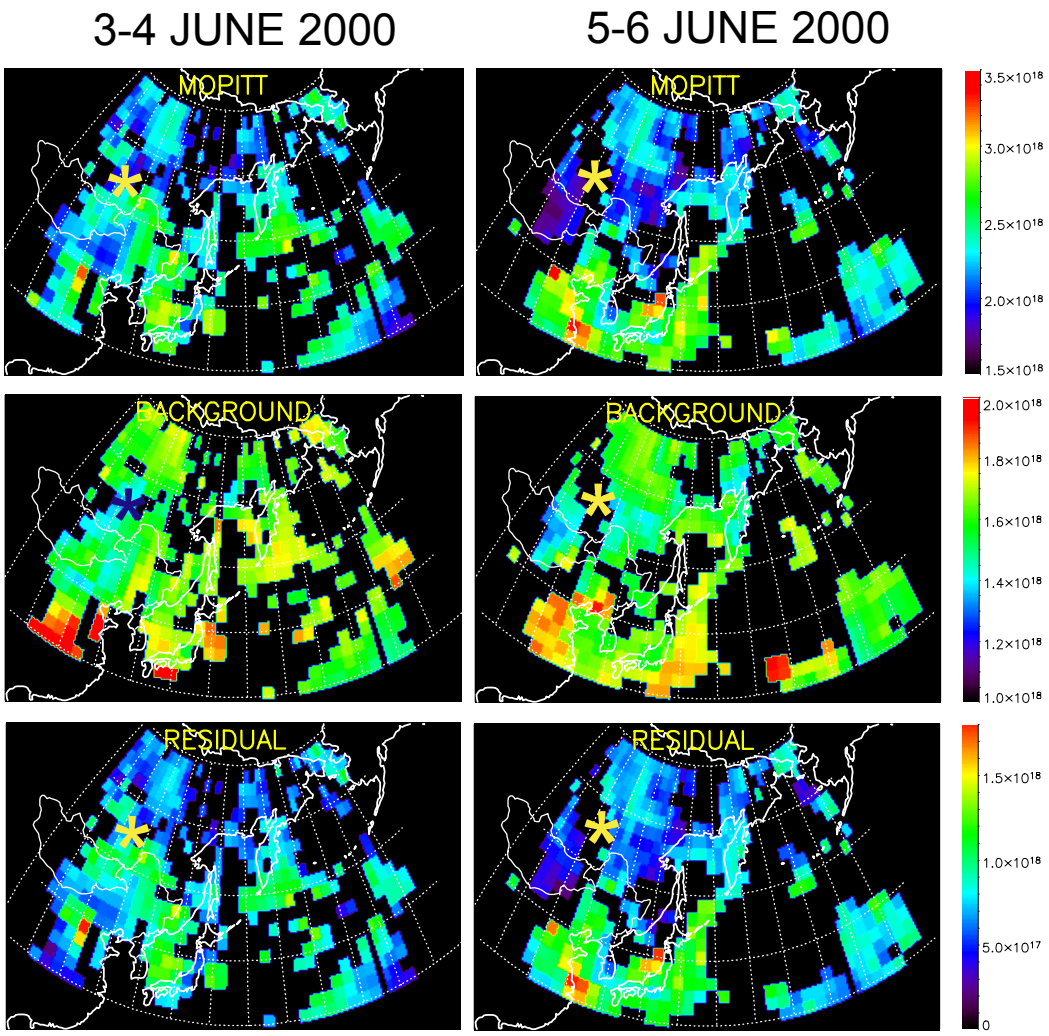

Figure 3-13. Maps of eastern Asia and the Pacific during a large fire event near the Russian border with Mongolia and China, 3-6 June 2000. Shown here are TC CO values gridded to a 2.5° by 2° grid. Data shown are a) TC CO from MOPITT data, b) TC CO from BACKGROUND simulation, and c) residual obtained by subtracting BACKGROUND simulation from MOPITT data. Approximate center of fire activity is marked with "*". Note that scales are different for each data set.

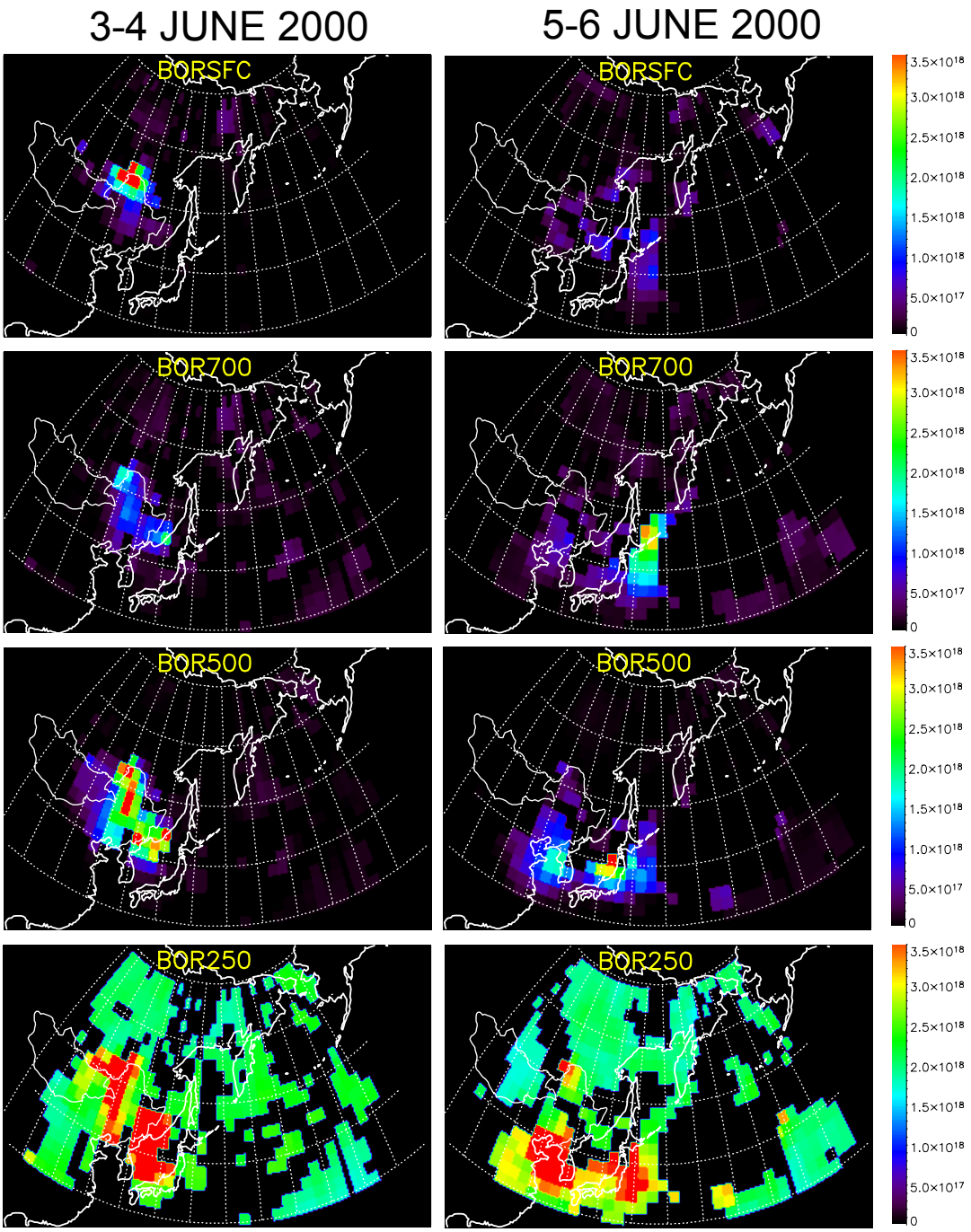

Figure 3-14. Modeled TC CO enhancement from boreal forest fires using single-layer injection. Cases shown are (top-bottom) BORSFC, BOR700, BOR500, and BOR250.

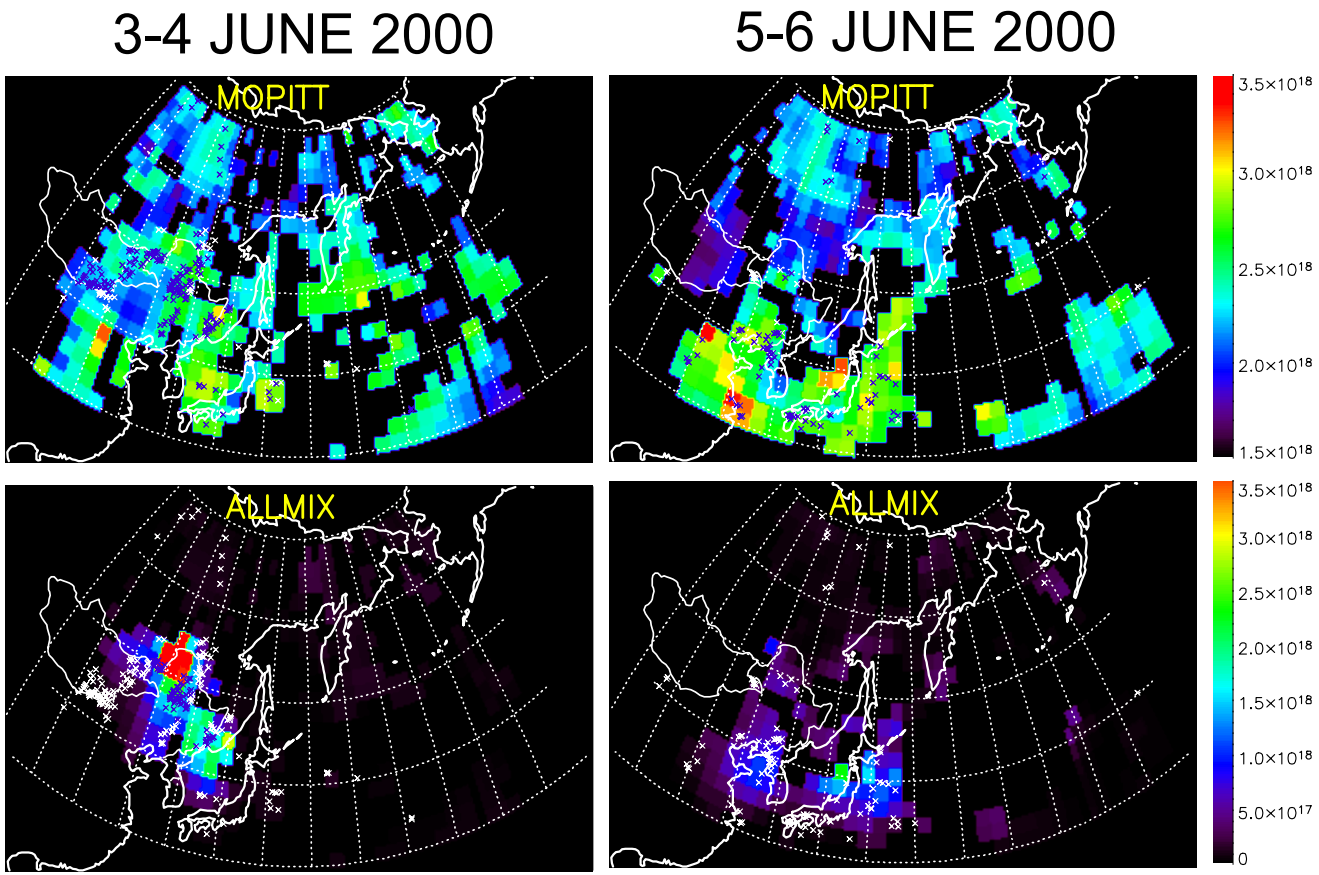

Figure 3-15. Locations of "Top-Heavy" retrievals, marked with "x". "Top-heavy" retrievals are retrievals that have TC CO more than 20% above the mean, and higher CO at 350mb than 850mb by at least 10 ppbv. These points are shown overlain on TC CO from a) MOPITT, and b) ALLMIX simulation.

Chapter 4. Evaluation of high-resolution temporal information in a boreal forest fire emissions model

1. Abstract

High-resolution inputs to a model of emissions from boreal forest fires were evaluated using a chemistry and transport model. Emissions of CO from boreal forest fires were estimated using daily resolution, and then aggregated to 7-day and 30-day composites. Comparison of daily and composite data indicate that much of the variability at the scale of the atmospheric model inputs (2° latitude by 2.5° longitude by 1 day) is lost when daily data are aggregated. Lag-correlation analysis showed no significant periodicity in the data sources, indicating that the temporal data were not subject to systematic reduction of the sampling rate, which had been identified in another study using fire detection data from AVHRR [*Heald et al.*, 2003]. Transformation of model outputs to simulate the sampling properties of surface CO flask measurements from the CMDL data set as well as continuous measurements of CO from Mace Head, Ireland, showed very little sensitivity to differences between daily and 7-day composite data. Analysis of model output transformed to match the sampling characteristics of MOPITT data showed that the discrepancy between daily and 7-day composite simulations dwindles rapidly with distance from the source. MOPITT retrievals were filtered to select "high-contrast" retrievals, where the difference between daily and 7-day simulations was more than twice the MOPITT measurement error, which yielded 35,000 retrievals during the study period, approximately 1% of the total retrievals in the HNH. Model output was compared with atmospheric measurements to assess the quality of the high-resolution temporal information. Temporal resolution did not significantly affect agreement between

model outputs and surface CO measurements from the CMDL data set. Agreement between the model and CO data from Mace Head was identical for daily and 7-day simulations, and worse for the 30-day composite simulation. Agreement between the MOPITT data and the model output from the daily simulation was highly variable and subject to large errors near the source, which likely relate to the mismatch in spatial resolution between the model and observations. Analysis of "high-contrast" retrievals gave consistently better results for the 7-day simulation relative to the 30-day simulation.

2. Introduction

Boreal forest fires are a large and concentrated source of trace gases to the atmosphere. These fires can account for as much as 20% of the global source of CO from biomass burning during large fire years [*Kasischke and Bruhwiler*, 2002], and have even greater impacts at higher latitudes and during the summer months [*Kasischke et al.*, 2005; *Novelli et al.*, 2003; *Yurganov et al.*, 2004b]. Fire activity is not distributed evenly through the boreal forest: even in the largest fire years, fire affects less than 2% of the forested area in the boreal zone. The bulk of emissions during any given year comes largely from a small fraction of the largest fires [*Stocks et al.*, 2002]. The temporal distribution of fire activity is likewise uneven: the boreal fire season extends from late April into September, but the majority of the area burned in most large fire events results from just a few days of intense activity [*Flannigan and Harrington*, 1988]. This spatial and temporal concentration of the source means that modeled atmospheric effects of these emissions will be strongly dependent on the spatial and temporal resolution of the input data.

Most temporally resolved global data sets for trace gas emissions give monthly averages of emissions. In many cases, such as with fossil fuel consumption, this is unavoidable due to data limitations. For biomass burning, however, the satellite data products used to monitor fire activity have much higher repeat rates, and the potential in many cases to generate daily data [*Justice et al.*, 2002; *Kaufman et al.*, 1998; *Reid et al.*, 2004]. Application of daily data sources may improve model representation of biomass burning emissions for studies of transport and chemistry. In order for this improvement to be realized, three conditions must be satisfied:

1. The high-resolution data must contain information not included in aggregate data;

2. The atmospheric simulation must be sensitive to the high-resolution variability in the source;

3. The high-resolution information must be accurate.

The purpose of this study is to evaluate a high-resolution emissions inventory for boreal forest fires. This inventory, hereafter referred to as BWEM-1, integrates satellite and ground-based information on fire size, location and timing with spatially resolved estimates of fuel loading to generate emissions estimates at a range of spatial and temporal scales [*Kasischke et al.,* 2005]. The information content of this high-resolution source will be evaluated using the gridded emissions estimates. The sensitivity of the atmospheric measurements to high-frequency variation in the source will be evaluated with simulations using a chemistry and transport model. The agreement between the high-resolution source data and observations will be evaluated by comparing simulated CO to surface measurements as well as data from the MOPITT instrument.

The remainder of this section describes selected pertinent results from the literature. The Methods section provides a detailed description of the temporal information used in the boreal emissions model, and outlines the data sources and models used in this study. Results and discussion are included in a separate section, and the last section offers a summary and some conclusions based on this research.

2.1. Recent research on high-resolution modeling of emissions

The use of daily data for monitoring of biomass burning has been a focus of the remote sensing research community for many years (e.g. *Malingreau et al.* [1996]). *Li et al.* [1997] evaluated daily satellite observations of hot spot activity for estimating area burned in the boreal forest. They found that when cloud cover is low, the daily data are in good agreement with ground-based observations of area burned. Daily fire products based on the approach of *Li et al.* are used for fire monitoring and management in Canada, and products based on MODIS data have begun to be applied worldwide [*Justice et al.*, 2002].

Very few global studies of trace gas emissions have attempted to use source data with daily resolution. *Heald et al.* [2003] used data from the World Fire Web (WFW) [*Stroppiana et al.*, 2000] to estimate daily fluctuations in biomass burning in southeast Asia. These fluctuations were applied to monthly emissions data from *Duncan et al.* [2003] to generate a daily estimate of trace gas emissions. *Heald et al.* found that the WFW product, which is derived from active fire (hot spot) detections made by the AVHRR instrument, had a strong dependence on scan angle, with detection efficiency decreasing dramatically away from nadir. Because of this scan angle dependence, they found that the data from WFW had an effective sampling rate of about every eight days

over tropical and subtropical Asia. To compensate for this incomplete sampling, *Heald et al.* used a persistence function to generate a continuous temporal data set. Comparison of model simulations to atmospheric trace gas observations from the TRACE-P experiment showed very small differences from applying the daily fluctuations, and no significant improvement in agreement with observations.

The temporal information used for the boreal emissions source examined in this study is largely derived from the same AVHRR instruments used for the WFW product. However, algorithms based on detection of hot pixels from polar orbiting satellites will have more efficient detection in the boreal zone than in the tropics. First, instruments on polar orbiting satellites have more dense coverage at higher latitudes. This increases the sampling rate, and decreases the maximum scan angle required for daily coverage. Second, the lower background temperatures in the boreal forest increase the contrast available for detection of fires (assuming an appropriate contextual algorithm is used). The next section describes in detail the temporal information used for the boreal fire emissions inventory BWEM-1.

3. Methods

3.1. Study period and region

Emissions from boreal forest fires during the 2000 fire season were modeled and used as input to a CTM. Area burned in the 2000 fire season (10.28 million hectares) was slightly lower than the annual average for 1996-2003 in the boreal forest [*Kasischke et al.*, 2005]. The 2000 season was chosen because of the availability of data from the MOPITT instrument, which is a unique data source for studying atmospheric effects of fires. The MOPITT retrieval was modified for data collected after May 2001, and data

from before and after this period are referred to as "Phase 1" and "Phase 2" MOPITT data, respectively. Validation of "Phase 2" MOPITT data [*Emmons et al.*, 2004] shows that the precision and accuracy of these data are comparable to "Phase 1" data. The MOPITT data analysis methods described in this study could therefore be used to study later years.

Atmospheric observations of CO concentrations during June-August 2000 were processed for comparison with model output. This study was restricted to observations from the Northern Hemisphere north of 30° N (HNH), which is the region most sensitive to boreal forest emissions. More than 60% of boreal fire activity during 2000 occurred before 1 June, but early season observations were not used because of interference from other Asian biomass burning sources geographically close to the boreal source.

3.2. Temporal information in BWEM-1

The BWEM-1 emissions model uses a flexible-resolution GIS framework to incorporate information on fire activity and fuels at a range of scales, and produce emissions estimates at a range of resolutions [*Kasischke et al.*, 2005]. The model includes a description of seasonal variability of fire behavior that connects the total emissions from a given burned area to the temporal profile of fire activity. Information on timing of fires used in this study comes from different sources, depending on the region. In many cases, these data also contribute to determining fire size and location. Data sources used for each region are described in detail in this section.

3.2.1. Russia

Burned area maps for Russia are generated at the Sukachev Institute of Forestry in Krasnoyarsk using AVHRR active fire detection as well as post-fire scar mapping

[*Sukhinin et al.*, 2004]. The data included in the 2000 data product used for this study were taken from daytime overpasses by the NOAA-12, NOAA-14, and NOAA-15 satellites. The active fire component of this dataset was then analyzed to construct temporal profiles of activity for each spatially contiguous burned area.

3.2.2. Canada

Area burned in Canada is taken from data reported at the provincial level and collected by the Canadian Forest Service (CFS, available online at http://www.nrcan-rncan.gc.ca/cfs-scf/science/prodserv/firereport). The BWEM-1 was built to incorporate the fire size and location data from the Canadian Large Fire Database (LFDB) [*Stocks et al.*, 2002]. These data are only available through 1999. Comparison over 1995-1999 shows good agreement between the reported provincial totals and the LFDB. For 2000 and later years, the total area burned for each province reported by the provincial fire management agencies was spatially distributed using the total annual density of hot spot detections from the Canadian Forest Service's FireM3 project (available online at http://cwfis.cfs.nrcan.gc.ca/en/current/cc_m3_e.php). FireM3 data for 2000 were derived from daytime overpasses by NOAA-14, using a "best-pixel" approach to reduce cloud contamination and avoid large scan angles [*Li et al.*, 1997]. The hot spot detections are clumped spatially into "fire areas", and temporal profiles are calculated for each "fire area" using the timing information in the FireM3 hot spot data. No operational data gaps appear in the 2000 data set, though hot spot detections from FireM3 are limited by cloud cover.

3.2.3. Alaska

Fire boundary polygons for large fires in Alaska are compiled annually by the Alaska Fire Service (available online from http://agdc.usgs.gov/data/blm/fire/index.html). The daily reports of fire activity from the National Interagency Coordination Center (available online at http://www.cidi.org/wildfire) are then used to construct a temporal profile of fire activity for the state. In the future, the BWEM-1 will construct individual profiles for each large fire, as is done in Canada and Russia, but this has not yet been implemented. The daily reports include both daily and year-to-date (YTD) area burned figures. For consistency, the year-to-date numbers are used. Negative changes in YTD area, which can be caused by detailed re-mapping of roughly sketched fire boundaries, are ignored. These reports are part of the operational work of the Alaska Fire Service, but boundaries of fires are not always updated daily, especially in limited protection areas.

3.3. CO emissions from boreal forest fires

CO emissions from boreal forest fires were modeled using the method described in detail in Chapter 3. For this study, a daily estimate of CO emissions from boreal forest fires was prepared. This estimate was aggregated to 7-day and 30-day resolution, and these three sources were used as input to the CTM. CTM outputs were transformed to simulate the sampling properties of the CO observations used in this study, as described below.

3.4. Transport model

Transport and chemistry of CO emissions were simulated using the University of Maryland CTM [*Allen et al.*, 1996]. This model has a spatial resolution of 2.5° longitude by 2° latitude, with 35 vertical layers, and produces output at 6-hour intervals. CO

sources other than boreal fires are as described in Chapter 3, and additional details of the transport model can be found in that chapter, as well as in *Park et al.* [2004]. The vertical injection of the boreal forest fire CO was parameterized by distributing the emissions through the low and mid-troposphere at the source. No injection in the boundary layer was included in this simulation, but previous results (Chapter 3) showed that CO in the lower troposphere is readily mixed down to the surface by the CTM.

3.5. CO observations

Atmospheric observations of CO concentration are obtained by several different methods, depending on the application of the measurements. In this study, three different types of measurement are examined, covering the types of measurements most commonly used for studies of the global atmosphere, as well as studies of long-range pollution transport. Each method has different sampling properties as well as different accuracy and precision, which are discussed in detail in this section.

3.5.1. Surface CO measurements

Surface measurements of CO concentration were obtained from the NOAA CMDL Cooperative Air Sampling Network (http://www.cmdl.noaa.gov/ccgg/flask.html). For this study, flask measurements collected from all fixed stations during the study period were used. These flask samples are intended to represent regional background conditions, and so are generally collected in remote areas and areas dominated by clean marine air masses. A quality control process is used to flag measurements that are not representative of background conditions [*Novelli and Steele*, 1992]. This process is primarily intended to eliminate influence of local sources in the data, but it also generally

removes measurements influenced by pollution plumes from regional sources. Flagged measurements were not included in this study.

The accuracy and precision of the flask data are very high. Analyzers used to take these measurements are calibrated using a series of standards traceable to a NIST Standard Reference Material. Absolute accuracy was estimated by analytical propagation of errors to be around 3.5 ppbv for the data used in this study [*Novelli et al.*, 2003]. The precision of the gas chromatography / mercuric oxide reduction method used for CO measurement was determined to be better than 2% [*Novelli et al.*, 1998].

A model output data set matched to the flask measurements was created by sampling the model output at the grid cell containing each measurement station, at the time step nearest to the collection date and time.

3.5.2. High-frequency *in situ* CO measurements

The environmental research station at Mace Head, county Galway, Ireland, provides high-frequency sampling of a range of atmospheric trace gases as part of the AGAGE network [*Prinn et al.*, 2000]. CO concentrations are measured every 40 minutes by a gas chromatograph analyzer (Trace Analytical, model RGA3) [*Derwent et al.*, 2001]. This analyzer uses the same method for CO detection as is used for the CMDL flask measurement data, and is regularly calibrated to standards from CSIRO [*Simmonds et al.*, 1996]. The absolute accuracy and precision of these data are comparable to the CMDL flask measurement data.

For comparison to these CO observations, model output was sampled in the grid cell containing the Mace Head research station, and interpolated to the temporal resolution of the measurement data. Since model output is only generated every six

hours, the CO measurements from this data set have greater temporal detail than the model output.

3.5.3. MOPITT CO data

The MOPITT instrument samples tropospheric CO globally with a 3-day repeat rate and a 22 km ground measurement footprint. For this study, total column CO (TC CO) retrievals from the MOPITT Level 2 data product were used. This analysis excludes retrievals with more than 40% *a priori* contribution at the 700 hPa nominal level, or estimated radiometric error greater than 25%. All cloud-free measurements from the HNH with a retrieval bottom pressure (surface pressure) greater than 850 hPa were analyzed, resulting in a total of about 40,000 retrievals per day during the study period.

Validation exercises comparing MOPITT data to profiles obtained from aircraft sampling give an estimate of the bias in the MOPITT TC CO retrievals of 0.7e17 +/- 1.9e17 molecules cm-2 (= 4.9% +/- 10.8%, 1 σ) [*Emmons et al.*, 2004]. Because there is no definitive way to measure the total column CO, this estimate gives only a general idea, as the aircraft measurements used to generate validation data have some error, and do not represent complete sampling of the atmospheric column.

For comparison with CTM output, each MOPITT retrieval was matched to its corresponding location on the output grid, and a vertical profile was extracted from CTM output by temporal interpolation between the two CTM output periods closest to the time of the retrieval. This profile was then interpolated to the nominal MOPITT pressure levels, and combined with the averaging kernel from the MOPITT retrieval according to the method described by *Deeter* [2000]. The result was a simulated MOPITT retrieval based on the CTM model output. Total column CO was calculated using the hydrostatic

relation, as described by *Emmons et al.* [2004]. The contribution of each source to the simulated MOPITT TC CO was obtained by subtracting the *a priori* component [*Arellano et al.*, 2004].

4. Results

4.1. Temporal Signal in modeled emissions

Table 4-1 shows the distributions of emissions from the gridded daily boreal fire CO emissions source as well as the 7-day and 30-day composite sources. The correlation between the sources is also shown in this table. From these data, it is clear that a large fraction of the variance in daily CO emissions is absent from 7-day and 30-day composite data.

To examine the temporal characteristics of the boreal fire data and look for evidence of periodicity, time-lag autocorrelations were calculated from the daily emissions data for Alaska, Canada and Russia (Figure 4-1). Autocorrelation for the entire data set is nearly identical to Russia, which had more than 80% of the CO emissions during the study period. All of the data show rapid decay of autocorrelation, indicating a very short characteristic period of just a few days. The Alaska data show some evidence of periodicity, which may be evidence of a systematic schedule of remapping active fire boundaries. Features at higher lags in the Alaska data are likely related to the time elapsed between major fires during the 2000 season. The Russian data also show qualitative evidence of periodicity, but this is not statistically significant, as the autocorrelation does not exceed 0.2 after five days.

The lag-correlation patterns seen in these data do not suggest sampling issues of the type encountered by *Heald et al.* [2003] in the WFW data. This does not mean that

these data have complete daily sampling, only that the data does not show systematic reduction of sampling rate, as this would result in evident periodicity in the data. The decay in the autocorrelation function is indicative of the real persistence of the fire process, but may also be affected by incomplete sampling due to cloud contamination.

Figure 4-2 shows the same lag-correlation calculation, repeated for source terms resampled to grids with resolutions of 4° latitude by 5° longitude and 8° latitude by 10° longitude. As the data are aggregated, the sample size decreases, and autocorrelation rises slightly, but the overall pattern, indicating rapid decay of autocorrelation with a short period, does not change. This suggests that the characteristic period of the fire activity, rather than the sampling inefficiency, is driving the decay of lag autocorrelation. A more stringent test of this would require data on cloud contamination, which are unavailable.

The comparison of source variance establishes that the daily gridded emissions product contains significantly greater variability than the aggregate products. The lag-correlation analysis establishes that the effective resolution of the daily data is actually daily, though the completeness of daily sampling has not been demonstrated conclusively. In the next section, simulated atmospheric measurements will be used to evaluate the magnitude of the signal from high-frequency variability in the source.

4.2. Signal of daily variability in atmospheric measurements

The atmospheric measurements used in this study have very different sampling properties, and are not expected to have the same response to the high-resolution information in the daily emissions source. To examine the sensitivity of these different measurements, the CTM output was transformed to match the sampling characteristics of

each data set. Results from the simulation using daily emissions were compared with results obtained using 7-day and 30-day composite emissions.

4.2.1. Flask sample measurements of surface CO

Boreal fire activity has been shown to explain much of the variability observed in surface measurements of CO [*Kasischke et al.*, 2005; *Novelli et al.*, 2003; *Wotawa et al.*, 2001]. These analyses were undertaken using monthly mean data from each measurement site or averaged over several sites, rather than the individual measurements, which are generally taken at 7-14 day intervals at a given location. These results therefore do not deal with the influence of high-frequency variability in the boreal fire source. Table 4-2 shows the simulated boreal contribution to surface CO concentrations for the daily and composite simulations, as well as the average difference between daily and composite simulations and the correlation between daily and composite simulations. The bias in the model output using the 30-day composite is less than 1 ppbv on average, with differences between the daily and 7-day (30-day) simulations exceeding 10% of observed CO in only 2(29) cases. The correlations among the model outputs reflect this, with essentially complete correlation between daily and 7-day composite simulations. These results suggest that no meaningful comparison of the daily and 7-day composite simulations will be possible using only comparisons between model output and flask sample measurements.

4.2.2. Temporal signal in long-range transport: Mace Head observations

The Mace Head atmospheric observatory has been shown to be sensitive to trace gases originating in the boreal zone [*Connellan et al.*, 2003; *Forster et al.*, 2001]. Model results from this study indicate a boreal contribution of around 25% of the observed CO

during the study period. This figure does not change when the "polluted" measurements are excluded from the sample, indicating that the boreal source is uncorrelated with the anthropogenic source in these measurements. The signal from variability in the source over short time scales is negligible, however, due to the distance between the source and measurement locations. Table 4-3 gives a statistical analysis of the boreal CO influence from the daily, 7-day and 30-day simulations. The daily and 7-day simulations are nearly identical, with the maximum deviation between them of only 5% of the observed CO value. As with the flask CO measurements, it appears that only the relative quality of the 30-day composite data can be assessed relative to daily and 7-day composite data using these observations.

4.2.3. Temporal signal in MOPITT data

The MOPITT data have a spatial coverage and data volume far greater than the other two measurement types described above, but with lesser accuracy and precision. Table 4-4 shows the simulated TC CO from the daily boreal source for the source geographic regions and the entire HNH, as well as a comparison of the results from the 7-day and 30-day composite simulations. The daily and 7-day simulations have very small differences in nearly all of the data, but the data volumes from MOPITT are sufficient to find a sample of retrievals where the differences are large enough to analyze.

Figure 4-3 represents graphically the procedure used to select a subset of data in which the differences between daily and composite simulations are large enough to analyze quantitatively. Figure 4-3a shows the distribution of differences in simulated MOPITT TC between daily and composite simulations, as well as the estimated error in the MOPITT TC retrievals. The vertical lines on the graph show the 90% cutoff for each

of these statistics. Figure 4-3b shows the distribution of differences in TC as a function of the retrieval error. The shaded part of Figure 4-3b shows high-contrast retrievals where the difference is more than twice the estimated error in the total column CO. For comparing the daily data to 7-day composites, this sample consists of fewer than 1% of the retrievals during the study period. However, even this small fraction of data is still enough to attempt a statistical comparison of the simulations.

The spatial distribution of the high-contrast retrievals (Figure 4-4) shows that these are generally concentrated near the source. The difference between daily emissions data and 7-day composite data declines rapidly outside of the immediate vicinity of the emissions source, but the inclusion of the retrieval error in the filter produces a more spread-out sample of high-contrast retrievals, because the retrieval error is generally higher over the source regions. Figure 4-5 shows the time series of emissions for daily and composite sources, together with the temporal distribution of high-contrast retrievals. The high-contrast subset follows the general pattern of fire emissions, but shows some effects of variable spatial sampling.

4.3. Accuracy of daily information

In the previous section, the model output was transformed to simulate the CO observations, and estimate the amount of variability in the observations simulated with emissions inventories of different resolution. This analysis showed that in the CMDL flask measurement data set and in the Mace Head CO data, resampled model output from the daily and 30-day composite simulations were highly correlated but different enough to allow potential use of these data to evaluate the quality of the high-resolution temporal

information. Differences between the daily and 7-day simulations were mostly within even the very small measurement error of the observations.

Analysis of the MOPITT data showed that while the overall differences between simulated CO values using daily and composite data sets were very small, the density of measurements permitted quantitative comparison of the simulations using a subset of the data where the differences are largest and most significant. This subset was found to be strongly concentrated near the emissions source.

To compare the model simulations of the boreal source to the observations, the influence of non-boreal sources on the CO observations must be accounted for. The results of CTM simulation of CO from non-boreal sources for MOPITT and CMDL flask measurements are described in detail in Chapter 3. This section will include details of the performance of the simulation of non-boreal sources compared with the observations from Mace Head, but will otherwise deal exclusively with the residuals obtained by subtracting the simulated CO from non-boreal sources from the CO observations. The quality of the agreement between model output and observations is thus dependent on the accuracy of the simulation of non-boreal sources, but this is unavoidable. The accuracy of the simulated non-boreal sources is sufficient to permit quantitative evaluation of different simulations of the boreal source.

4.3.1. CMDL flask measurements

Table 4-5 presents the mean and standard deviation of model errors, as well as the correlation between model and measurements. The daily and composite simulations are nearly identical, and differences in the agreement with the observations are negligible.

Differences between the simulations using daily and 30-day composite data do not affect model agreement with these observations.

This result demonstrates the effectiveness of the filtering algorithm applied to remove plume-influenced data from the CMDL data set. Boreal fires contribute a substantial fraction of the simulated CO in these measurements, and the observations are correlated to variability in the boreal CO source, but the lack of sensitivity to high-frequency variability of CO sources indicates that the measurements effectively sample only well-mixed air masses.

4.3.2. Mace Head CO measurements

Figure 4-6 presents a time series of Mace Head CO measurements. Observations marked in red are flagged as "polluted" by the quality control algorithm used for this data, which is based on simultaneous measurements of CFCs and therefore indicates influence of anthropogenic sources. The shaded portion of the graph indicates the simulated CO from non-boreal sources, and the lines on the graph indicate simulated CO from boreal fires using daily and composite data.

The variability in CO observed at Mace Head during the study period is almost entirely due to intrusion of polluted air masses. During much of the month of June, the model shows substantial contribution of CO from boreal forest fires, and the features of this CO enhancement are reflected in the observations. After June, the boreal fire CO enhancement is smaller, and generally highly correlated to the enhancement from industrial sources. As expected, the CO enhancement from the daily and 7-day simulations of boreal fire CO is identical, but the results from the 30-day simulation show some differences. The weighting of fires in the high-resolution source toward the

beginning of June can be seen in these data, as the daily and 7-day sources exceed the 30-day source early in the month, and are lower in late June and early July.

Table 4-6 gives the mean and standard deviation of model errors, as well as correlations for the Mace Head simulations. The non-boreal sources are compared directly with the observations, and the simulated boreal CO is compared with the residuals. Daily and 7-day simulations produce identical results. Both daily and 7-day simulations produce better correlations with observations and smaller scatter in model errors than simulations from 30-day composite data. Because of the strong autocorrelation in these measurements ($r > 0.2$ up to 4.5 days = 160 measurements), the statistical significance of the differences in model error is difficult to assess quantitatively.

Figure 4-7 shows (a) the CO observations compared with the simulated CO from non-boreal sources, and (b-d) the CO residuals compared with the simulated boreal fire CO. Variability in the "polluted" measurements is much greater than the "background" measurements, and much of this variability is not captured by the model. The difference between the 30-day composite simulation and the high-resolution simulations is also qualitatively evident in these plots. High concentrations (>30 ppbv) of boreal CO in the daily and 7-day simulations correspond qualitatively to enhanced residual CO, a relationship that does not hold for the 30-day simulation results.

4.3.3. MOPITT CO

Table 4-7 presents error statistics for the model simulation of non-boreal sources. The model underestimates MOPITT CO throughout the HNH, and the bias is larger in the

source regions. The regional differences in the model bias are due to the influence of regional CO sources both within and outside the boreal forest.

The results for the high-contrast retrievals show higher bias and scatter for model errors, consistent with a large contribution from boreal sources, except in Canada, where model bias and scatter are lower for the high-contrast subset than for the entire dataset, but model simulation of non-boreal sources still captures very little of the variability in the observations. This indicates either poor representation of Canadian fires in the model, or problems with representation of other CO sources by the model.

Total CO burden for the HNH was calculated by interpolation of the MOPITT TC CO and simulated TC CO from the model simulations. The results are shown in Figure 4-8. Fire activity in the boreal forest is also shown on this graph, and it is evident that the response of both the model and MOPITT to emissions from fire is slow and highly smoothed. The contrast between the simulation with daily data and the 30-day composite simulation is somewhat different from Figure 4-6, with the higher-resolution simulations showing enhanced CO starting in mid-June and the 30-day composite producing higher values during the rest of the month in June. This suggests that boreal fire CO is arriving at Mace Head relatively quickly, and therefore relatively more concentrated, compared with the rest of the HNH.

Time series for each source region (Figure 4-9) shed light on the results for non-boreal CO sources as well as the question of temporal resolution in the boreal source. Results over Russia show a much faster response to fire activity in the MOPITT data, compared with the simulation over the entire HNH. CO enhancement over Alaska from the boreal source is largely from Russian fires, and the effects of fires in Alaska are only

evident during one period in late June. CO enhancement over Canada shows no influence from regional fire activity. MOPITT data over Canada show several distinct features with no analogues in the CTM simulation, which is reflected in the poor agreement between the CTM simulation and MOPITT data in this region.

A statistical depiction of the relationship between MOPITT data and model outputs is shown in Figure 4-10. The simulated CO from non-boreal sources was subtracted from the MOPITT observations to yield a residual, which was then compared with simulated boreal CO from CTM outputs.

Results from Russia show the least influence of model transport error, since most of the boreal source is from Russian fires. The differences between results for Alaska and Russia are indicative of the effects of long-range transport on this CO simulation. The CO data over Russia agree best with the 7-day composite simulation, and worst with the 30-day simulation. The data over Alaska agree better with the 30-day composite simulation. Since much of the boreal fire CO over Alaska during the study period is actually in smoke transported from Russian fires, the two regional comparisons are actually sampling many of the same plumes, especially during June. With greater distance from the source, two changes in the boreal fire CO signal will occur. First, the high-frequency variability will be smoothed during transport. Second, the transport error will accumulate. The relatively poor performance of the daily and 7-day simulations over Alaska may be because they produce a more concentrated pattern of CO which produces larger errors if the modeled transport is inaccurate.

Figure 4-11 shows the results for the high-contrast subset of retrievals. The overall mean bias shows that this subset has higher CO influence from the high-

resolution simulations, but the boreal CO influence from all simulations is much higher in this subset compared to the entire data set. The error statistics for this subset also differ from the overall pattern in that the scatter of model errors and the correlation between the model and observations are not closely linked. The connection between scatter and correlations is strong when transport error is the dominant error term. In the case of this subset of the data, however, representation error is a larger component of the total model error. Representation error, in this case, results from the coarse resolution of the emissions source related to the process. Active fires and fresh smoke plumes will occupy only a small fraction of the 2.5° by 2° grid cell. All simulated values within the grid cell will have high CO, even if the area with active fire within the grid cell does not overlap with any MOPITT retrievals. This type of representation error drives the scatter in model errors for this subset. Because of this effect, the daily simulation shows the worst performance in this metric, despite having the highest correlation with the observations.

When the entire HNH is considered as a whole, temporal resolution of the source does not greatly affect model agreement with observations. In the high-contrast subset of the data, the 7-day composite simulation consistently produces better correlation with observations than the 30-day composite simulation. Results for the simulation with daily data are highly variable. Results for regional subsets vary due to a range of causes both inside and outside the model, of which the most important are model depiction of non-boreal sources and representation error near the fire CO source. But the results presented here indicate that the temporal information at the weekly level can improve agreement between transport model results and observations compared with monthly averaged source data.

5. Summary and Conclusions

To evaluate the quality of temporal information in a model of CO emissions from boreal forest fires, daily emissions data, as well as 7-day and 30-day composites, were used as input to a model of atmospheric transport and chemistry. The model output was transformed to simulate various sources of CO concentration data, and these simulations were compared to CO observations.

Transformation of gridded daily emissions to 7-day composite emissions reduced the variance in the emissions input by more than half. Some evidence of periodicity was found in the Alaskan emissions data, but otherwise autocorrelations were small and decayed rapidly, indicating that any incompleteness in sampling of fire activity was not systematic. This method did not determine the sampling efficiency of the data sources used, but ruled out systematic detection problems such as those described by *Heald et al.* [2003].

Model output was compared to three different atmospheric data sets: surface CO from flask measurements in the CMDL Cooperative Air Sampling Network, continuous *in situ* CO measurements from Mace Head, Ireland, and satellite retrievals of total column CO from MOPITT.

The flask measurements use a mathematical algorithm to filter measurements not representative of well-mixed tropospheric air. The flask measurements showed very little sensitivity to high-resolution variability in the boreal CO source, which demonstrates the effectiveness of the filtering algorithm. Agreement between the model and observations was not significantly different among simulations.

Time series data from the Mace Head observatory provide a clear indication of the smoothing effect of long-range transport on high-frequency variability of CO. The boreal source contributes 25% of the total simulated CO at this site, but the difference in simulated CO from daily and 7-day data is less than 5% of simulated CO in 99% of cases. Daily and 7-day simulations did produce markedly lower error than the 30-day simulation.

The simulated MOPITT data showed that differences related to source resolution dwindled rapidly away from the source. Overall, the effects of source resolution on model agreement with the MOPITT data were small. A subset of data where the simulated CO from daily and 7-day composite sources varied by more than twice the estimated error in the MOPITT total column CO included roughly 35,000 retrievals, slightly over 1% of the retrievals in the HNH during the study period. Comparison of model agreement using the high-contrast subset showed that the 7-day emissions data had consistently higher correlations than the 30-day data, but the differences were small even in the high-contrast subset. The model agreement with simulations using daily data was dominated by representation error near the emissions source.

The temporal information driving the BWEM-1 is accurate at scales down to 7 days, but model skill did not improve with daily data. The difference between daily and 7-day composite emissions diminished rapidly with distance from the source. Proper evaluation of the daily emissions data would require high-frequency measurements of CO at a location nearer the source.

The importance of resolving the temporal profile of fire events for transport investigations is intuitively obvious, but the results of this study indicate that lack of

temporal resolution is not a significant source of model error at all scales, and that other sources of error may obscure the high-frequency signal from sources with daily resolution. Thus, the results obtained from using daily sources depend strongly on the observations used, and the distance from the source region.

6. Tables

	GLOBAL GRID		ACTIVE CELLS			
	MEAN	**SD**	**N**	**MEAN**	**σ**	**r vs. Daily**
Daily	18.27	2205.22	4287	20439.28	70881.92	1.00
7-day	18.27	1448.03	12201	7181.64	27799.94	0.66
30-day	18.27	944.37	25770	3400.20	12429.19	0.43

Table 4-1. Statistics for daily and composite emissions product. The "global grid" statistics are for the entire 2° latitude by 2.5° longitude by 366-day input grid, while the "active cells" statistics are for only those cells with emissions activity. Correlations were calculated with all cells.

		Daily	7-day	30-day
All Data	**Mean (ppbv)**	14.5 +/- 30.5	15.0 +/- 31.4	14.3 +/- 31.4
N=506	**Difference from daily (ppbv)**	-	-0.5 +/- 6.2	0.2 +/- 14.9
	Correlation vs. daily (r)	-	0.98	0.88
HNH only (>30°N)	**Mean (ppbv)**	22.4 +/- 30.8	23.3 +/- 31.5	22.1 +/- 32.8
N=283	**Difference from daily (ppbv)**	-	-0.9 +/- 8.1	0.3 +/- 19.6
	Correlation vs. daily (r)	-	0.97	0.81
Rest of World (<30°N)	**Mean (ppbv)**	4.5 +/- 14.8	4.5 +/- 15.0	4.4 +/- 14.2
N=223	**Difference from daily (ppbv)**	-	-0.0 +/- 1.5	0.1 +/- 4.8
	Correlation vs. daily (r)	-	1.00	0.95

Table 4-2. Statistics of CTM simulation of boreal fire influence on surface CO measurements from the CMDL flask network for the entire globe, the high northern hemisphere only, and the rest of the world (lat < 30°N), for June-August 2000. Confidence limits are at 95%.

		Daily	7-day	30-day
All Data	**Mean (ppbv)**	23.0 +/- 19	23.8 +/- 20	20.6 +/- 16
N=2700	**Difference from daily (ppbv)**	-	-0.7 +/- 3	2.4 +/- 12
	Correlation vs. daily (r)	-	0.99	0.78
"Background"	**Mean (ppbv)**	23.4 +/- 20	24.1 +/- 21	20.4 +/- 16
Data Only	**Difference from daily (ppbv)**	-	-0.7 +/- 3	3.0 +/- 12
N=2192	**Correlation vs. daily (r)**	-	0.99	0.80

Table 4-3. Statistics from CTM simulation of boreal fire influence on CO observations at Mace Head. All error estimates are 95% confidence.

			Sim. w/ daily data[a]		7d vs 1d sim[b]		30d vs 1d sim[b]	
	N(MOPITT)	**N(grid)**	**Mean**	**s.d.**	**Mean**	**s.d.**	**Mean**	**s.d.**
HNH	3,251,253	79,123	2.33E+17	2.59E+17	0.8%	48.1%	0.8%	78.1%
RUSSIA	284,318	9,596	3.76E+17	5.04E+17	-0.2%	73.7%	-0.1%	106.6%
CANADA	296,097	9,612	3.27E+17	1.35E+17	1.3%	9.6%	3.6%	18.9%
ALASKA	269,944	10,583	3.84E+17	2.43E+17	2.6%	22.4%	9.5%	40.1%

[a]Units of molecules cm^{-2}

[b]Percentage of simulated TC CO from daily source.

Table 4-4. Statistics for CTM simulation of boreal fire influence on MOPITT TC CO. Mean and standard deviation of differences between simulations are reported as percentages of the mean TC CO from the daily simulation. The N(MOPITT) reported here is the number of MOPITT retrievals in the sample, the N(grid) is the number of different locations in the CTM output grid (1-day resolution) to which those retrievals correspond. Complete sampling of the HNH during the study period would yield N=544,608.

		Non-boreal sources[a]	Simulated Boreal Forest Fire CO[b]		
			daily	7-day	30-day
All Data	**Bias (ppbv)**	-0.5 +/- 32.5	+14.0 +/- 31.6	+14.5 +/- 31.4	+13.8 +/- 31.3
N=506	**R**	0.66	0.30	0.31	0.32
HNH only	**Bias (ppbv)**	-6.5 +/- 39.0	+15.9 +/- 38.9	+16.8 +/- 38.6	+15.6 +/- 38.6
N=283	**R**	0.56	0.21	0.23	0.23
Rest of World	**Bias (ppbv)**	+7.0 +/- 19.4	+11.5 +/- 18.3	+11.6 +/- 18.3	+11.4 +/- 18.0
(below 30°N)	**R**	0.48	0.34	0.34	0.38
N=223					

[a]Compared with CO measurements

[b]Compared with residuals obtained by subtracting non-boreal sources from CO measurements

Table 4-5. Model error and fit statistics for CTM simulation of surface CO measurements from the CMDL flask sampling network. Positive values indicate overestimation of CO by the simulation. Confidence limits for bias are 95%. All correlations are significant ($p < 0.001$).

		Non-boreal sources[a]	Simulated Boreal Forest Fire CO[b]		
			Daily	7-day	30-day
All Data	**Bias (ppbv)**	+2.0 +/- 15.8	+25.0 +/- 15.9	+25.7 +/- 15.9	+22.6 +/- 16.7
N=2700	**R**	0.77	0.30	0.31	0.14
"Background"	**Bias (ppbv)**	+1.7 +/- 14.5	+25.1 +/- 14.6	+25.8 +/- 14.6	+22.1 +/- 15.5
Data only	**R**	0.63	0.35	0.36	0.18
N=2192					

[a]Compared with CO measurements.

[b]Compared with residuals obtained by subtracting non-boreal sources from CO measurements.

Table 4-6. Model bias and fit statistics for CTM simulation of Mace Head continuous CO measurements.

		HNH	RUSSIA	CANADA	ALASKA
ALL	**mean error (molecules cm^{-2})**	-5.21E+17	-5.73E+17	-5.73E+17	-6.09E+17
	σ of error	2.48E+17	2.31E+17	2.25E+17	2.19E+17
	R	0.59	0.60	0.65	0.61
CONTRAST	**mean error (molecules cm^{-2})**	-6.65E+17	-7.02E+17	-5.92E+17	-6.7E+17
	σ of error	3.52E+17	3.21E+17	2.13E+17	3.23E+17
	R	0.60	0.65	0.30	0.44

Table 4-7. Error statistics for comparison of MOPITT measurements to CTM simulation of non-boreal sources for source regions, as well as regional high-contrast subsets.

7. Figures

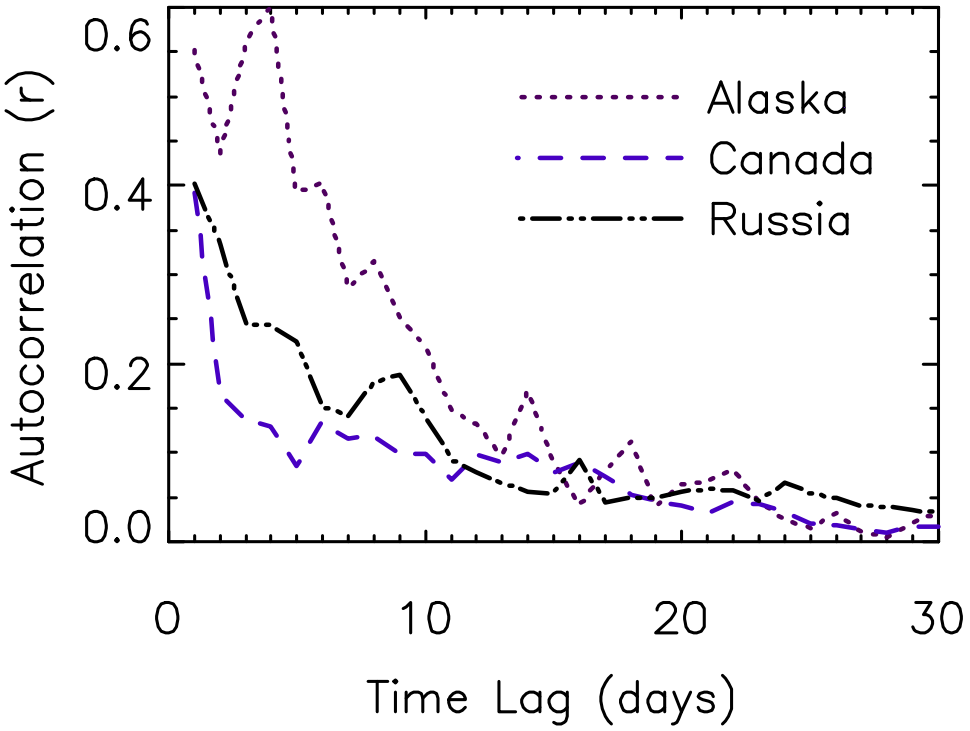

Figure 4-1. Lag-correlation function for gridded emissions. By definition, lag correlation is equal to 1 at lag = 0.

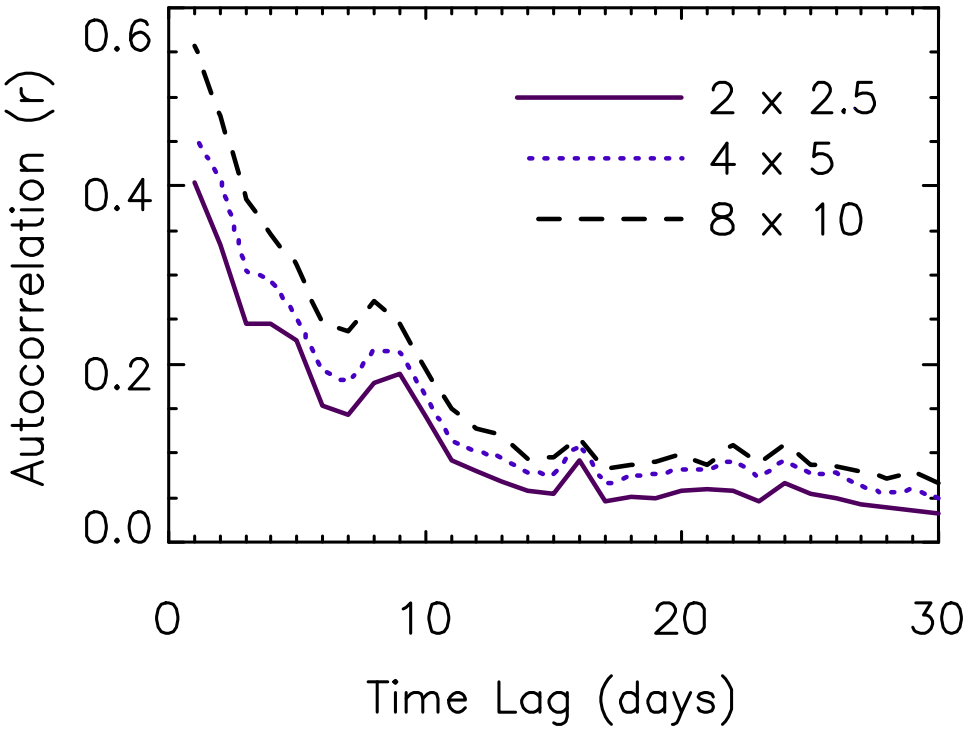

Figure 4-2. Lag-correlation function for gridded emissions, resampled to different grid-cell resolutions. Resolutions are expressed in degrees of latitude by degrees of longitude.

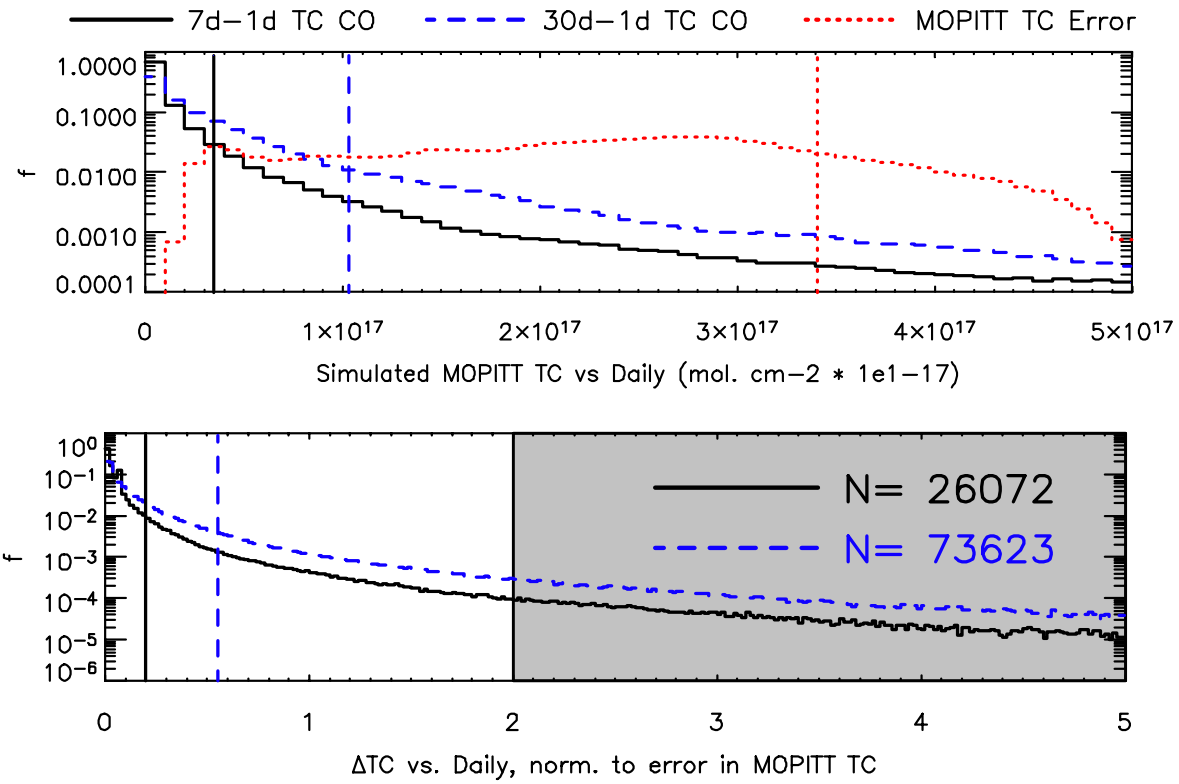

Figure 4-3. Cumulative distribution of difference in simulated TC CO using daily vs. composite inputs. A) Absolute difference in simulated MOPITT TC CO. For comparison, the cumulative distribution of errors in MOPITT TC CO is shown (dotted line) . B) Difference in simulated TC CO normalized to the error in each MOPITT TC retrieval. Vertical lines on both graphs show 90% limit of data in this study, i.e. 90% of data have values below the line. Labels in shaded area of (B) show number of retrievals where the difference in simulated TC CO is more than twice the error in the MOPITT TC.

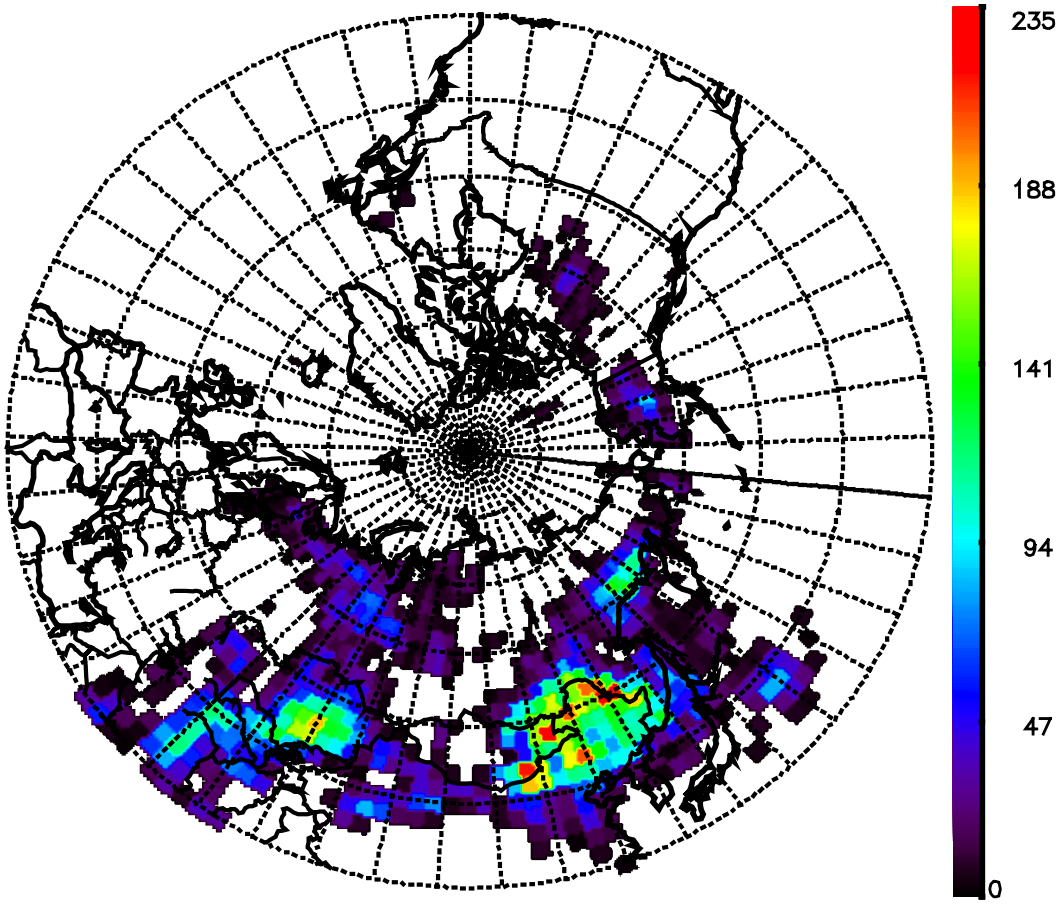

Figure 4-4. Spatial distribution of retrievals where CTM-simulated MOPITT TC CO using daily differs from simulated TC using 7-day composite emissions by more than twice the error in the MOPITT TC.

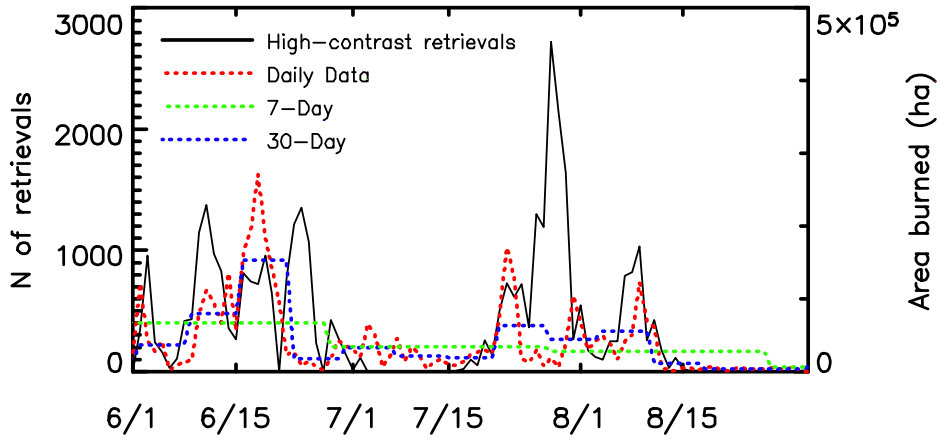

Figure 4-5. Timing of high-contrast retrievals, compared with timing of fire activity from daily and composite data.

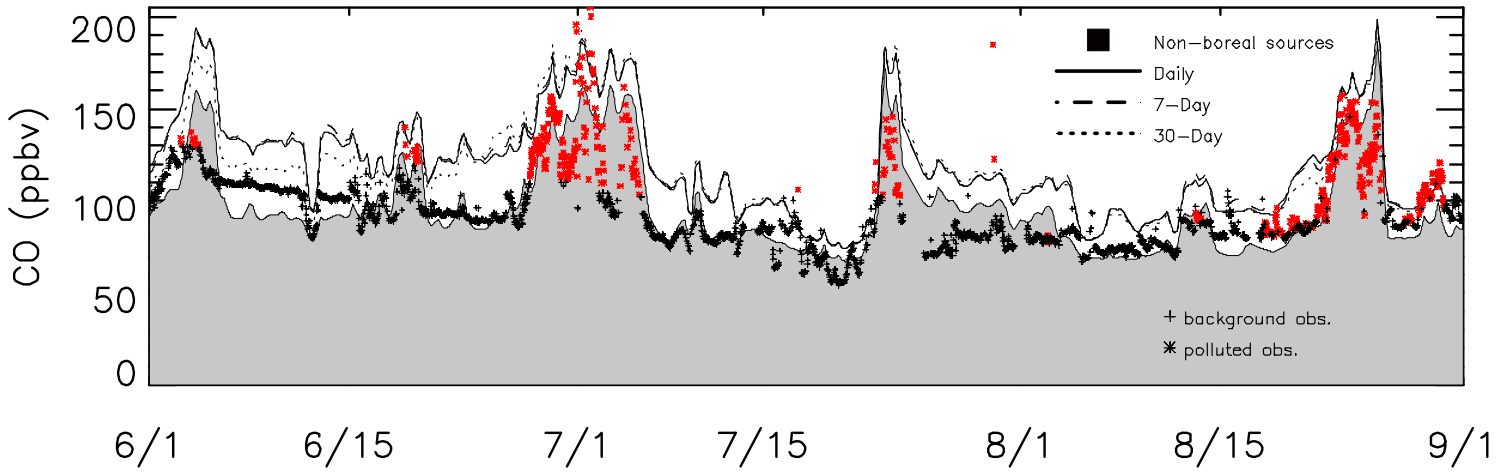

Figure 4-6. Time series of CO observations from Mace Head, Ireland (+ symbols). Observations flagged as "polluted" are shown in red. Shaded area of graph is simulated CO from non-boreal sources, and lines show CTM-simulated CO with boreal source included.

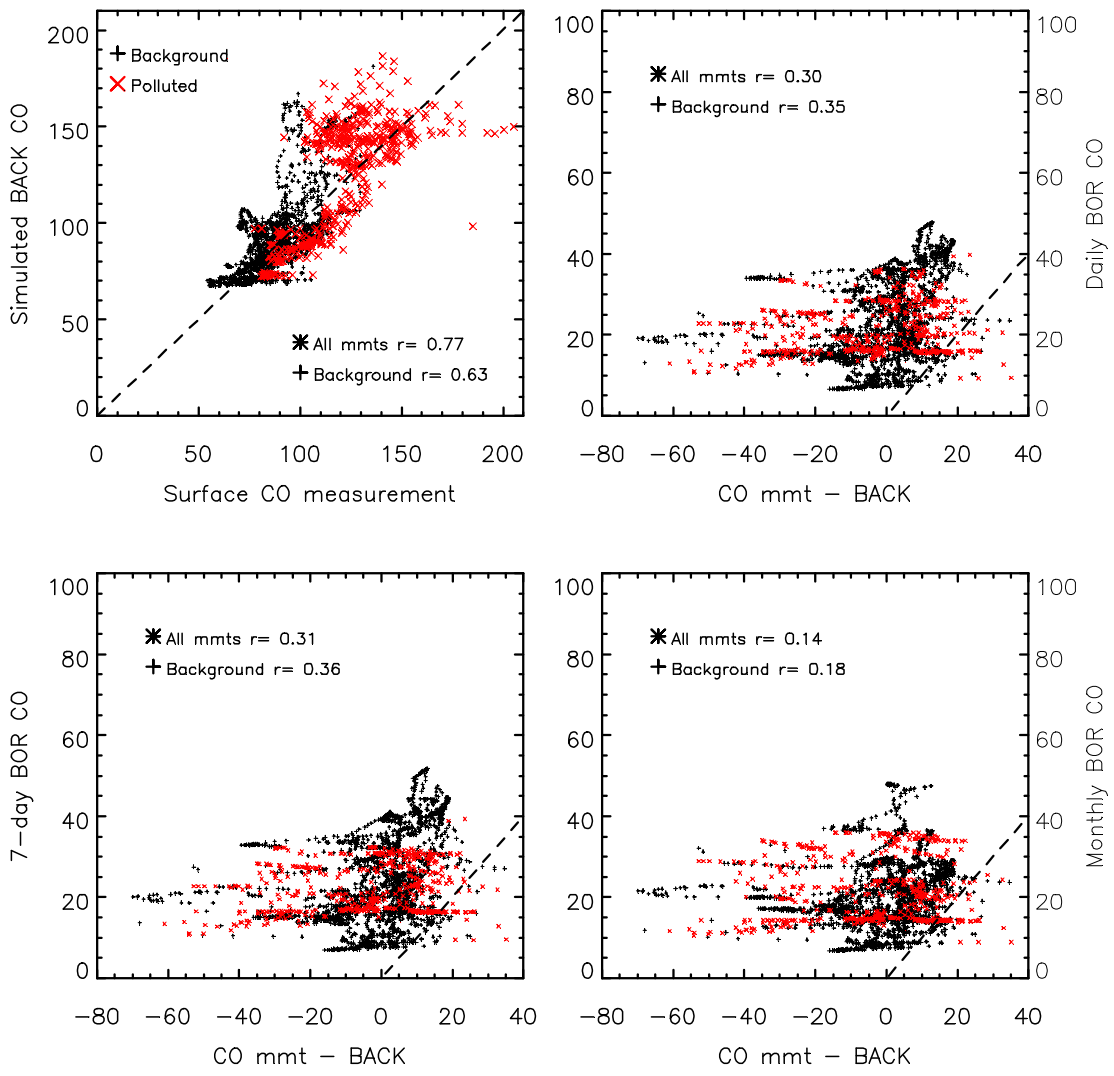

Figure 4-7. Scatter plot of simulated CO vs. observed CO from Mace Head. (a) Simulated non-boreal sources vs. observed CO and (b-d) simulated CO from boreal fires modeled at different resolutions vs. residuals of CO observations with simulated non-boreal CO sources removed.

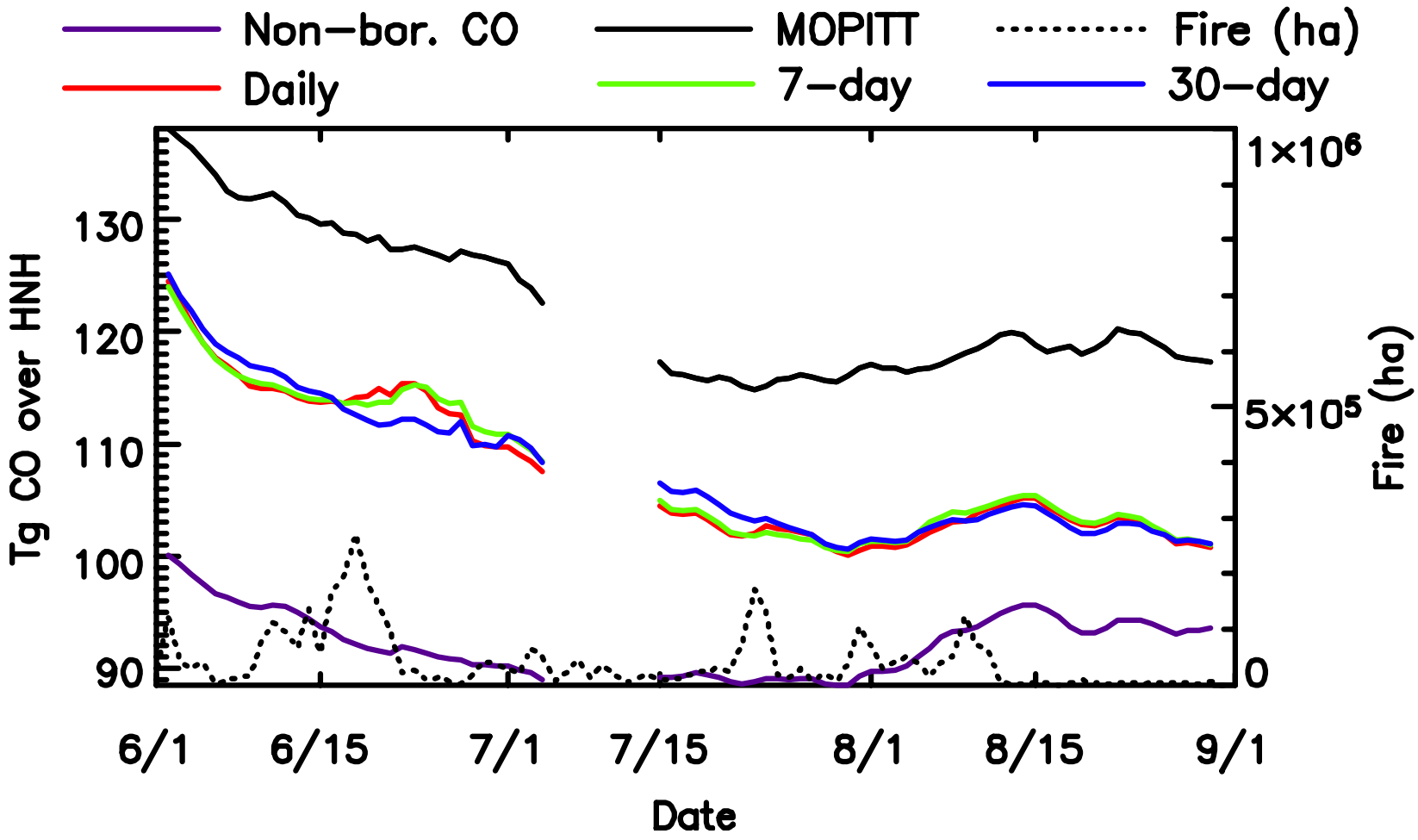

Figure 4-8. CO burden in the HNH estimated from MOPITT data and model outputs.

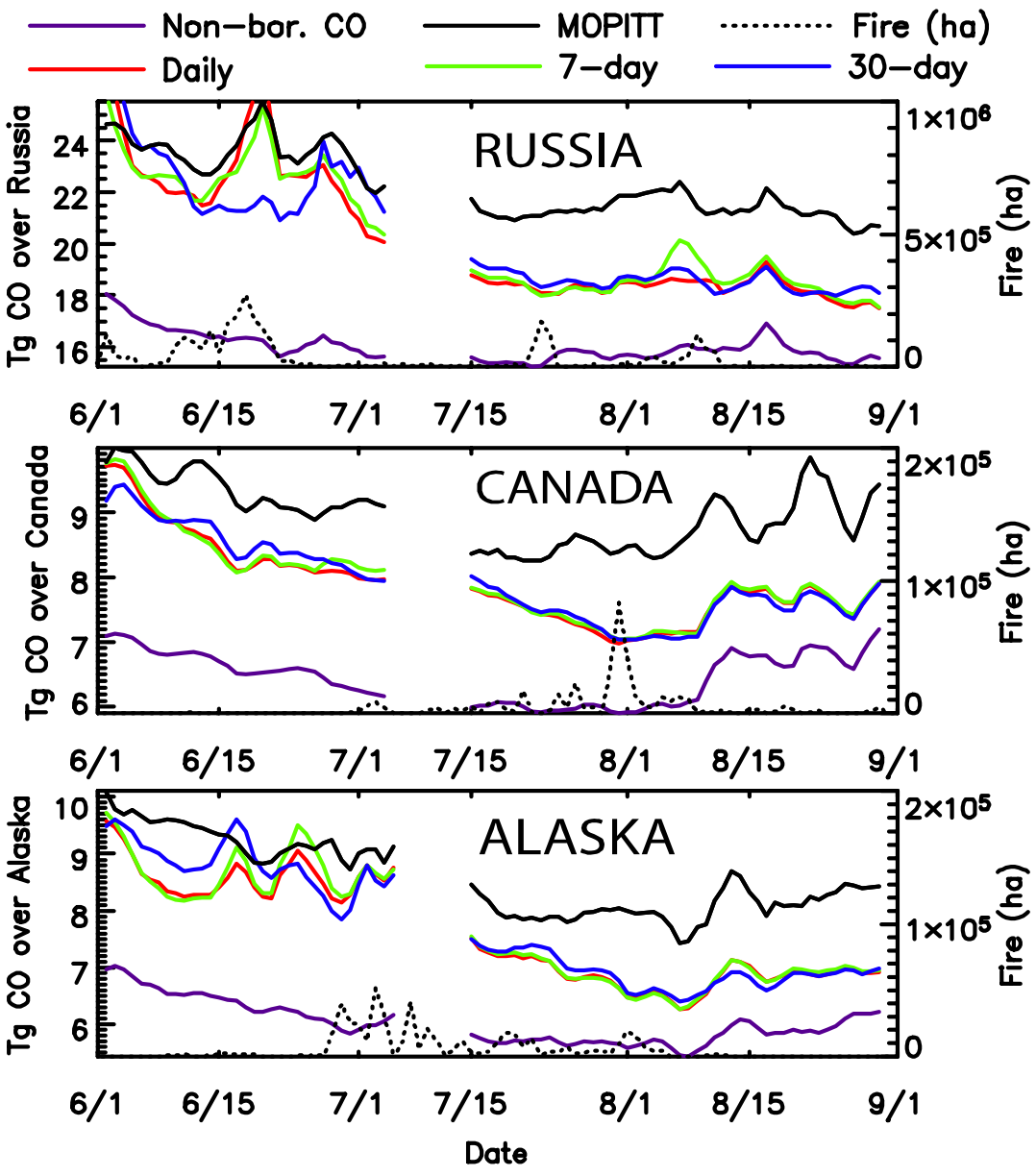

Figure 4-9. CO burden over source regions estimated from MOPITT data and model outputs.

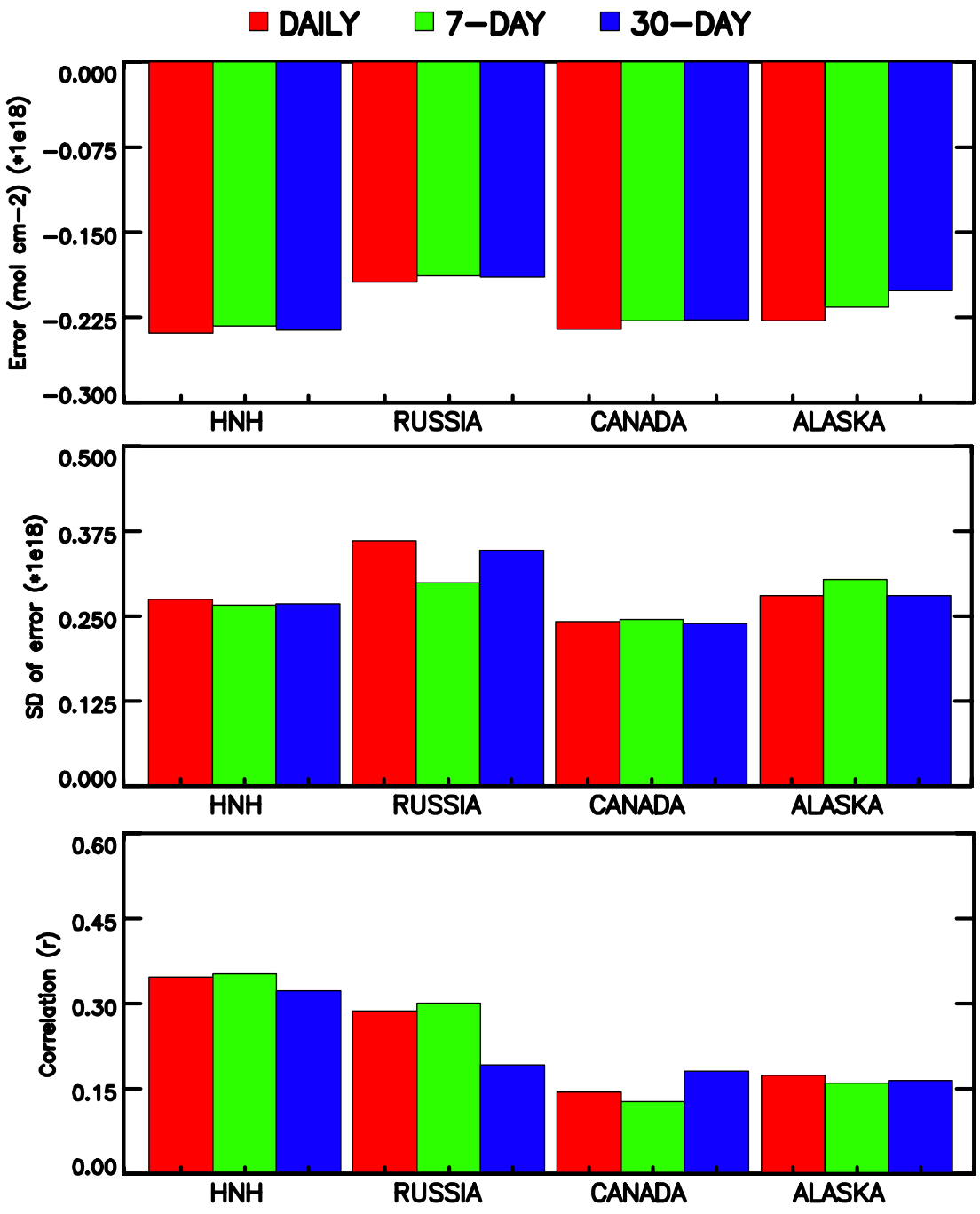

Figure 4-10. Error statistics for comparison of simulated boreal contribution to total column CO to residual obtained by subtraction of simulated non-boreal CO from MOPITT data. Negative bias indicates underestimate of CO by the model.

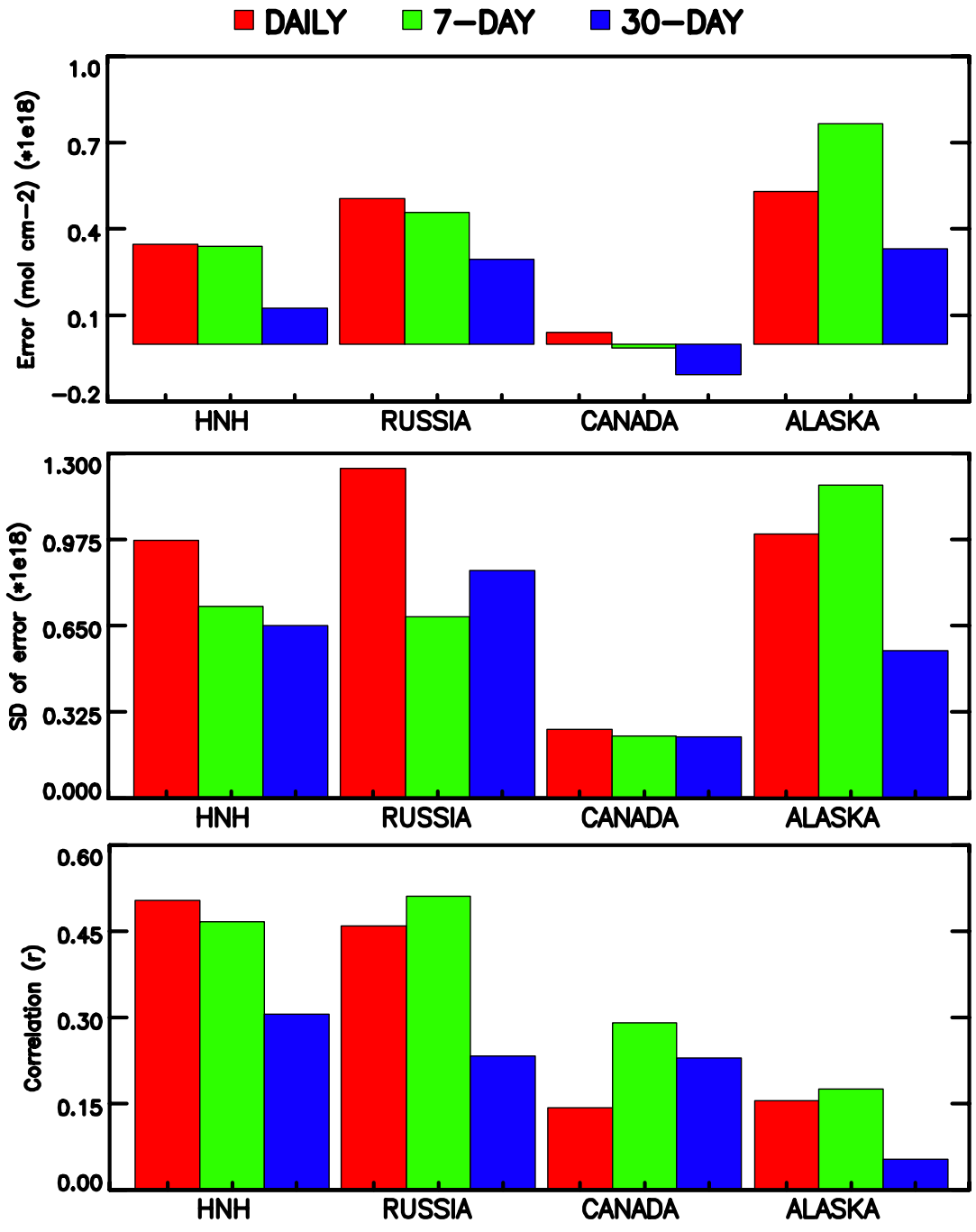

Figure 4-11. Error statistics for comparison of high-contrast subset of CO retrievals.

Chapter 5. Comparative evaluation of burned area products in terms of their consequences for atmospheric patterns of CO

1. Abstract

Three different estimates of burned area for the boreal forest were compared: the burned area sources from *Kasischke et al.* [2005], incorporating several different remotely sensed and ground-based data sources, the GLOBSCAR burned area product [*Simon et al.*, 2004], and the GBA-2000 burned area product [*Tansey et al.*, 2004a]. These products were qualitatively evaluated and systematic problems with each product were discussed in terms of their effect on estimated emissions. Spatial agreement among the products was high at coarse scales, and worse at finer scales. The temporal profile of emissions differed greatly among products, even in regions where spatial patterns were very similar. In terms of the atmospheric impact of fire emissions, the discrepancies in the seasonal cycle of each product are likely more important than the spatial differences. The BWEM-1 emissions model [*Kasischke et al.*, 2005] was used to simulate CO emissions based on each product, and the simulated emissions were used as input to the University of Maryland chemistry and transport model (UM-CTM). The output of the UM-CTM was compared with MOPITT observations. The BWEM and GBA-2000 burned area estimates produced better overall agreement with atmospheric observations than the GLOBSCAR product, the seasonal trend of the simulations was different from the trend observed from MOPITT. This analysis showed significant differences between different burned area estimates at all scales, and demonstrated that these differences have important consequences for modeling spatial and temporal patterns of atmospheric CO.

2. Introduction

Burned area is widely recognized as the chief uncertainty in biomass burning emissions estimates at the global scale [*Kasischke and Penner*, 2004]. Recent global emissions estimates have used widely varying approaches to estimate the area affected by fire, reflecting a lack of scientific consensus on the best methods [*Hoelzemann et al.*, 2004; *Ito and Penner*, 2004; *van der Werf et al.*, 2003]. Several large projects have focused on attempts to monitor fire activity using globally consistent methodologies [*Stroppiana et al.*, 2000; *Tansey et al.*, 2004a]. However, studies using a wide assortment of products have consistently shown that detection methods designed for fire monitoring in tropical ecosystems will encounter problems in other parts of the globe [*Kasischke et al.*, 2003; *Silva et al.*, 2004]. This issue is complicated by the fact that different applications make different demands of burned area estimates.

The boreal forest accounts for only a small fraction of global area burned annually, but boreal forest fires can have a disproportionate influence on atmospheric composition and the global carbon cycle because of their high fuel loads and low combustion efficiency [*Cofer III et al.*, 1996]. Estimates of emissions from boreal forest fires have generally developed around the model of *Seiler and Crutzen* [1980], with trace gas emissions estimated as a function of area burned, fuel loading, fire severity, and trace gas emissions factors. The emissions model described in *Kasischke et al.* [2005] estimates area burned using the best available multi-year databases for Canada, Alaska and Russia. *Kasischke et al.* found that while the agreement between their emissions estimates and atmospheric observations was sensitive to fuel loading and fire behavior

assumptions, area burned was the largest source of inter-annual and inter-continental variability. In the remainder of this paper, the emissions model used in *Kasischke et al.* [2005] will be referred to as BWEM-1, and the area burned data from that study will be referred to as BWEM-BA.

For this study, in addition to the sources used by *Kasischke et al.* [2005] (BWEM-BA), two global products prepared for the year 2000, GLOBSCAR [*Simon et al.*, 2004] and GBA-2000 [*Tansey et al.*, 2004a], were examined. Differences in spatial and temporal patterns among these products were calculated at several scales, and CO emissions estimates from each product were used as input to a chemistry and transport model (CTM) simulation for comparison to observations from the MOPITT instrument.

The next section outlines the properties of burned area estimates most critical to emissions modeling. In Section 4, each product is described, and its potential evaluated in terms of the relevant criteria. The Results section (Section 5) consists of three parts: first gridded emissions estimates from the three burned area products will be compared, then CTM simulations of atmospheric CO with each product will be compared, and finally, simulated CO using each product will be compared with measurements from the MOPITT instrument.

3. Estimating burned area for emissions modeling

Estimation of trace gas emissions is only one of many scientific applications of burned area data. Area burned is a single parameter in the formula for calculation of total emissions, but in the context of a spatially and temporally resolved emissions model, three pieces of information are needed to describe the patterns of fire: fire size, location,

and timing. For a global estimate, only the total area burned is required, but spatially explicit calculation of emissions requires the location of fires so that spatial variability in fuel loading can be incorporated. Time-resolved calculation of emissions requires additional information about the timing of fires. Atmospheric modeling of trace gas emissions requires spatially and temporally explicit estimates of emissions at scales appropriate to atmospheric observations.

For atmospheric studies, the spatial and temporal variability in the modeled trace gas flux should be considered the signal, and all other sources of variability in trace gas concentrations are noise. In the context of fire emissions, this means that the most important criterion for burned area information is accuracy of the spatial and temporal pattern of fire activity, at the scale relevant to the atmospheric measurements, which can be best examined in terms of fire size, timing and location.

Fire size refers simply to the amount of area affected by fire within a given space. This is often treated in emissions modeling as a fractional amount at the resolution of the model (e.g. [*Heald et al.*, 2003]; [*Ito and Penner*, 2004] [*Kajii et al.*, 2002]). Different methods for estimating area burned are subject to various low and high biases, but as long as the bias is consistent, fine-scale studies can be used to determine a correction that can be applied to broad-scale area estimates [*van der Werf et al.*, 2003]. Therefore, in terms of estimating trace gas emissions, a consistent proportional response to fire activity may be more important than absolute accuracy of total area.

Atmospheric models range from regional models run at resolutions of a few kilometers, to global models such as the one used in this study, which is run at a

resolution of 2° by 2.5°. These are coarser scales than used for land cover change studies, and the evaluation of burned area location data should reflect this. *Boles and Verbyla* [2000] compared fire detection algorithms in the Alaskan boreal forest, and evaluated them by comparison with field observations. Much of the error they detected was caused by poor georeferencing of the AVHRR satellite data, causing a spatial shift in the location of burned area detection. While important for cartographic and fine-scale land-cover applications, location error at this scale is unlikely to have much effect on estimated emissions, and almost no effect on modeled trace gas concentrations. Fire location information for atmospheric applications should therefore be evaluated at broader scales more relevant to atmospheric observations, ignoring variability at finer scales that may be important for other applications. In terms of estimating carbon consumption and trace gas release, it should be noted that fine-scale location information can be important in certain contexts. For instance, in partially cleared areas, high-resolution location information may be necessary to distinguish fires associated with land clearing from burning of agricultural residues on cleared land.

Atmospheric models have very high temporal resolution, generally modeling atmospheric transport internally with a time step of only a few minutes, and delivering output at daily or better resolution. The model used in this study produces output every six hours. This is a finer scale than any systematic burned area product. However, for atmospheric modeling purposes, the diffusive effect of modeled long-range transport means that sub-monthly variability in emissions has only a small effect outside of the source region (see Chapter 4). For accurate modeling of atmospheric effects of fires, the

appropriate resolution of fire timing information will be determined by the atmospheric model and measurements used.

In the next section, each of the different methods used to estimate burned area in this study is introduced, including a description of the specific properties of each relative to its potential for atmospheric applications, in terms of the criteria described above.

4. Overview of burned area products in this study

Fire size and location are generally determined from the same input data, but not always. Depending on the methodology used, these data may or may not also be appropriate for determination of fire timing. The initial runs of the BWEM-1 had the goal of producing a consistent multi-year data set, and the data sources for fire size, location, and timing were chosen from those that were consistently processed for multiple years.

Two different global estimates of burned area for the year 2000 were produced using different methods applied to different satellite data inputs. The differences between the burned area maps obtained by these methods and those in the BWEM-BA shed light on some of the general issues associated with mapping of burned area, and some of the specific issues of burned area mapping in the boreal forest. It is important to note that none of these products represent definitive information about fire size, location, and timing in the boreal forest.

In this section, the technical details of each of these products will be introduced, and the products will be compared in terms of fire size, location, and timing. Selective comparisons will be made to illustrate the qualitative differences between the products.

4.1. BWEM-BA burned area

There currently are no multi-year data products that provide information on fire activity for the entire boreal forest. In Canada and Alaska, the best information about fires comes from the governmental agencies responsible for fire management, rather than from a third party. Therefore, the BWEM-BA uses separate data sources for each of these regions.

In Canada, mapping of fires in the boreal forest is undertaken by the agencies responsible for fire management at the provincial level. These data are compiled by the Canadian Forest Service into national reports, which are available daily during the fire season. The mapping of individual burns by provincial agencies is done with a combination of satellite data, aircraft observation, and ground surveys. Fire boundary information for all of Canada was collected and validated by the Canadian Forest Service, which produced a Large Fire Database of fires larger than 200 hectares during the years 1959-1999 [*Stocks et al.*, 2002]. The provincial totals in this database show good agreement with the totals reported by the Canadian Forest Service, which are used to estimate fire size in the BWEM-1 from 2000-2003. Timing of fires is derived from the thermal hot spot detections from the FireM3 system. With provincial area totals used to estimate fire size, and hot spot detections used to estimate fire timing, what remains is to construct a better estimate of fire location for the years when the Canadian Large Fire Database is unavailable. The spatial distribution of these hot spot detections was used to estimate fire location for 2000-2003, including the data shown in this paper, by application of a spatial clustering and region-growing approach. The hot spots were

buffered to 2500 meters to produce clusters, and clusters with fewer than 10 hot spots are removed. The area burned estimated for each province is assigned to each cluster proportionally to the buffered area. Separate temporal profiles are calculated for each cluster. Fine-scale maps in this chapter depict the clusters, which are proportional to area burned within each province, but direct comparison between products is only possible with the gridded emissions model outputs.

Mapping of fires in Alaska is undertaken by the Alaskan Fire Service, which maps fire boundaries using aircraft observations and ground surveys [*Kasischke et al.*, 2002]. Fire boundaries are compiled annually in GIS format and distributed through the Alaska Geospatial Data Clearinghouse (http://agdc.usgs.gov/data/blm/fire/). The fire perimeters compiled by the Alaskan Fire Service are the basis for the fire size and location estimates used in the BWEM-1. Fire timing for Alaska is derived from daily reports from the National Interagency Fire Center (available at http://www.cidi.org/wildfire). In the present implementation, all fires in Alaska are assigned the temporal profile corresponding to fire activity in the entire state.

Mapping of fires in Russia requires the use of satellite observations because of the large area which is unprotected and unmonitored by the state agencies. A project at the Sukachev Institute of Forestry in Krasnoyarsk using AVHRR observations resulted in the production of a database of fire boundaries for 1996-2003 for eastern Russia (east of 60°E), including most of the fire-prone areas of the Russian boreal forest. This database was compiled using a combination of thermal hot spot detections and post-fire scar mapping, and details can be found in *Sukhinin et al.*[2004]. This product is the basis for

fire size, location, and timing estimates for Russia used in the BWEM-1. Temporal profiles are calculated for each contiguous area burned.

4.2. GLOBSCAR

The GLOBSCAR product [*Simon et al.*, 2004] was developed using 12 months of daytime imagery from the ATSR-2 instrument on the ERS-2 satellite. This product uses two burned area detection algorithms in tandem to improve accuracy and minimize false detections. These two algorithms, based on different combinations of visible, near-infrared, shortwave infrared, and thermal wavelengths, both detect the fundamental changes in land surface radiative properties following fire, *viz.* higher thermal emissions and lower near-infrared reflectance. The ATSR-2 satellite data have a repeat rate of 3 days at the equator, and generally have daily coverage at boreal latitudes. These data are re-sampled to a consistent resolution of 1km before application of the burned area detection algorithms. The accumulated burned area detections were compiled for each month in 2000, and the cumulative total of the previous month was subtracted to obtain a monthly burned area estimate. If multiple detections occurred in the same area, they were counted only once, in the first month of detection.

The GLOBSCAR product is available for download in several different formats (http://shark1.esrin.esa.it/ionia/FIRE/BS/ATSR/format.html). For this study, the vector product was used, containing outlines of burned areas. These outlines correspond to pixels of a regular grid with a resolution of about 32 arc-seconds, which corresponds to 1 kilometer at the equator. Monthly data were assembled for April-October and clipped to include only Canada, Alaska and Russia. The monthly data were overlaid to produce an

annual area burned map, and a monthly profile of emissions was calculated for each contiguous polygon on the annual map, according to the fraction of total area from each month.

A qualitative analysis of the GLOBSCAR product revealed some important quality issues relevant to burned area detections in the boreal forest. First of these is a data gap related to a descoping of the ATSR-2 instrument, which was an engineering decision to accommodate other instruments on board the ERS-2 satellite. This gap caused some missing data in central Siberia, as shown in Figure 5-1. This area has substantial area burned in the GBA2000 product, but not much in the BWEM-BA.

Another issue with the GLOBSCAR product identified by Simon *et al.* is the lack of any region-growing mechanism. Region-growing algorithms attempt to capture the complete extent of large burned areas by rechecking areas adjacent to high-confidence burned area detections using a less strict algorithm. Figure 5-2 shows the effects of the region-growing algorithm used by the GBA-2000 product, as compared with the unconnected burned areas in the GLOBSCAR and Sukhinin *et al.* products. This deficiency results in evident problems with fire boundaries at finer scales, but its effect on overall bias and the consistency of the product's response to fire activity is harder to determine.

Finally, Simon *et al.* documented the tendency of the algorithms used for the GLOBSCAR product to pick up burn scars from previous years in the boreal region. This is shown quite clearly in Figure 5-3, where areas of fire activity from 1996-1999 in Alaska are included in the GLOBSCAR burned area. The GLOBSCAR product did not

show sensitivity to fires before 1996, but fires from 1998 produced burned area detections across the entire boreal forest. Despite the good agreement between the GLOBSCAR and other products in areas of 2000 fires, the detections of area burned in previous years makes the error in this product highly variable and difficult to correct. In the context of operational use of this method, however, Simon *et al.* point out that these detections could be avoided by including data from the previous fall in the burned area estimation for the first month of the fire season.

The GLOBSCAR product also shows some of the problems with ATSR thermal fire detection described by *Kasischke et al.* [2003], such as a string of burned area detections at high elevations in the Brooks Range of Alaska, as shown in Figure 5-4. But in terms of its potential for modeling trace gas emissions, the largest problem with the GLOBSCAR product in the boreal zone is detection of older burn scars, which erroneously enlarges the area burned, distorts the seasonal profile of fire activity, and does not lend itself to simple post-processing correction. This deficiency could likely be corrected in operational use of this method [*Simon et al.*, 2004].

4.3. GBA-2000

The Global Burned Area product (GBA-2000) is actually a composite of several different regional products, all based on input data from the VGT sensor on the European SPOT-4 satellite [*Tansey et al.*, 2004a; *Tansey et al.*, 2004b]. This product differs from the GLOBSCAR and BWEM-BA in that thermal detection of hot spots was not part of the burned area detection methodology. Instead, the GBA-2000 methods used only the visible, NIR, and SWIR bands from VGT to detect burned areas. This makes the

comparison of this product to the BWEM-BA and GLOBSCAR burned areas very interesting, as the other two are heavily dependent on the elevated thermal emissions associated with fire activity.

The GBA-2000 product is available for download as a vector database and also as a point database of burned area locations. For this study, the vector database was converted into a map of burned area for the entire season. Temporal profiles of each contiguous burned area were calculated using the proportion of the total burned area detected in each month.

Two algorithms are used for the GBA-2000 product in the boreal zone. In Canada and Alaska, the algorithm applied to the SPOT VGT data was developed at the Canadian Center for Remote Sensing. This method uses an NDVI compositing method to remove cloudy pixels, and detects burned areas based on change detection in the SWIR band of SPOT VGT [*Fraser et al.*, 2003]. *Fraser and Li* [2002] tested a change-detection algorithm using SPOT VGT data and hot spot detections from AVHRR, and found that the resulting burned area agreed well with areas mapped using air photo interpretation. The algorithm used for GBA-2000 did not include any hot spot detection data. In algorithms using both hot spot and burn scar detection, hot spot detections are used to eliminate false detections of change in reflectance not accompanied by any fire activity. Without hot spot data, the change detection algorithm has to be made more rigorous [*Fraser et al.*, 2000].

Figure 5-5 shows fire activity in a region of northwest Canada from the GBA-2000 product, the FireM3 hot spots, and digitized fire boundaries obtained from

Environment Saskatchewan. These data were mapped by hand from aircraft by expert observers using GPS (J. Xie, Saskatchewan Environment, personal communication, 2002). Fire statistics from the Northwest Territories indicated roughly 120,000 ha burned during 2000, but fire boundary data obtained from the Forest Management Division of the Government of the Northwest Territories did not include any fires in this region (B. Croft, Forest Management Division, Government of the Northwest Territories, personal communication, 2002).

It is important to note that areas shown in Canada in Figure 5-5 represent the location information used in the BWEM-BA, derived from the FireM3 hot spot detections. The actual area burned assigned to each of these polygons was weighted so that provincial totals would match statistics from the Canadian Forest Service.

The burned area estimates from GBA-2000 and the BWEM-BA agree well in the largest fires, and both show burned area considerably larger than the mapped boundaries. Of the fires detected by only one of the RS methods, examples can be seen in this figure of both GBA-2000 (above the Slave river north of Riou Lake) and FireM3 (bottom right, near Pasfield Lake) capturing fire activity missed by the other. Overall, the FireM3 detections are the most generous, including large areas in the southern Northwest Territories where the GBA-2000 product did not detect any fire activity. The GLOBSCAR product (not shown) also did not detect fire activity in the areas in NWT with FireM3 hot spots and no burned area in the GBA-2000 product. These detections may represent error in the FireM3 product, such as sun glint off of small lakes [*Li et al.*, 1997].

In Russia, the GBA-2000 product is based on an algorithm developed at the International Forest Institute of the Russian Academy of Sciences in Moscow, which is based largely on change detection, primarily in the NIR. This product is thus likely to be sensitive to any stand-killing disturbance that would result in reduced NIR reflectance.

Spatial patterns of burned area in Russia differ a great deal among the three products. In southern Russia, where the largest fires in 2000 were located, the products all show general agreement as to the location of the largest concentrations of fires (for instance, the area in Figure 5-2), but the GLOBSCAR product includes large areas which correspond to older burn scars, and the GBA-2000 also includes large areas not included in the other two products.

The differences are particularly striking in northern parts of Russia, as shown in Figure 5-6. While the products show some common concentration of burned area in the largest features in the Sukhinin *et al*. product, each product shows substantial burned areas which are detected by neither of the other products. In the case of GLOBSCAR, possible causes are discussed above, including detection of older burn scars and false detections caused by low solar angles. The GBA-2000 product should not be susceptible to either of these problems, since it is based entirely on change detection within the study period and since it does not use thermal wavelengths.

Figure 5-7 shows an area in central Russia where large areas are denoted as burned in the GBA-2000 product, and very little activity is detected by the other products. The pattern of detection in the GBA-2000 product is highly concentrated near the rivers Ob and Irtysh. This pattern suggests an anthropogenic component to the

phenomenon, which is not apparent in the patterns of either of the other products. One possibility is that the GBA-2000 algorithm is picking up sites along the river where clear-cut logging has taken place, either in 2000 or earlier years, which would have a similar signature in the NIR and visible bands, but would not be detected by the other products because logging does not result in a thermal signal.

All three of these burned area products include some fires in non-forest ecosystems. Since the BWEM-1 emissions model does not treat these fires differently, they are potentially a large source of error in estimated emissions. The next section gives an outline of this problem and how it affects emissions estimates with the products used in this study.

4.4. Fires in non-forest ecosystems in the boreal zone

Burning of agricultural residues and fires in steppe grasslands near the border of Mongolia account for much of the non-forest biomass burning in Russia. The emissions estimation algorithm of the BWEM-1 does not explicitly account for non-forest fires. When used in conjunction with the burned area product of Sukhinin *et al.* [2004], this does not cause large errors, for two reasons. First, the areas of Russia where non-forest fires might be included in the *Sukhinin et al.* product are near the forest-steppe ecotone, and have low fuel loading estimated from the biomass maps used as input. Second, to the extent that agricultural and steppe burning is a factor, it is confined to early in the fire season in the areas covered by the *Sukhinin et al.* product. The BWEM-1 estimates low emissions for early-season fires because of the assumed predominance of surface fires,

and so the estimated carbon release is comparable to what would be obtained from an explicit treatment of agricultural and steppe fires.

In Western Russia, beyond the extent of the *Sukhinin et al.* product, large burned areas in the GBA-2000 and GLOBSCAR products along the Kazakh border are likely fires of agricultural origin. These detections in southwestern Russia pose a specific problem when processed with the emissions estimation algorithm of the BWEM-1. *Tansey et al.* [2004b] state that agricultural fires occur in April and May and again in September and October. However, the August data from the GBA-2000 product show large areas of burning in western Russia where a high proportion of agricultural fires would be expected, and the GLOBSCAR product shows burning throughout May-August in this region. When processed with the BWEM-1 algorithm, these fires result in carbon release that is likely a substantial overestimate, especially for activity later in summer.

In North America, agricultural burning occurs mainly in the southern areas of the Prairie Provinces (Saskatchewan, Manitoba, and Alberta). The BWEM-BA and GBA-2000 show very little fire activity in this area. About 15% of the GLOBSCAR burned area for Canada is in this region, mostly during the months of June and July. As with Russia, the emissions estimation algorithm of the BWEM-1 is predicted to overestimate emissions from agricultural fires after May.

The application of the BWEM-1 emissions algorithm burned area products that include substantial non-forest burned area is a potentially serious source of error in estimated carbon release.

In summary, the three burned area products generally show sensitivity to the same events in Canada, Alaska, and southern Russia. In the rest of Russia, however, large discrepancies exist, and the area of agreement between the products is a minority of the area in each of them. In the next section, the burned area estimates will be compared at the resolution of the atmospheric model, to evaluate how the differences between products will affect patterns of simulated CO emissions.

5. Comparison of gridded burned area and emissions

Emissions were estimated using fire size, location and timing inputs from each product. The "moderate" emissions scenario described in *Kasischke et al.* [2005] was used for estimation of carbon and trace gas emissions. Monthly burned area and estimated emissions were gridded to a 2° by 2.5° grid, suitable for input to the chemistry and transport model.

5.1. Comparison of area burned and spatial distribution

Table 5-1 lists total area burned and carbon consumption for each product for Canada, Alaska and Russia during 2000. The estimated area burned in Russia varied greatly, but agreement between the BWEM-BA and the GBA-2000 burned area was good in Canada and Alaska. In Russia, the GLOBSCAR and GBA-2000 products estimated similar total area, despite large differences in spatial distribution. For the part of Russia covered by the BWEM-BA, the GLOBSCAR burned area was about 50% higher than the BWEM-BA, and the GBA-2000 burned area was nearly twice the BWEM-BA.

The GBA-2000 product shows higher fuel consumption on average in North America because of a much higher percentage of fire activity late in the fire season (when

modeled fuel consumption is higher, see Chapter 6). The fuel consumption estimates for each individual month during the fire season (not shown) were very similar for all three burned area products, indicating that biases in fuel consumption related to the spatial distribution of burned area are very small.

Figure 5-8 to 5-10 show burned area for each product for all of 2000 and monthly for May-August. With the exception of Western Russia, which is not included in the BWEM-BA, all three products captured the general spatial characteristics of the 2000 fire season, with the largest concentration of burned area occurring near the border with China in all three products. All three showed large fires in northeastern Russia, but the spatial distribution of activity within this region varied considerably among products.

Table 5-2 shows the linear correlation (r) between the different fire products, evaluated at spatial resolutions of 2° by 2.5, 4° by 5°, and 8° by 10° (degrees latitude by degrees longitude). The nominal input scale for the atmospheric model used in this study is 2° by 2.5°, but in terms of long-range transport, it is likely that emissions transport will be similar or different according to input data correlations at coarser resolution.

Agreement between GBA-2000 and the BWEM-BA is very good for all areas where the BWEM-BA data coverage extends. The GLOBSCAR product agrees better at coarser scales with the other products. This coarse-scale agreement likely reflects the patterns of fire-prone ecosystems on the landscape. Agreement between BWEM-BA and GBA2000 is not sensitive to spatial resolution.

Boschetti et al. [2004] performed a comparison of burned area products that included the GLOBSCAR and GBA-2000 products. Their analysis was conducted with a reference grid made up of hexagons of nearly equal area, to avoid latitudinal distortions associated with a lat/long grid. The grid cells in their analysis were approximately $1/10^{th}$ the size of the 2° by 2.5° grid cells in the boreal latitudes. They analyzed correlations among products and presented aggregate statistics for several different regions. None of these regions correspond to the regions used in this study, but a comparable extent of correlation between GLOBSCAR and GBA-2000 was reported.

Overall, the area burned estimated by these three products show some agreement at the scale of the atmospheric model, with the exception of areas not included in the BWEM-BA data, which comprise substantial fractions of the area burned in Russia estimated by the other two products. Systematic problems with the various products, including detection of previous years' fire by GLOBSCAR and the lack of data for western Russia in the BWEM-BA, manifest themselves in poor spatial agreement between the products at fine scales, and in widely differing regional and global estimates of total area burned, but the spatial patterns of biomass consumption captured by each product are similar at scales relevant to atmospheric studies at the global scale.

5.2. Comparison of fire seasonality

The seasonal pattern of area burned varied greatly between products; only in Alaska do all three products agree on the month of maximum fire activity (Figure 5-11). Timing of fire activity has a large impact on fuel consumption in the BWEM-1 algorithm, as can be seen in Table 5-1. The majority of Russian area burned from the GBA-2000

product is in April and May, which results in lower estimated fuel consumption relative to the other products.

In North America, fuel consumption estimated by GBA-2000 is higher than the other products due to a larger fraction of late fires. The Alaskan Fire Service reported fewer than 10,000 hectares of fire after 1 August 2000, of which fewer than 500 hectares were in September. The GBA-2000 product shows a very different pattern of burning in Alaska, with nearly half of the total area burned after 1 August.

Differences in fire timing will result in different patterns of emissions and a different distribution of CO in the atmosphere. Correlations between gridded monthly emissions from the three burned area products are much lower compared to correlations of annual totals (Table 5-3). Even in regions where spatial patterns are quite similar, the temporal profiles of emissions differ widely between products. The differences in timing of fires will have an effect on the simulated distribution of atmospheric CO equal to or greater than the differences in spatial pattern. The comparison of the CO transport simulation to atmospheric measurements will attempt to separate the effects of spatial and temporal pattern by making separate comparisons of time series of CO burden and spatial patterns observed over shorter time periods.

6. Comparison to atmospheric observations: Methods

6.1. Modeling of transport and chemistry

The gridded emissions were used as input to the University of Maryland Chemistry and Transport Model (UM-CTM) [*Allen et al.*, 1996; *Park et al.*, 2004]. This model was run at a resolution of 2° latitude by 2.5° longitude with 35 vertical levels, 17

in the troposphere. The model was driven using the GEOS-3 assimilated meteorological fields from the NASA Data Assimilation Office [*Hou et al.*, 2003].

Non-boreal CO sources used were the same as those described in Chapter 3. Injection of boreal fire emissions was parameterized by a pressure-weighted distribution of emissions throughout the tropospheric column, equivalent to a constant vertical concentration profile from the surface to the tropopause at the emissions source.

The model simulation was run for the period 1 January – 31 August 2000, and output was analyzed from May-August 2000. CO concentration was output from the model at 6-hour intervals.

6.2. Atmospheric observations

MOPITT Level 2 total column CO observations were used for this study. All daytime MOPITT data were ingested for the period 1 May – 31 August 2000. Data quality filters were chosen as a compromise between data coverage and data quality. Retrievals were filtered to exclude retrievals with estimated error in total column CO greater than 25%, and retrievals with greater than 40 percent *a priori* contribution to the 700mb layer of the retrieval. Application of these filters resulted in approximately 30,000 usable retrievals north of 30° N per full day of instrument operation. There is a data gap from July 4-14 related to an instrument calibration activity [D. Ziskin, *personal communication*, 2004].

6.3. Processing of model output for comparison to MOPITT data

CTM output was processed to match the spatial and temporal sampling properties of each MOPITT retrieval, and vertical averaging kernels were applied to each MOPITT

retrieval according to the method of *Deeter* [2000]. This resulted in a dataset with comparable spatial and temporal characteristics suitable for direct comparison with the MOPITT observations.

Because of the inclusion of *a priori* data in the retrieval, the simulated MOPITT CO is not a linear sum of constituent sources. In order to compare individual sources with MOPITT data, the method described by *Arellano et al.* [2004] was used to estimate the contribution of constituent sources to simulated MOPITT total column. For this study, MOPITT observations were compared to simulations of all non-boreal sources, and the simulated contribution of each boreal fire source was compared to the residual obtained by subtracting the simulated non-boreal CO from the MOPITT observation. To reduce sampling bias related to the MOPITT resolution, both model outputs and observations were re-sampled back to the CTM output grid for statistical comparisons.

7. Results of CO transport simulation

Figure 5-12 shows the simulated HNH CO burden from each simulation in this study, as well as from the MOPITT data (black line). The BACK simulation (purple line) does not include any boreal fire source. Boreal fires contribute more than 20% of simulated HNH CO during much of the study period. The dramatic increase in boreal CO after 1 August is a consequence of the seasonal assumptions in the BWEM-1 algorithm. The effects of fire seasonality on atmospheric CO are examined in more detail in Chapter 6. The CO burden calculated from the MOPITT data has a downward trend throughout the study period.

7.1. Simulation of CO from non-boreal sources

The simulation of non-boreal CO sources was evaluated in Chapter 3, but since this study uses a different input dataset for non-boreal biomass burning and a different subset of MOPITT data, the comparison will be repeated here. Table 5-4 shows error statistics for the BACK simulation compared with MOPITT observations for the whole HNH as well as the two continental source regions, for each month of the study period. Agreement of CO values over Eurasia is better than over North America, in terms of absolute error as well as the scatter of model errors.

7.2. Comparison of simulated boreal fire CO to MOPITT data

Figure 5-13 shows correlations between simulated boreal fire CO and the residuals obtained by subtraction of BACK simulated CO from MOPITT observations. Similar to the results for the BACK simulation, agreement is better for individual months than for the entire study period. The GLOBSCAR product is uncorrelated with observations over the entire study period, but shows a relationship to MOPITT observations of the same order as the other simulations for each month, even besting the other two products in August. To better understand what drives the relationship between simulated and observed CO, two subsets of the simulation will be examined in more detail: May over Eurasia and August over North America.

Figure 5-14 shows BACK model output, MOPITT observations and residuals averaged over August for North America. All retrievals over land during August (N=76,921) were aggregated to a 1° by 1° grid to prepare these maps. The observations

and BACK simulation have units of TC CO (molecules cm^{-2}). The residuals are plotted as z-scores (standard deviations from mean).

The most prominent features in the MOPITT data are in the East, on the coasts of Maine and Newfoundland, as well as inland just east of the Hudson Bay and on Baffin Island. All of these features are reflected to some extent in the simulation of non-boreal sources, though the residuals clearly indicate aspects of the spatial pattern not captured by the BACK simulation. West of Hudson Bay and in the northern parts of the Northwest Territories, as well as in western Alaska, elevated CO features can be seen that have no analog in the BACK simulation.

Figure 5-15 shows the model-simulated boreal fire CO from the three different simulations. None of the simulations agree well with observations over North America during August. All of the simulations show large features of highly elevated CO in central Canada that are absent from the observations. This suggests that all of the products are subject to false positive detections, or at least substantial overestimates of the magnitude of August fire events. Some of this disagreement may also be attributed to overestimation of late-season fuel consumption by the BWEM-1 algorithm (see Chapter 6).

The largest feature in the GLOBSCAR simulation over North America is a large region of elevated CO in Saskatchewan and the Northwest Territories, which has no analog in the MOPITT data or the MOPITT residuals. In spite of this, the GLOBSCAR simulation agrees better with observations than either the BWEM-BA or GBA-2000

simulations. Areas of better agreement are eastern Canada and Alaska. The GLOBSCAR simulated CO over Alaska matches well with the MOPITT residuals.

MOPITT sampling properties are different above 65°N because of a difference in processing [*Deeter et al.*, 2003]. This is related to the implementation of the cloud-clearing algorithm using MODIS cloud products [*Warner et al.*, 2001]. MOPITT data on either side of this parallel have the same mean and approximate distribution, but the data density is considerably lower north of 65°N. This results in a shorter positive "tail" in the MOPITT data, and lower means in the simulated data sets sampled to match MOPITT. The strength of this effect in the simulations of boreal fire CO may be an indication of bias in this experiment.

The GBA-2000 simulation appears qualitatively to match better with the MOPITT residuals than the BWEM-BA simulation, however the correlations are similarly low for both. The GBA2000 simulation has a much larger CO source in Alaska during August. Most of the CO enhancement over Alaska in the BWEM-BA simulation is transported from Asia, which likely explains the enhanced CO over Alaska in the BACK simulation.

Overall, the results from North America from August 2000 suggest serious shortcomings in model representation of CO emissions from boreal fires. To some extent, this may be caused by problems with the fuel consumption and CO production components of the model, but many large features in the simulation have no analogs in the MOPITT data, suggesting false detections of fire activity.

Figure 5-16 shows simulated and observed CO over Eurasia during May 2000. These maps are considerably easier to interpret than the previous case, because of better

data coverage, lower spatial variability, and improved representation of anthropogenic and other non-boreal CO sources by the BACK simulation (r=0.62, compared with r=0.37 for NA August, see Table 5-4).

Numerous features in the MOPITT data over northern China and eastern Russia can be unambiguously attributed to boreal forest fire activity. The chain of features, seen most clearly in the MOPITT residuals, extending northward from the Chinese border up to the Siberian Sea is actually two different plume events a few days apart early in May. Figure 5-17 shows areas of TOMS aerosol optical depth greater than 1.5 for 5-12 May. Two distinct events are shown in this graph. The first originated along the Russian-Chinese border on 6 May and was transported northeast over the Kamchatka Peninsula to the Pacific. The second began in a very similar location on 10 May and was transported almost directly northward to the Sea of Siberia. Neither of these events was directly detected over the source by MOPITT, but both plumes strongly influenced the monthly average CO of locations to the north. The BWEM-BA simulation shows the most similarity to the observed patterns of MOPITT CO in this region, and the GBA-2000 simulation shows similar patterns, but neither appears to capture the northward extent of the later plume.

Farther west, large areas in western Russia along the Kazakh border show enhanced CO in the GLOBSCAR simulation with no corresponding signal in the MOPITT data. This discrepancy is likely from a combination of causes. The GLOBSCAR product may have false positive detections in that region, resulting from detection of old burn scars or other factors. Also, if the fires in that region are

predominantly small agricultural fires, the burned area could be substantially overestimated by the 1-km resolution of the product. Finally, the model-estimated fuel consumption may be too high, although early in the season this is less likely to be a problem. The GBA-2000 and BWEM-BA simulations do not show large enhancements in this western region, and therefore have better agreement with MOPITT observations during this period.

The GBA-2000 burned area product agreed better with the MOPITT data than did the BWEM-BA during May over Russia. The principal differences between the two are in central Russia, where the GBA-2000 burned area is greater and produces CO enhancement over a larger area. This suggests that the BWEM-BA may be missing some fires in this region.

The overall agreement between simulated and observed CO is dominated by the opposing seasonal trends in the observation and the simulation. This may be partly a consequence of the seasonal parameterization of fuel consumption in the model (see Chapter 6). Model results for individual months are highly variable and indicate that each of the burned area products has serious limitations. The BWEM-BA and GBA2000 products show better performance in most cases than the GLOBSCAR product. This is consistent with the widely observed tendency of regionally specific burned area products to have better accuracy than products using uniformly applied global algorithms. The GBA-2000 product gives the best agreement with observations overall, while the BWEM-BA product agrees better with observations during three of four months of the study period. This result suggests that the BWEM-BA gives a better depiction of the

spatial pattern of area burned, while the GBA-2000 has a more realistic seasonal cycle. However, the best results obtained by this experiment still show only weak agreement with observations, indicating that substantial improvement in burned area estimation is possible.

8. Conclusions

The comparison of three different estimates of area burned for the boreal forest showed that all three capture the same general features of fire activity in the boreal zone at very coarse spatial scales. This agreement diminishes at finer scales, where the area of overlap between estimates is much smaller than the area of disagreement. The spatial agreement between GLOBSCAR and the other two estimates does not necessarily extend beyond matching the spatial distribution of fire-prone ecosystems in the boreal zone. Each estimate has specific liabilities, and none can lay claim to systematic validation at broad scales, with the possible exception of the mapped burn scars from the Alaskan Large Fire Database, which have no analog in Canada or Russia. The lack of agreement between estimates of timing of fire activity is of particular concern, since the behavior of fire on the landscape and the atmospheric fate of emissions vary strongly with timing of fires.

The comparison of emissions estimates with observations from MOPITT showed that none of the burned area estimates used result in good agreement with MOPITT either spatially or temporally. Depending on the month and location, there were instances of each product giving the best agreement with observations. Overall, the best agreement

came from the BWEM-BA product, but agreement between simulations and observations was so low for all of the products that much improvement is evidently possible.

This experiment is not able to estimate the absolute error in area burned, because the total emissions are dependent not only on the area burned but on the assumptions in the emissions model, and comparison with atmospheric observations will depend on the magnitude of simulated CO from other sources. Likewise, this experiment does not indicate the correct seasonal cycle of fire activity for the study period, because the fuel consumption of fires varies with season in ways that are not well-understood.

This experiment serves as an evaluation of the utility of currently available burned area products for estimating the spatial and temporal distribution of the boreal fire CO source. The results obtained indicate that substantial discrepancies exist between the sources, and that these discrepancies have important impacts for both the spatial and temporal distribution of CO in the HNH.

9. Tables

		Area burned (Mha)	Carbon release (Tg)	CO release (Tg)	Fuel Consumption (t C ha-1)
Alaska	**BWEM-BA**	0.30	4.55	1.66	15.02
	GLOBSCAR	0.21	3.10	1.11	15.03
	GBA2000	0.25	5.46	2.14	21.42
Canada	**BWEM-BA**	0.62	12.05	4.66	19.31
	GLOBSCAR	3.65	63.74	24.05	17.48
	GBA2000	0.53	12.75	5.11	23.99
Russia	**BWEM-BA**	NA	NA	NA	NA
	GLOBSCAR	19.85	254.84	97.16	12.84
	GBA2000	21.79	199.04	72.10	9.13
E. Russia	**BWEM-BA**	9.36	103.84	36.09	11.09
	GLOBSCAR	14.26	189.60	71.09	13.30
	GBA2000	18.39	166.55	59.70	9.06

Table 5-1. Total area burned, emissions and fuel consumption for 2000 as estimated with each burned area product.

		BWEM-BA vs. GLOBSCAR	BWEM-BA vs. GBA2000	GLOBSCAR vs. GBA2000
2° by 2.5°				
	Alaska	0.42	0.96	0.43
	Canada	0.52	0.91	0.56
	Russia	0.29	0.51	0.71
	E. Russia	0.67	0.75	0.82
	All	0.29	0.51	0.70
4° by 5°				
	Alaska	0.56	1.00	0.58
	Canada	0.66	0.94	0.68
	Russia	0.29	0.50	0.82
	E. Russia	0.71	0.77	0.85
	All	0.29	0.50	0.81
8° by 10°				
	Alaska[a]	0.86	1.00	0.88
	Canada	0.74	0.95	0.81
	Russia	0.31	0.48	0.88
	E. Russia	0.73	0.76	0.89
	All	0.31	0.48	0.87

[a]At a resolution of 8° latitude by 10° longitude, almost all of Alaska falls into a single grid box, making the comparison of spatial pattern invalid. The GLOBSCAR product has a correlation less than 1.0 because of a small area on the Aleutian Islands.

Table 5-2. Correlations between gridded total area burned for 2000 for 3 different burned area products, calculated at 3 different spatial resolutions.

	BWEM-BA vs. GLOBSCAR	BWEM-BA vs. GBA2000	GLOBSCAR vs. GBA2000
Alaska	0.11	0.48	0.10
Canada	0.19	0.45	0.30
Russia	0.10	0.24	0.34
E. Russia	0.23	0.37	0.44
All	0.10	0.24	0.33

Table 5-3. Correlations between gridded (2° by 2.5°) monthly area burned for 2000 for 3 different burned area products.

		HNH		N. America		Eurasia	
All	**R**	0.50		0.42		0.55	
	mean error[a]	-4.34E+17	-27%	-4.42E+17	-29%	-4.03E+17	-25%
	s.d. of error[b]	2.72E+17	63%	3.16E+17	71%	2.43E+17	60%
May	**R**	0.52		0.60		0.62	
	mean error	-5.88E+17	-32%	-6.34E+17	-37%	-5.53E+17	-31%
	s.d. of error	2.17E+17	37%	1.97E+17	31%	1.96E+17	35%
June	**R**	0.47		0.46		0.51	
	mean error	-5.05E+17	-31%	-5.37E+17	-35%	-4.77E+17	-30%
	s.d. of error	2.68E+17	53%	2.47E+17	46%	2.63E+17	55%
July	**r**	0.41		0.41		0.50	
	mean error	-4.02E+17	-26%	-4.16E+17	-29%	-3.58E+17	-23%
	s.d. of error	2.62E+17	65%	2.86E+17	69%	2.21E+17	62%
August	**r**	0.48		0.37		0.58	
	mean error	-3.72E+17	-23%	-3.39E+17	-22%	-3.52E+17	-22%
	s.d. of error	2.67E+17	72%	3.73E+17	110%	2.15E+17	61%

a. Errors are given in molecules cm^{-2} and as a percentage of the mean MOPITT TC.

b. S.D. of errors is given in TC units (molecules cm^{-2}) and as a fraction of the mean error (coefficient of variation).

Table 5-4. Statistical comparison between simulated model CO without any boreal fire source included and MOPITT observations. Errors are given as mean absolute error in molecules cm^{-2}, and as a fraction of MOPITT TC. Scatter in model errors is estimated using the standard deviation of model errors, which is shown in TC units as well as CV.

10. Figures

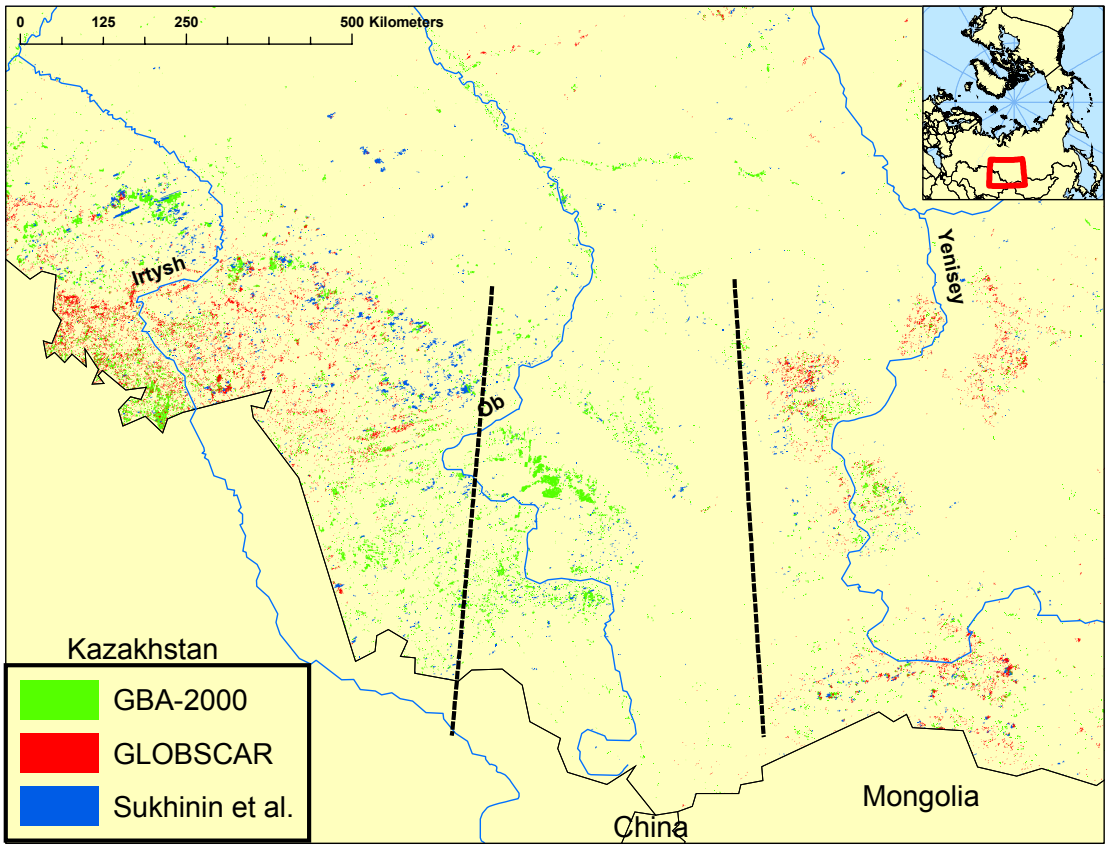

Figure 5-1. Data gap in GLOBSCAR burned area. Burned area detections from GLOBSCAR are shown in red. The area of the data gap is between the dotted lines. From this figure, it is clear that that BWEM-BA (in blue) has very few fires in this region, while the GBA-2000 product (green) shows substantial burned area.

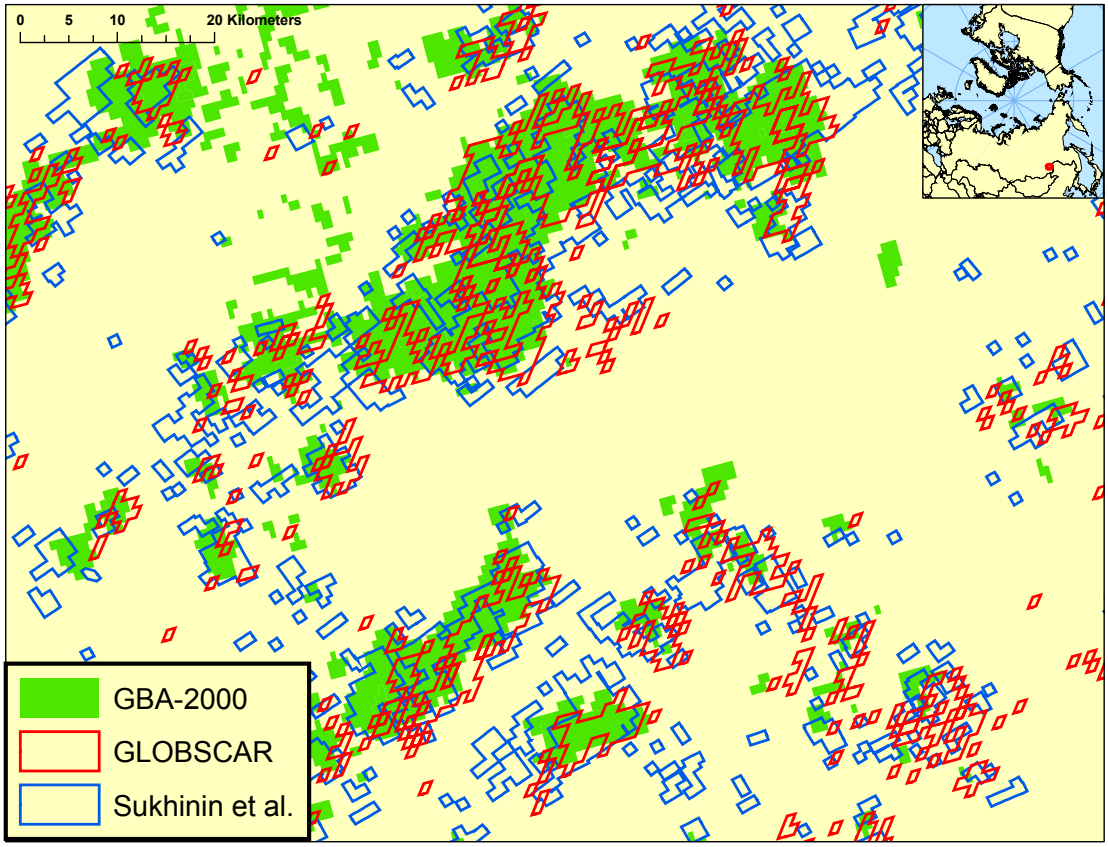

Figure 5-2. Difference in spatial pattern resulting from application of region-growing algorithms. The contrast between the GBA2000 burned areas (green) and the other products shows clearly the effects of the region-growing mechanism used to fill in burn scars in the GBA-2000 product.

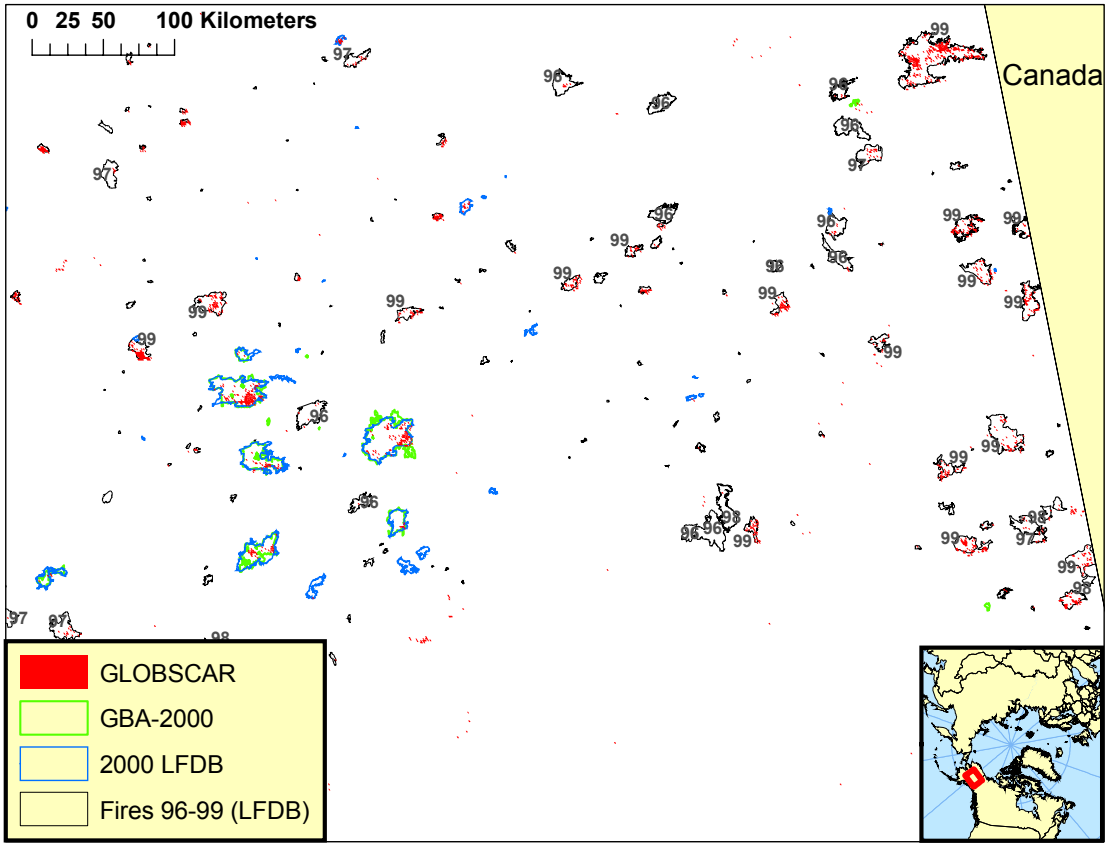

Figure 5-3. Recent fire history from the Alaska Large Fire Database (2000 in blue, 1996-1999 in gray) showing the tendency of the GLOBSCAR product (red) to include burned areas from previous years' fires.

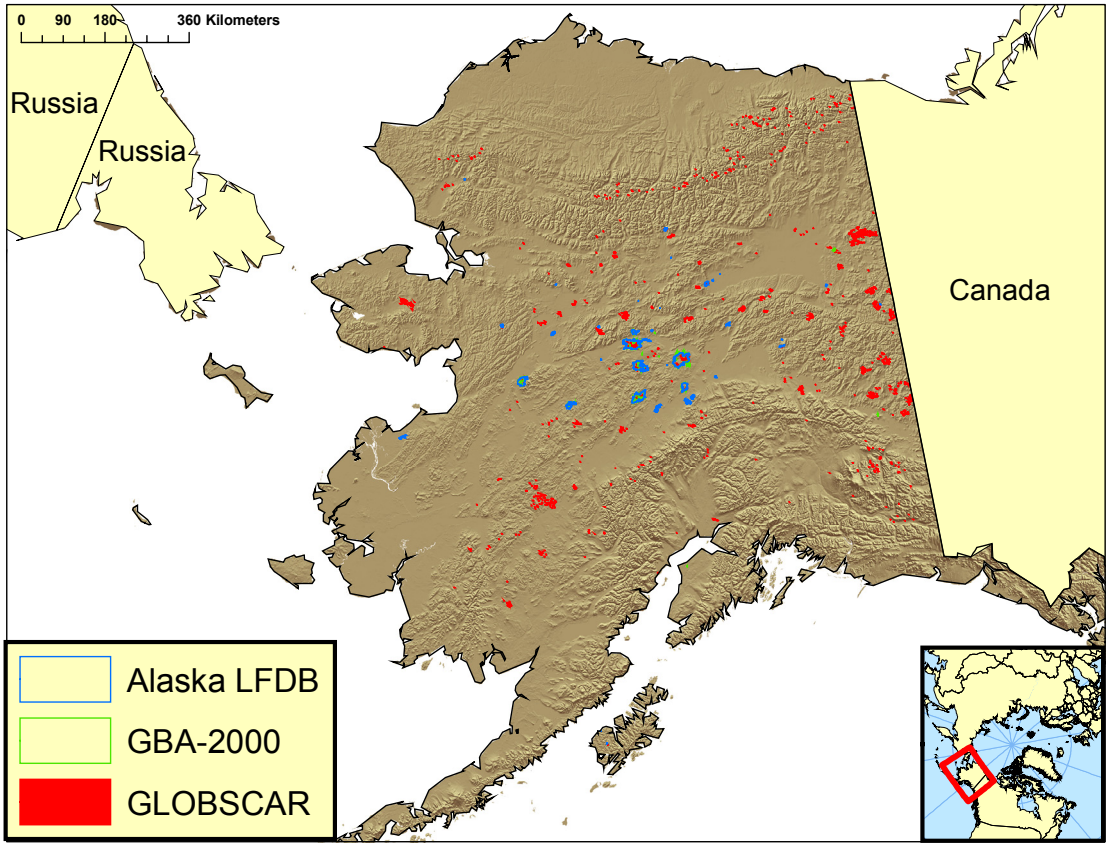

Figure 5-4. Burn scars from the Alaska LFDB as well as GLOBSCAR and GBA2000 burned areas for 2000. Note the numerous detections in the GLOBSCAR product (red) at high elevations in the Alaska and Brooks ranges.

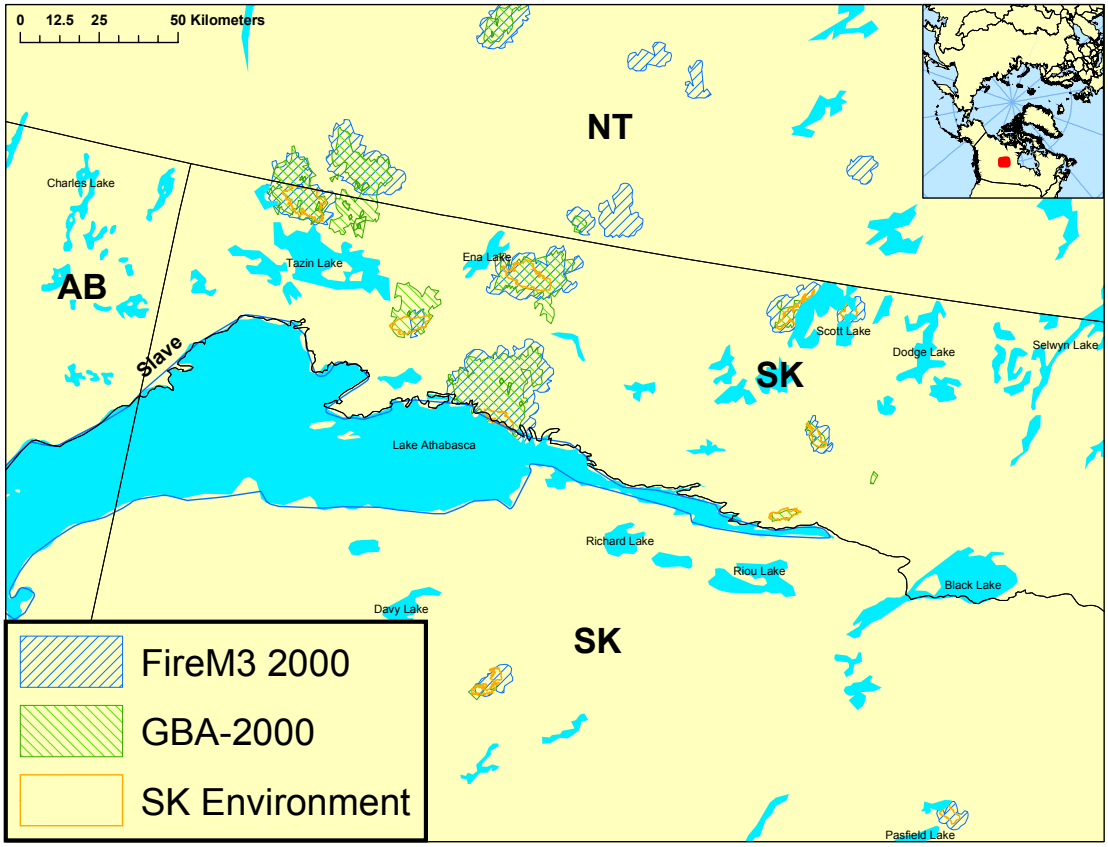

Figure 5-5. Comparison of FireM3-derived fire areas (blue) with burned areas from the GBA2000 product (green) and burn scars mapped by Saskatchewan Environment (orange). All burned areas from the Saskatchewan Environment data were captured by one of the other burned area products, but neither product captured all of the mapped burns. Burned area estimates from GBA2000 are considerably larger than the mapped scars. Areas of boundaries from FireM3 are scaled before use in BWEM-BA emissions calculations; see text for details.

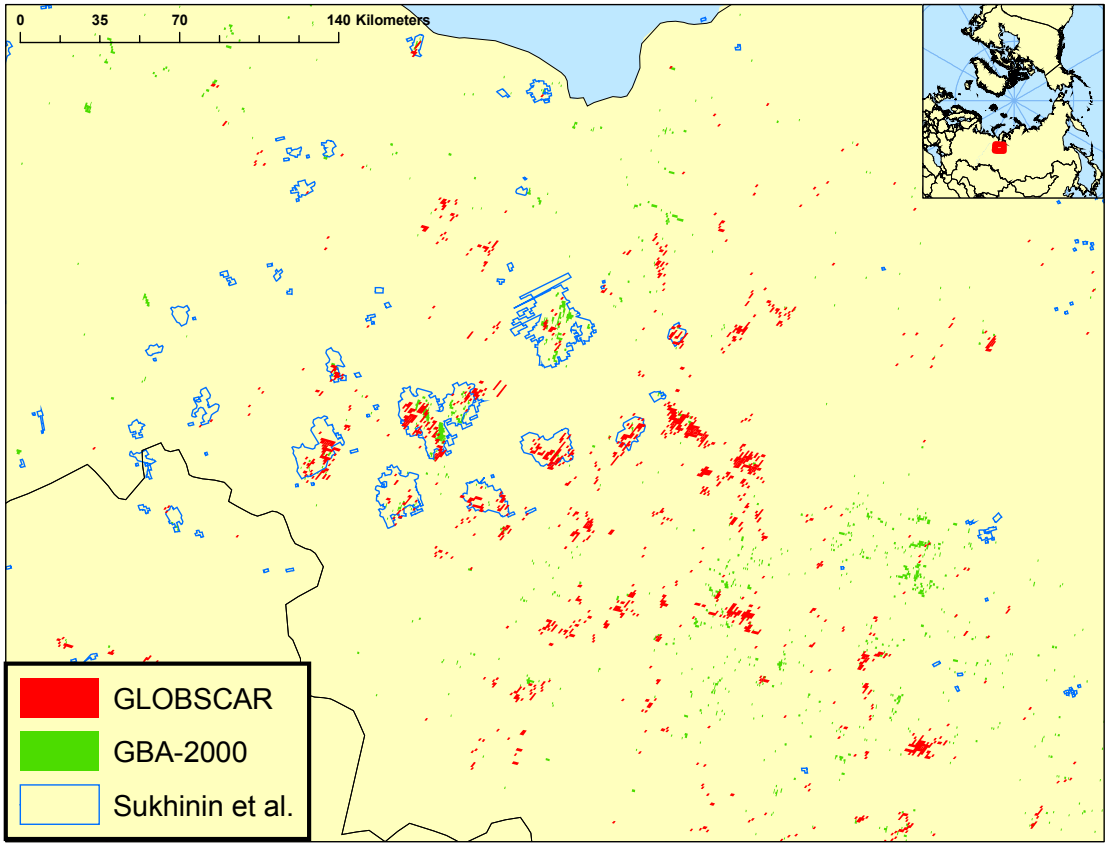

Figure 5-6. Burned area in a region of north-central Russia estimated by three different methods. Area of overlap is a small fraction of total area burned in each product.

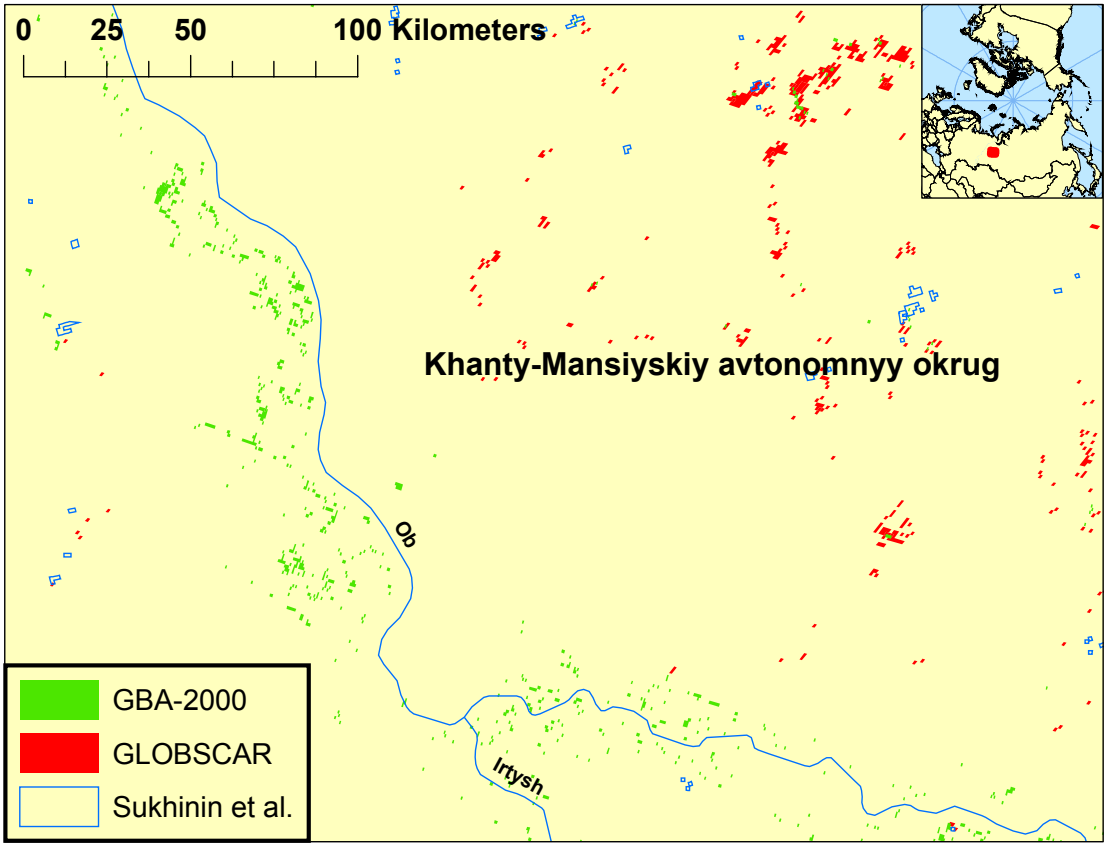

Figure 5-7. Burned area detections along the Ob and Irtysh rivers in Khanty-Mansiskiy. The concentration of GBA-2000 detections (green) near the major rivers suggests that this product may actually be picking up anthropogenic disturbances as well as forest fires.

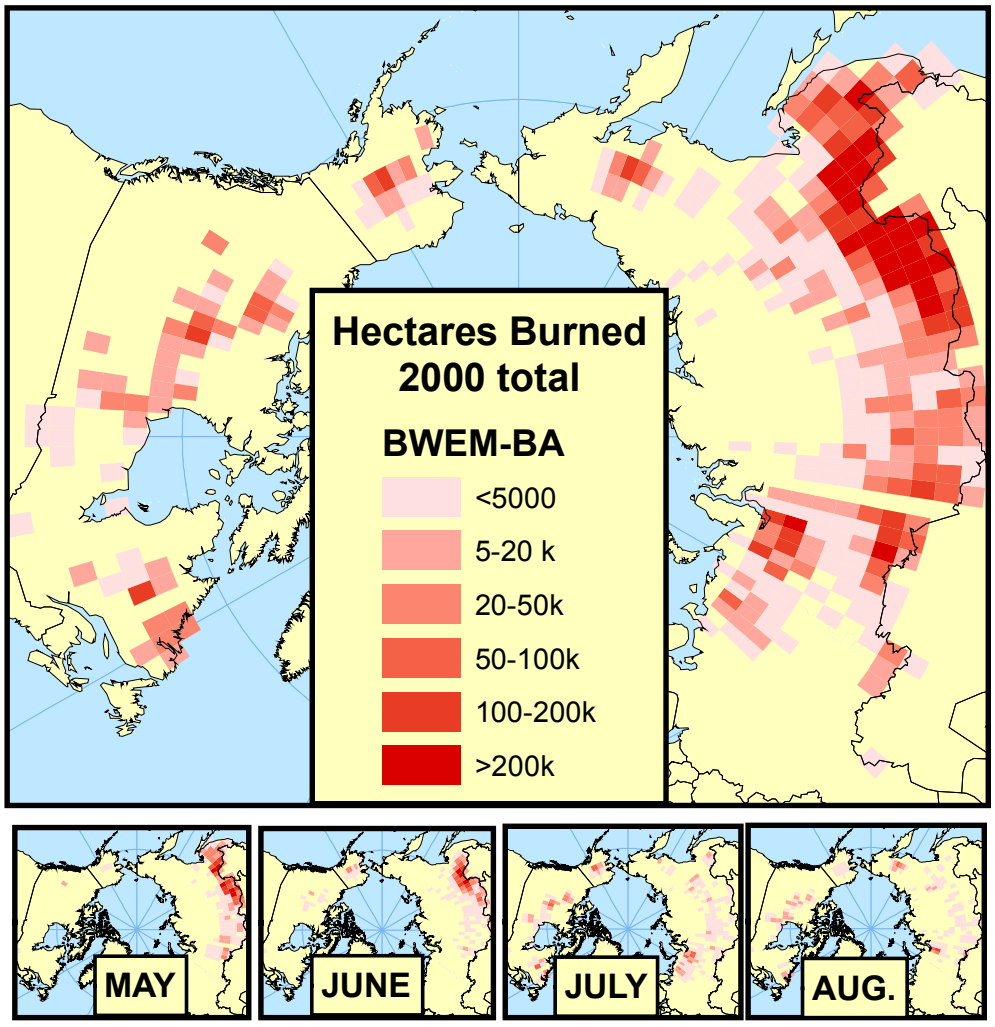

Figure 5-8. Burned area from the BWEM-BA, gridded to a resolution of 2° latitude by 2.5° longitude.

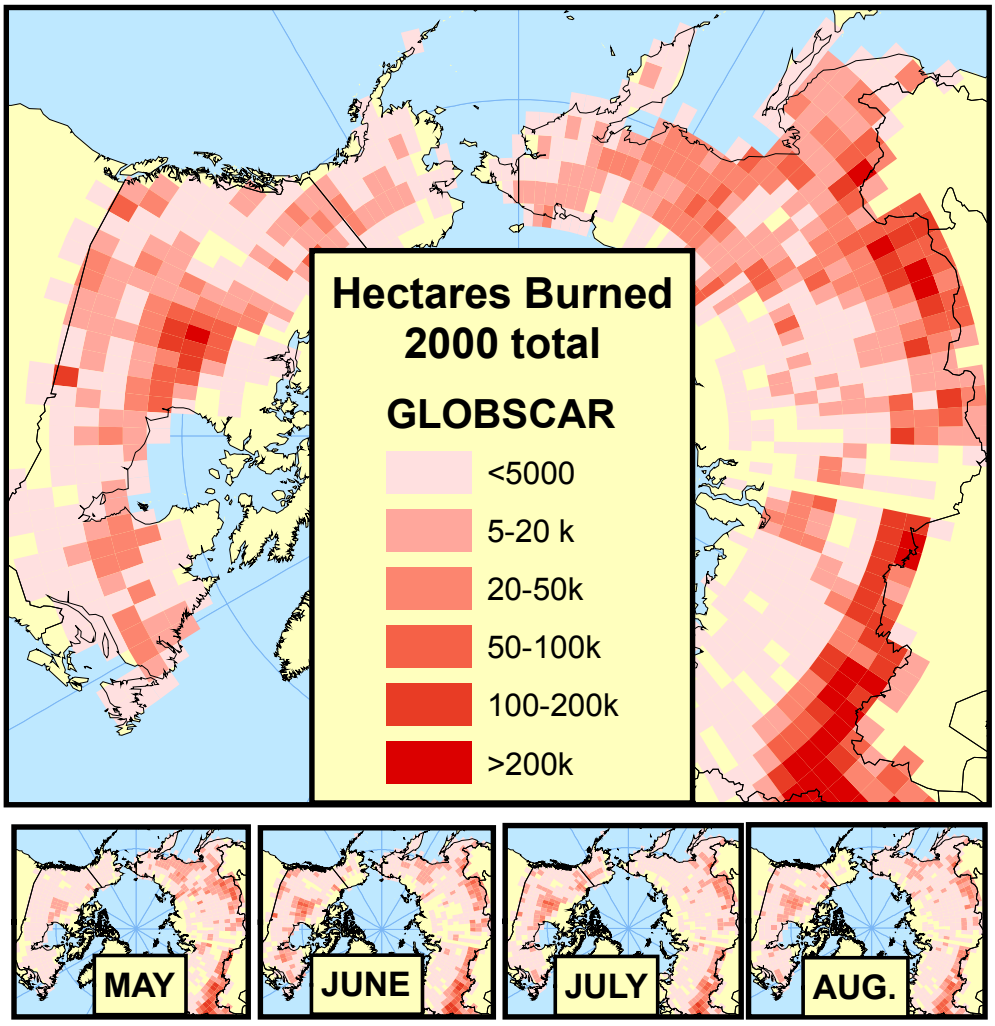

Figure 5-9. Burned area from GLOBSCAR, gridded to a resolution of 2° latitude by 2.5° longitude.

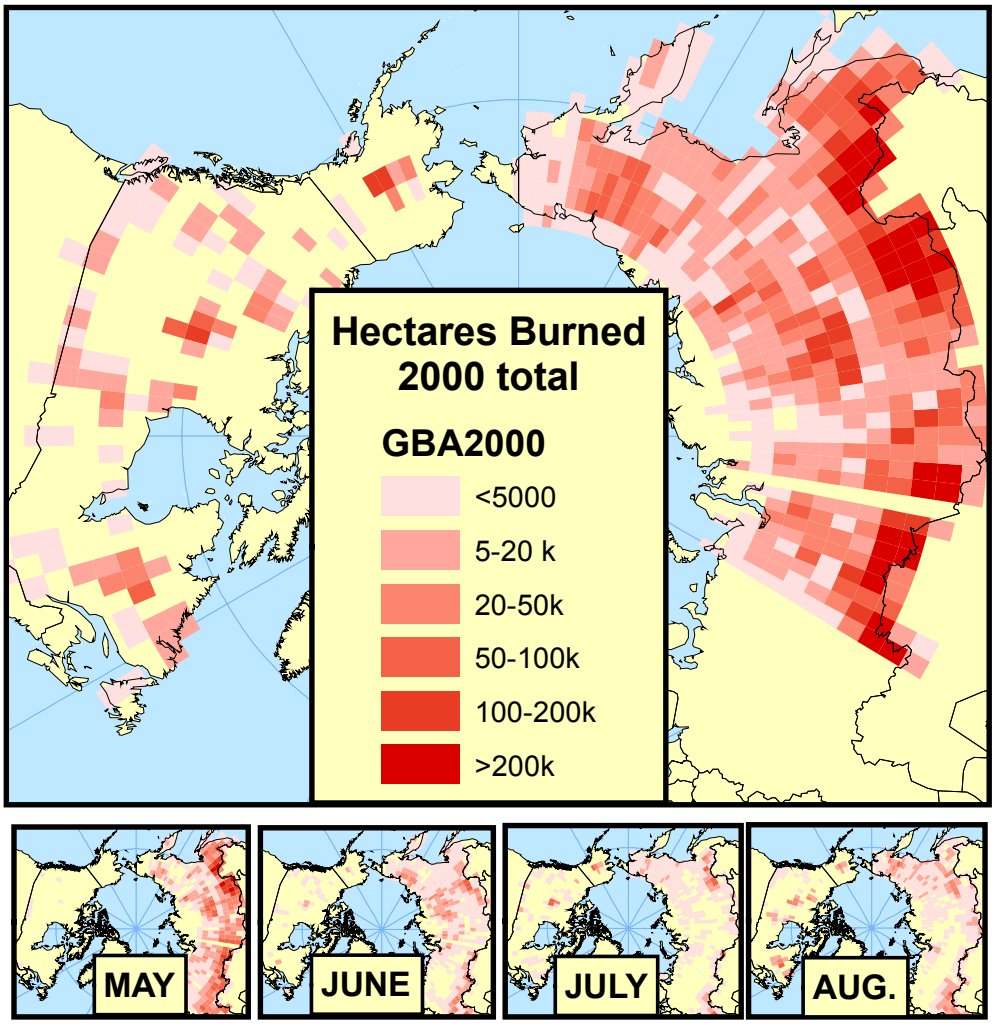

Figure 5-10. Burned area from GBA2000, gridded to a resolution of 2° latitude by 2.5° longitude.

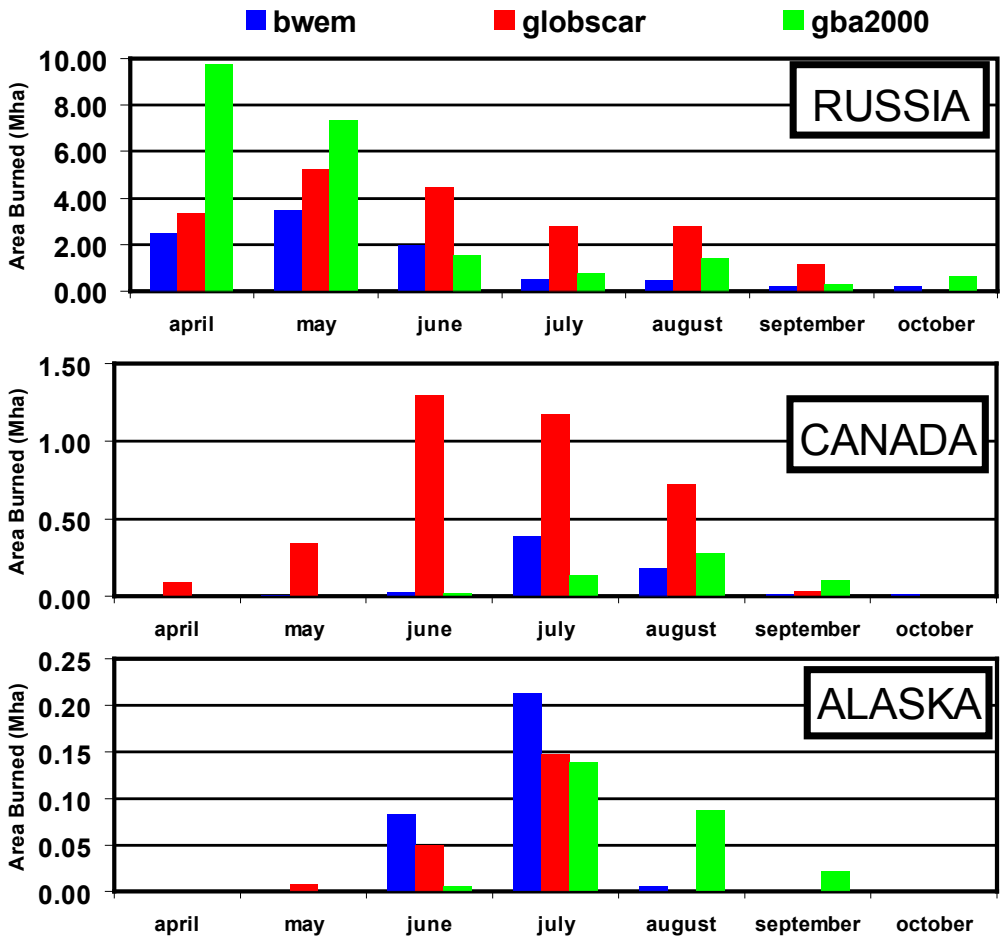

Figure 5-11. Monthly area burned for Alaska, Canada and Russia from BWEM-BA, GLOBSCAR and GBA-2000 products.

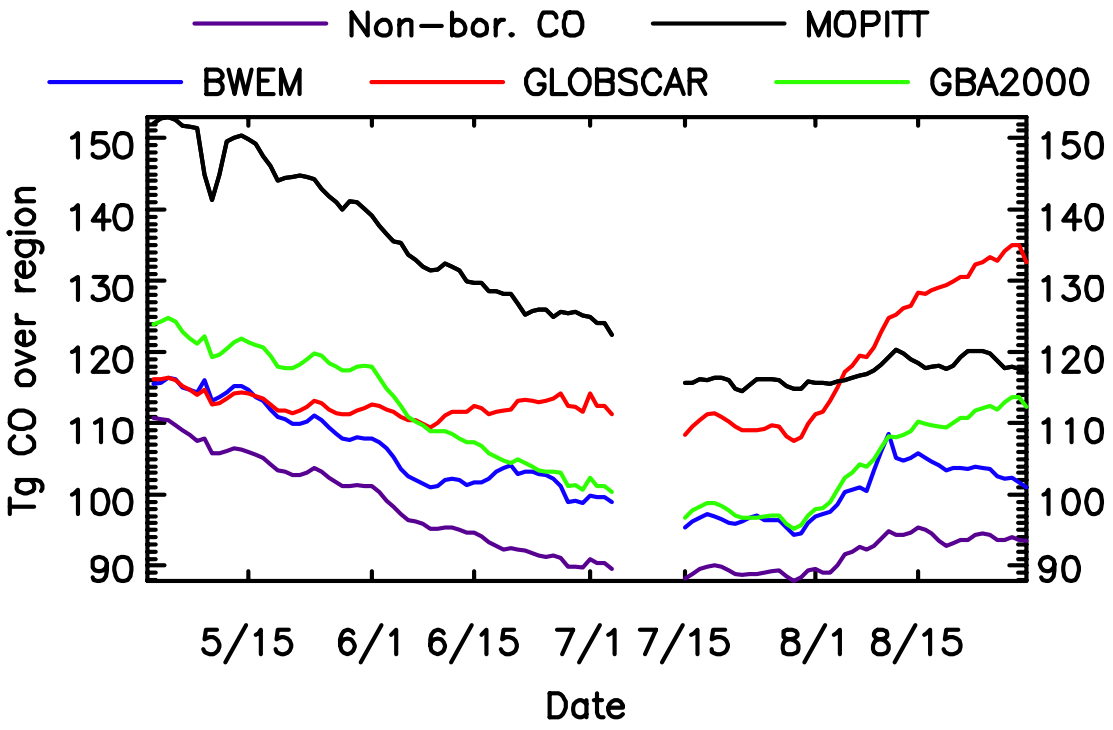

Figure 5-12. Time series of HNH CO burden from MOPITT data and simulations. A three-day moving average is applied to this series to minimize errors related to the sampling rate of MOPITT.

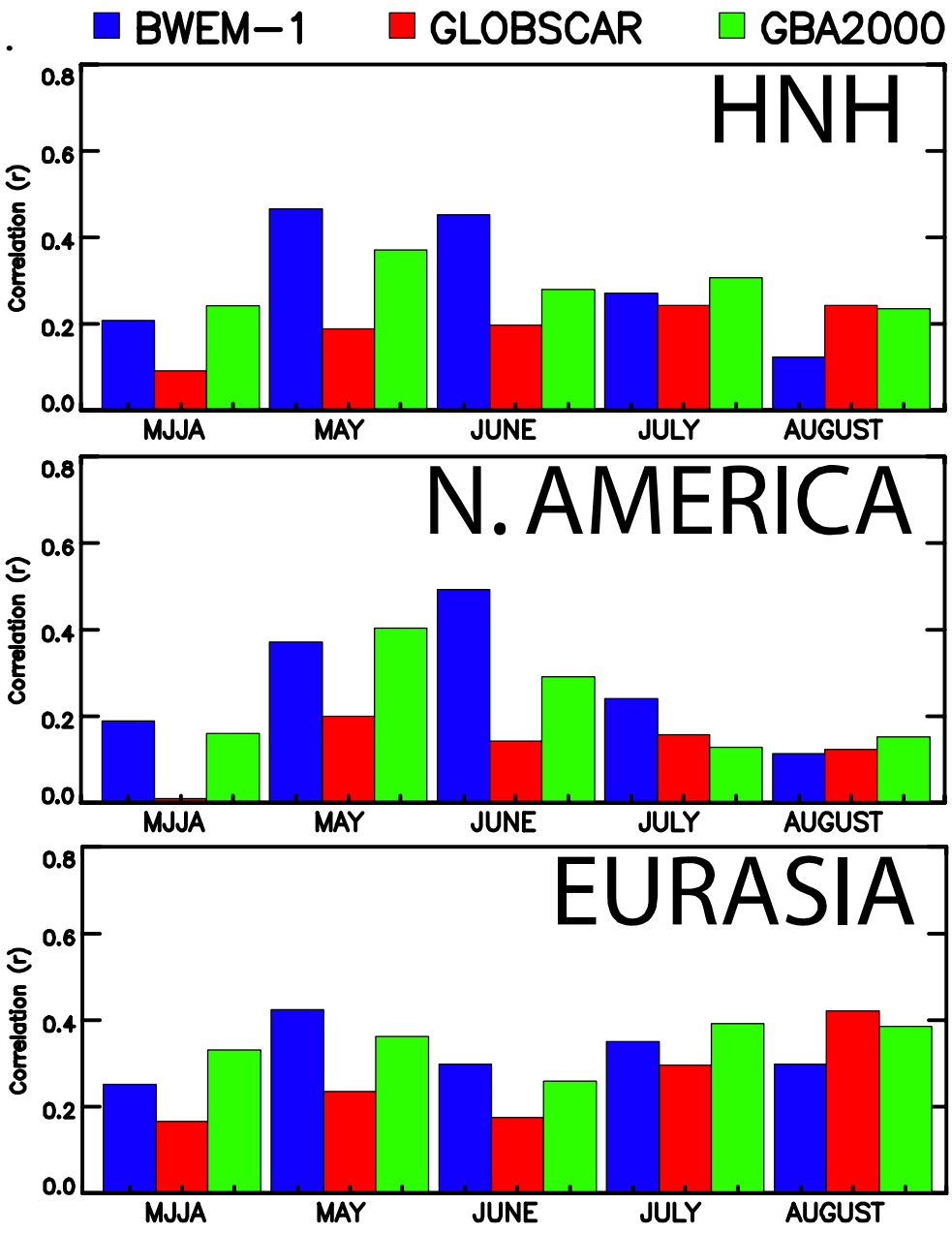

Figure 5-13. Correlations between simulated TC CO and MOPITT observations, broken down by month and region for each of the simulations. Correlations were calculated by first subtracting simulated CO from non-boreal sources from MOPITT observations, and then comparing simulated boreal CO to the residuals thus obtained.

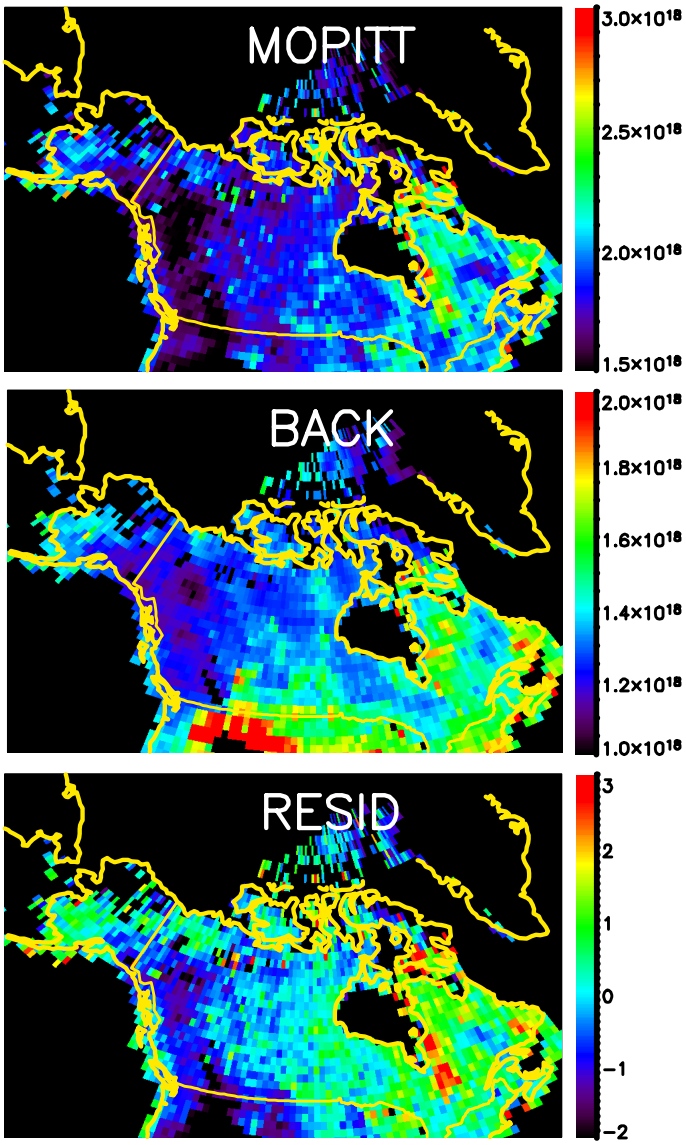

Figure 5-14. MOPITT observations and simulations results. Shown here are MOPITT retrievals over North America during August 2000 aggregated to a 1 by 1 degree grid. (a) MOPITT observations and (b) the BACK simulation are shown in units of total column CO (molecules cm-2), but note that the scales are different. The bottom map (c) shows residuals obtained from subtraction of the BACK simulation from the MOPITT data. These residuals are shown as z-scores (standard deviations from the mean).

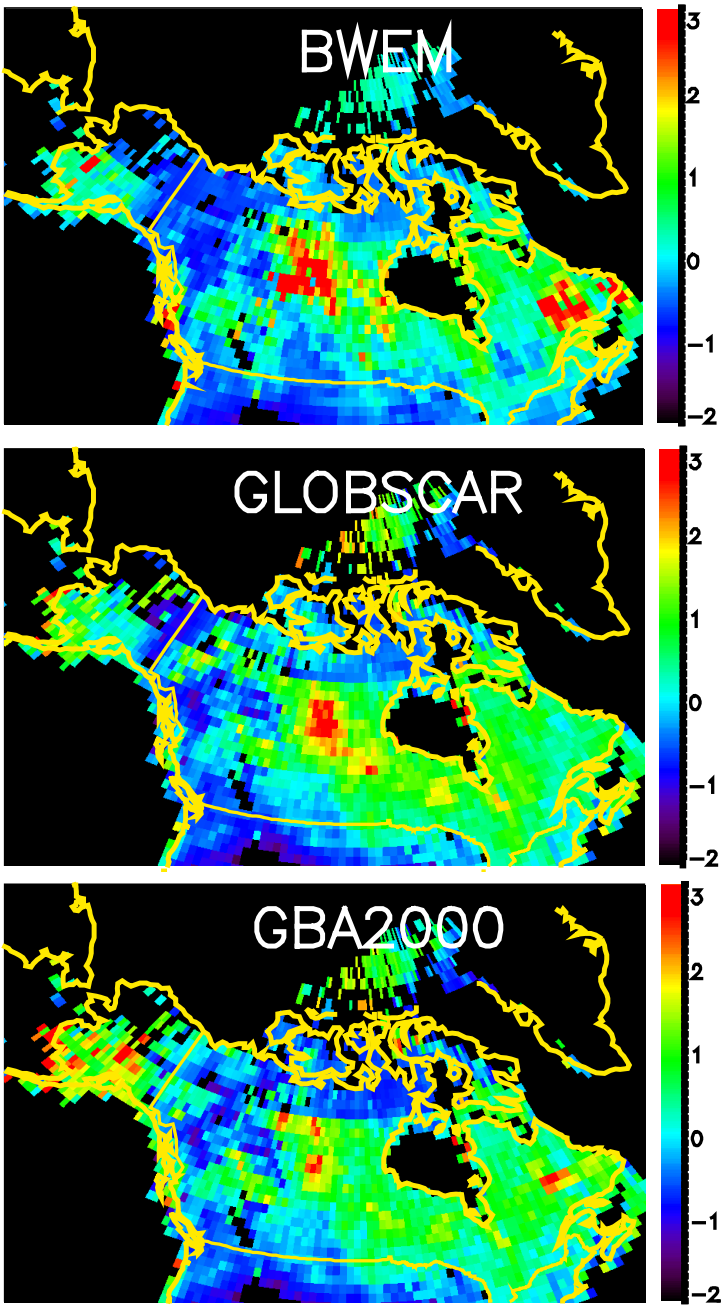

Figure 5-15. Simulated CO contribution from boreal fires over North America during August 2000, from CTM simulations using three different burned area products. Units are z-scores.

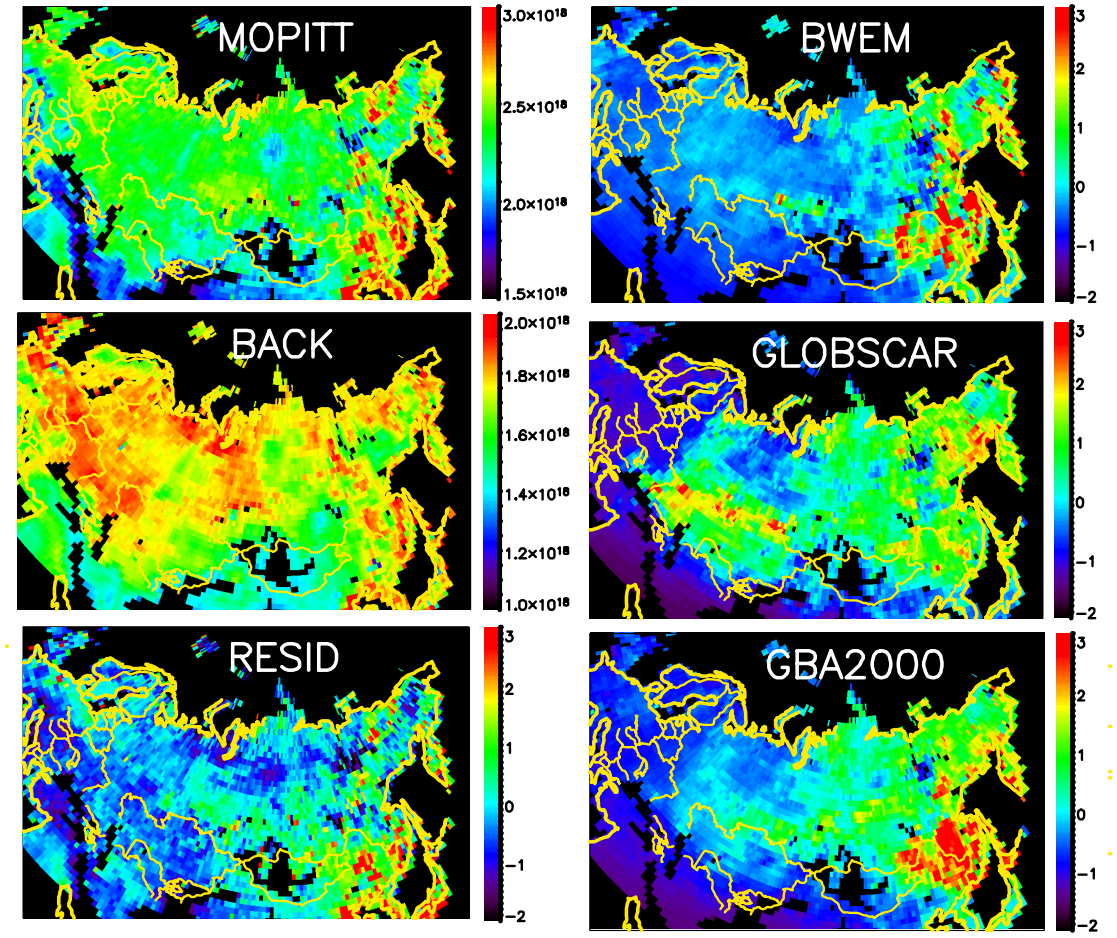

Figure 5-16. MOPITT observations and model results for Eurasia in May 2000.

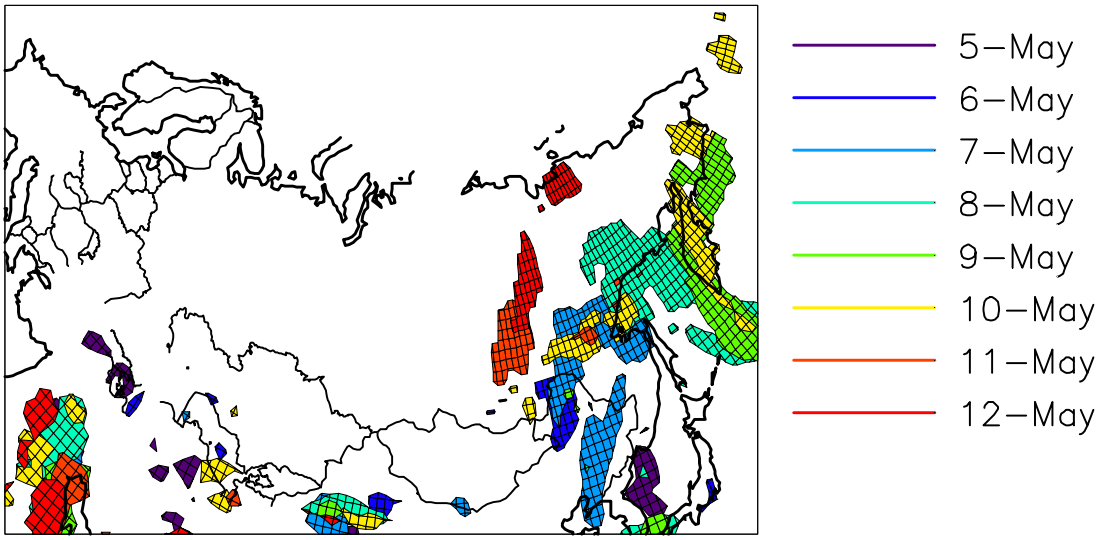

Figure 5-17. Contours of areas with TOMS aerosol index greater than 1.5 during 5-12 May. The evolution and northward transport of two different events can be seen in this graph.

Chapter 6. Quantifying the atmospheric signal from spatial variability of fuel consumption in the boreal forest

1. Abstract

Carbon and trace gas emissions from the boreal forest during 2000 were simulated using a spatially and temporally resolved emissions model. Three different algorithms were applied to the same source data to produce emissions estimates for comparison. Comparison of the carbon emissions estimates showed that at the scale of a global emissions model (2° latitude by 2.5° longitude), area burned was by far the most important determinant of emissions per grid cell. Seasonal variations in fuel consumption were a larger source of variance than spatial variation at the scale of the atmospheric transport simulation. The largest source of variation in fuel consumption per area burned came from the seasonal parameterization of fire type and severity in the algorithm used by *Kasischke et al.* [2005]. CO emissions estimates were used in a CTM to simulate atmospheric patterns of CO from boreal forest fires. Comparison of these estimates with observations from the MOPITT instrument showed that the seasonal assumptions of *Kasischke et al.* [2005] result in differences between early and late-season fires for 2000 that do not match observations. The best agreement with observations over North America was obtained with a model using broad regional estimates of fuel consumption. Spatially resolved fuel models produced better agreement with observations for each month of the study period when compared with a tracer with fixed fuel consumption. Over the entire study period, fuel models without strong seasonal variability gave better agreement than the fixed-fuel tracer. More research is needed to construct a more

complete description of fire behavior and its seasonal trends, and determine if the conclusions of this study can be applied to years with different levels of fire activity.

2. Introduction

Estimates of global trace gas emissions from biomass burning are based on estimates of area burned, fuel density, and fractional fuel consumption developed through spatial extrapolation of limited experimental and field survey data [*Hao and Liu*, 1994; *Laursen et al.*, 1992; *Seiler and Crutzen*, 1980]. Regional studies of African biomass burning showed the importance of interannual variability and the potential of remotely sensed data to improve estimates of area burned and interannual variability [*Barbosa et al.*, 1999; *Hely et al.*, 2003; *Korontzi et al.*, 2003a; *Korontzi et al.*, 2003b; *Scholes et al.*, 1996]. A recent modeling study by *van der Werf et al.*[2003] used remotely sensed data to determine fire size, location and timing, and also incorporated a biogeochemical model, the Carnegie-Ames-Stanford Approach [*Potter et al.*, 1993], to dynamically estimate available fuel. This approach resulted in considerable spatial variability in fuel loads both between and within ecosystems, and indicates that applying average fuel estimates over broad regions may be a source of considerable error in spatially resolved emissions estimates.

Recent estimates of carbon emissions from boreal forest fires have used spatially explicit approaches to estimate fuel consumption, based on newly available maps of above-ground and ground-layer biomass [*French et al.*, 2000; *French et al.*, 2002; *Kajii et al.*, 2002; *Kasischke et al.*, 2005; *Soja et al.*, 2004]. The biomass data are used as input to fuel consumption algorithms to yield spatial patterns of carbon release that vary

depending on model assumptions. In all of these approaches, the model assumptions are developed from a small set of field observations extrapolated to describe the process over broad spatial scales. Comprehensive validation of fuel consumption using field measurements is challenging for individual fire events, and impossible for broad-scale averages.

In this study, the spatial variability in fuel consumption was examined indirectly using atmospheric carbon monoxide measurements from the MOPITT instrument. Carbon monoxide is used in this study as a proxy for total carbon emissions, in the absence of reliable data to constrain the variability in emissions factors [*Hyer,* 2001]. Several variations of a model of boreal forest fire emissions were used as input to a global chemistry and transport model (CTM), and the output of this model was compared with observations. The goal of this study was to determine how much effect spatial variability in fuel consumption has on atmospheric composition as observed from space, and to examine whether the inclusion of spatially explicit treatments of fuel consumption could improve agreement with these observations.

3. Variability in fuel consumption of boreal forest fires

Kasischke et al. [2005] developed a spatially and temporally explicit model of boreal forest fire emissions, which they refer to as the BWEM-1. This model integrates spatially explicit maps of fuel loading with information about fire size, location, and timing to produce estimates of carbon and trace gas emissions that are useful at a range of scales. This model has the flexibility to accommodate a wide variety of parameterizations of fire behavior, as well as different data sets for fire activity and fuel loading. This study

uses four emissions estimates, each based on a different treatment of spatial and temporal variability in fuel consumption. This section provides an overview of the treatment of fuel loading and fuel consumption in the BWEM-1.

3.1. Fuel loading data sources for the BWEM-1

The fuel loading information for the BWEM-1 comes from a variety of published regional databases. Aboveground and ground-layer biomass are critically important pieces of information for any kind of carbon cycle study. However, no systematic surveys have ever been undertaken of these variables. Regional-scale estimates of these ecosystem properties are constructed by extrapolation of scattered field measurements in small plots. *Alexeyev et al.* [2000] divide regional-scale estimates of ecosystem properties into two methodological categories: geobotanical and statistical. Both of these approaches rely heavily on detailed measurements taken at small plots to constrain complex ecosystem properties at broad scales. The difference between these methods lies in how the extrapolation is achieved from small isolated plots to a continuous regional database.

The statistical approach is used when a systematically sampled database of an ecosystem property related to the target characteristic is available. In this case, extrapolation is performed by describing the relationship between the property catalogued in the database and the target characteristic using intensive plot measurements, and then applying that relationship to the statistical database. The geobotanical approach is used when no such systematically sampled database exists. In this case, data from intensive

field plots are extrapolated using available data about landscape characteristics, such as physiography and drainage, which govern the distribution of ecosystem types.

The BWEM-1 estimates fuel consumption separately for aboveground and ground-layer fuels. In the next section, the data sources used to estimate total aboveground and ground-layer biomass will be described. The following section (3.2) deals with the model assumptions that are used to estimate fuel consumption.

3.1.1. Above-ground fuel loading in the BWEM-1

Above-ground biomass in Russia is taken from a published database by *Alexeyev and Birdsey* [1998] (available from *Schlesinger and Stone* [2001]). This database is based on application of statistical model of biomass density to a map of timber stocks based on forestry surveys and classification of aerial photography. This database has sufficient resolution to capture the variability in fuel loading caused by regional differences in ecosystem types and species composition, but variability at finer scales related to stand age and disturbance is not included. Thus, this database does not provide the spatial coverage and up-to-date data of approaches using dynamic vegetation models driven by satellite observations (e.g. *van der Werf* [2003]), but does offer reasonable absolute accuracy of fuel loading in diverse ecosystem types of Russia from northern tundra to southern mixed forest-steppe.

Canadian above-ground biomass is estimated by a similar method from surveys of forest stocks undertaken as part of a regular forest inventory activity in Canada [*Lowe et al.*, 1996; *Penner et al.*, 1997]. This database uses data that is generally more recent than

the Russian data, but like the Russia data, this dataset is not current and does not account for recent stand aging or disturbance.

Above-ground biomass for Alaska was constructed using a geobotanical method, extrapolating carbon estimates from intensive field plots using a physiographic database [*Kasischke et al.*, 1995b].

All of these databases give total aboveground biomass as an output parameter. This parameter is used directly by the emissions estimation algorithm in the BWEM-1. Details of that algorithm are given below, in section 3.2.

3.1.2. Ground-layer fuel loading in the BWEM-1

Ground-layer databases for both North America and Russia were constructed from soil surveys with a geobotanical extrapolation method. The soil survey data for both databases were far more numerous than intensive plots for above-ground biomass. However, the soil survey represents a non-statistical evaluation of soils taken from measurements at sites selected to be typical of a given soil type. Russian soil carbon data comes from *Stolbovoi and McCallum* [2002]. A 1:2.5 million soil classification map [*Fridland*, 1988] was used to extrapolate data from intensive field plots to a continuous regional database. These data include the estimated carbon content in the top 30 centimeters, which is used as an indicator of carbon density by the BWEM-1 fuel consumption algorithms. These data cover the entire geographic extent of Russia, but the information they provide is essentially potential carbon storage, because this database has no accounting for disturbance and land cover change.

North American soil carbon is taken from a database constructed from soil survey data [*Lacelle et al.*, 1997]. These data were constructed by a similar process of extrapolation from intensive measurement sites to regional coverage using physiographic characteristics. The soil characteristics in this database are generalized estimates that do not account for disturbance or land cover change. Technical details of this database can be found in *Lacelle* [1997]. The data set relevant to fuel loading estimation is the total carbon content of the organic soil horizon.

3.2. Parameterization of fuel consumption in the BWEM-1

To derive fuel consumption from these biomass estimates, a number of model parameters are employed which describe the fuel structure and fire behavior. The choice of parameters is intended to permit flexible investigation of the key uncertainties in forest fire behavior, and also to correspond as closely as possible to observable properties of boreal forest stands. The choice of values for these parameters reflects the results of field investigations of fire behavior and carbon cycling, and the best current scientific understanding of the biomass burning process in the boreal forest. This discussion is adapted from *Kasischke et al.* [2005], and deals separately with consumption of aboveground and ground-layer fuels.

3.2.1. Consumption of above-ground fuels

Maps of aboveground biomass provide an estimate of the total carbon in living and dead tissue in a given stand. To begin applying this information to a model of fuel consumption, the first factor that must be considered is the fraction of fuel available for burning. In mature stands, it is well-established that the majority of the biomass will be in

thick stems which are not available as fuel [*Kasischke et al.*, 1994]. The overall fraction of fuel consumed is therefore quite low for these forests, even though areas of lower productivity may have a large fraction of biomass in flammable reservoirs. The BWEM-1 model estimates the fraction of biomass in the flammable fuel types—leaves, fine twigs, and dead woody debris—as a function of the total stand biomass: stands with higher biomass have proportionally less fuel available for burning.

The fraction of available fuel that is actually consumed by fire is dependent on fuel moisture and fire type. Fuel moisture is determined on short time scales (days to weeks) by meteorological factors, and on longer time scales (weeks to months) by water availability in soils [*Johnson*, 1992]. The short-term variability in fuel moisture can be parameterized with meteorological inputs [*Amiro et al.*, 2001; *Stocks et al.*, 1989]. These inputs are not included in the BWEM-1, and so fine-scale variability in fuel consumption is not represented in the BWEM-1. Fuel moisture is parameterized by a seasonal approximation based on observations of variation in fire severity with timing of fire in the growing season [*Kasischke et al.*, 2000].

Fire type is represented in the model by separate fuel consumption values for crown and surface fires, and parameterization of the fraction of each type in each part of the season. In the North American boreal forest, most of the area burned is in stand-replacing crown fires [*Stocks*, 1987; *Stocks and Kauffman*, 1997]. The behavior of fires in the Russian boreal forest falls along a continuum from fires burning intermittently through surface fuels and causing almost no tree mortality to stand-replacing crown fires similar to those common in North America. Surface fires have generally been assumed to

dominate area burned in the Russian boreal forest [*Shvidenko and Nilsson*, 2003], but studies using remotely sensed imagery of burned areas suggest canopy mortality greater than is consistent with only surface fires [*Isaev et al.*, 2002; *Kasischke et al.*, 1999]. The division of Russian burned areas into crown and surface fires in the BWEM-1 varies by season, with early-season fires assumed to burn mostly in surface fuels, and a higher fraction of crown fires later in the season.

The range of available fuels in the input biomass data is larger than the range of fuel consumption estimates after application of the algorithm for determining the fraction of fuel available for burning. The parameterization of fire types further suppresses this spatial variability, while introducing a seasonal dependence into the estimates. Application of the fuel consumption algorithm to the aboveground biomass data results in seasonal variability that exceeds spatial variability: late-season fires in areas with low biomass density will have higher fuel consumption than early fires in areas with high biomass density.

3.2.2. Consumption of ground-layer biomass

Burning of ground-layer fuels is responsible for one-half to two-thirds of the carbon release estimated by the BWEM-1 [*Kasischke et al.*, 2005]. This proportion is higher in the largest fire years. The contribution of ground-layer fuels to CO emissions is proportionally greater, because of the predominance of inefficient smoldering combustion in this layer [*Yokelson et al.*, 1997].

Consumption of ground-layer fuels is parameterized in the BWEM-1 by using spatial data to estimate the vertical profiles of carbon density, and then estimating

average depth of burn based on fire type and seasonality. Field measurements in several different boreal forest types indicate that carbon density in the first few centimeters is constant and consistent across forest types [*Kasischke et al.*, 2005]. Therefore, the carbon density from the soil carbon database is used only to estimate the carbon content of deeper layers, which are only consumed in severe fires. Thus, for the most part, the variability in ground-layer fuel consumption varies mostly depending on the fire type and timing during the fire season, and only in late-season fires does it show a strong dependence on the soil carbon map. Given that fire type and severity are strongly linked to timing of fires in the BWEM-1, the temporal variability in ground-layer fuel consumption is again greater than the spatial variability. The variability in overall CO emissions will show a proportionately stronger influence of this seasonal variability.

4. Methods

Estimates of carbon emissions constructed using three different scenarios of fuel consumption were compared for this study. These scenarios used the same inputs of fuel loading, fire size, location and timing. The differences between these scenarios related only to the description of fire behavior and the algorithms used to estimate fuel consumption. These three estimates of fuel consumption were first evaluated in terms of the extent and magnitude of variability in fuel consumption, both spatially and temporally. CO emissions from each scenario were then used as input to a chemistry and transport model, to produce a simulated distribution of carbon monoxide from boreal forest fires. Model output was compared among estimates and then compared with atmospheric observations from the MOPITT instrument. These comparisons provide

insight into the effects of spatial variability in fuel consumption on the atmospheric signal from boreal forest fires. These results also provide a preliminary indication about the agreement of emissions estimates produced with different algorithms with atmospheric observations.

4.1. Estimates of fuel consumption

Three different estimates of fuel consumption will be tested in this study. Table 6-1 gives an overview of some of the fuel consumption parameters of these estimates.

The first estimate (MOD) is the "moderate" estimate described by *Kasischke et al.* [2005]. This estimate uses a consistent algorithm throughout the boreal forest, with parameters adjusted to account for differences in fire behavior in North America and Russia. Aboveground fuel consumption is estimated as a fraction of available fuel as described above. Fuel availability is parameterized according to the total aboveground biomass, and fractional fuel consumption is determined by fire type, which varies with the timing of fires during the growing season. Ground-layer fuel consumption is calculated in terms of depth of burn, with the carbon density profile of each burn determined by the soil carbon database. Carbon density is fixed in the first five centimeters of the soil profile, so spatial variability is only a factor in mid- and late-season crown fires and late-season surface fires.

The second estimate (NS for "No Seasonal effects") is equal to the MOD estimate with all seasonally variable parameters fixed at the mid-season values. Comparison of the MOD and NS estimates should make it possible to separate the effects of spatial and temporal variability in fuel consumption.

The third estimate (VAR) is an earlier model that predates the BWEM-1 by several years. This estimate uses different approaches to emissions estimation for North America and Europe. Emissions in North America are parameterized using a single value of fuel consumption for each terrestrial ecozone [*Amiro et al.*, 2001; *Bourgeau-Chavez et al.*, 2000; *French et al.*, 2000]. In Alaska, for instance, forested areas are divided into two ecozones, the Alaskan Interior and the Boreal Cordillera, but all areas burned in 2000 were in the Alaskan Interior forest. *Amiro et al.* [2001] use this approach, arguing that spatially inaccurate and outdated information in the biomass maps is a source of error potentially greater than the error of using regionally aggregated fuel consumption values.

In Russia, the VAR estimate estimates fuel consumption as a fraction of aboveground and ground-layer biomass according to fire type. This estimate has the greatest dependence on spatial patterns of biomass in Russia, and the least dependence in North America. It is included here because of its use in the studies presented in Chapters 3 and 4 of this dissertation.

Patterns of CO derived from CTM output from each of these estimates will be compared with the spatial patterns obtained from fire information alone with no fuels information included. The atmospheric model used is linear in concentration, so the time-resolved area burned was scaled and used as input to the model, and the resulting simulated emissions can be rescaled to have the same mean CO enhancement as any of the other three estimates. This tracer (HA) represents CO emissions with a constant fuel consumption and combustion efficiency, and permits easy assessment of the signal from variability in fuel consumption.

4.2. Study Period

An estimated 10.3 million hectares burned in the boreal forest during 2000, of which about 90% was in Russia. The largest concentration of fire activity occurred during April-June in southern Russia along the borders of China and Mongolia, but isolated large fires occurred throughout the boreal zone during June-August. Carbon and CO emissions from forest fires during the 2000 fire season were simulated using data on fire size, location and timing from various sources. These data are described in detail in Chapter 5 and in *Kasischke et al.* [2005].

4.3. Transport model

Daily emissions estimates were aggregated to a 2.5° longitude by 2° latitude grid, and used as input to the University of Maryland CTM [*Allen et al.*, 1996; *Park et al.*, 2004]. The model was also used to simulate the other principal sources of CO to the atmosphere. Details of sources used, and more information about the model, can be found in the above references and in Chapters 3-4. Model outputs were transformed to simulate the sensitivity and sampling characteristics of the atmospheric observations used. Details and quantitative evaluation of this transformation can be found in Chapter 3.

4.4. MOPITT data

CO measurements were taken from the Level 2 MOPITT data product. Total column CO estimates were used for this study. The MOPITT data were filtered to exclude retrievals with greater than 40% contribution of the *a priori* profile at the 700mb level, and retrievals where the estimated error in the total column CO was less than 25%. Only daytime retrievals were used. Application of these filters resulted in approximately

30,000 usable retrievals per full day of instrument operation. More details of the MOPITT data processing can be found in Chapters 3 and 4.

5. Results

5.1. Spatial and temporal variability in emissions estimates

Table 6-2 shows total emissions, as well as fuel consumption and mean emissions per hectare burned, for each of the estimates for Canada, Alaska, and Russia. Overall fuel consumption is different for each estimate. The area burned in Canada is slightly different for the VAR estimate because of a small area (around 7,000 hectares) burned in an area in southern British Columbia in an ecozone not included in the VAR model.

The VAR model has considerably higher emissions than the MOD and NS estimates. The total carbon emissions for Russia in this estimate are more than double the other estimates. In North America, emissions from all three models are relatively similar. Differences in total emissions between the MOD and NS estimates relate to the timing of fires. These estimates are very similar for Alaska because nearly all of the area burned occurred during the mid-season period, when the fuel consumption in the MOD and NS estimates is identical. Area burned in Russia was greatest during the early part of the fire season, so the NS model gives higher overall fuel consumption; the opposite is true for Canada.

Table 6-2 are the mean and standard deviation of fuel consumption for each grid cell containing emissions in the 2° by 2.5° daily gridded emissions used as input to the atmospheric model. The grid cell mean is different from the global mean because the grid cell mean is weighted toward isolated fires. In Russia, this effect is very strong: isolated

late-season fires significantly raise the mean fuel consumption per grid cell by 50% compared with the overall mean.

The MOD estimate had the highest variability in fuel consumption, with a coefficient of variation of 67% for Russia, more than triple that of the NS estimate. This indicates that temporal variability eclipses spatial variability in modeled fuel consumption in North America and Russia for the MOD estimate.

The combustion efficiency is similar in each estimate, and reflects a high percentage of smoldering combustion, with higher CO emissions than would be expected for comparable fuel consumption in a grassland or woodland ecosystem.

The temporal variability in each estimate, and the magnitude of temporal variability overall, are shown by Figure 6-1, which shows the time series of carbon emissions for each estimate. All estimates track very closely to area burned, indicating that area burned is clearly the major determinant of temporal variability of emissions. The effect of the seasonal changes in fuel consumption in the MOD estimate is evident from comparison with the NS estimate. The two are identical during June and July, while the MOD estimate is lower in the early part of the season and higher in the late part, to the point of actually estimating higher carbon emissions during August than the VAR estimate, which has more than double the MOD emissions over the entire fire season.

Spatial variability for each of the models used is shown in Figure 6-2 through 6-4. These show the mean carbon emissions per hectare burned aggregated to a 2.5° by 2° grid. Temporal variability is incorporated in these results: for instance, emissions in Canada are higher for the same fires in the MOD estimate compared to the NS, because

of the timing of these fires. Fuel consumption in the VAR estimate has a very coarse spatial grain in North America because of the aggregated estimates used. In Russia, the VAR and NS estimates reflect the spatial pattern of biomass on the landscape, with the VAR estimate more strongly influenced by the pattern of belowground biomass. The MOD fuel consumption in Russia, meanwhile, is largely driven by the temporal pattern of fire activity, with very low fuel consumption throughout the southern part of Russia where fires occurred mostly before June 1, and much higher fuel consumption further north, in contrast with the pattern of the NS estimate.

Table 6-3 shows the correlation between gridded CO emissions from each estimate and gridded area burned. It is evident that at the scale of the 2.5° by 2° grid cells, area burned is the source of nearly all of the variability in emissions. The MOD estimate is the only one that shows significant deviations in pattern of emissions, indicating that the seasonal variation in this model is the most significant source of variability at this scale after area burned.

Each of the estimates shows a distinct spatial and temporal pattern of fuel consumption. The greatest variability in fuel consumption in these estimates comes from the seasonal parameterization in the MOD estimate. At the scale of the input grid for the CTM, spatial variability in fuel consumption is a small fraction of the variability in emissions per grid cell. In the next section, the signal produced by this spatial and temporal variability in fuel consumption will be examined using simulated atmospheric measurements.

5.2. Fuel consumption signal in simulated MOPITT measurements

CO emissions from each estimate were used as input to the CTM to produce a simulation of the atmospheric distribution of CO from the boreal fire source. The gridded area burned (HA) was also run as a tracer in the model, with the same chemistry as the CO runs. The model is linear in concentration, so output from the HA tracer can be freely scaled to match the mean CO enhancement from the other estimates. CTM outputs were processed to simulate the spatial and temporal sampling properties of MOPITT retrievals.

The filters used yielded 2.6 million usable retrievals in the HNH during the study period. Table 6-4 shows the mean total column CO from MOPITT as well as simulated total column CO from non-boreal sources (BACK) and boreal CO from each simulation.

Table 6-5 shows the correlation between simulated total column CO from each estimate and CO values estimated from the HA tracer. This is considerably lower than the correlation of the inputs, indicating substantial sensitivity of the atmospheric patterns of CO to spatial and temporal variability in fuel consumption. This sensitivity arises out of highly correlated source patterns because a large fraction of the retrievals have very low nonzero contribution from boreal CO, and the correlation is disrupted near source regions where CO concentrations are high. Figure 6-5 illustrates this, showing the spatial distribution of deviation between the MOD estimate and the scaled HA tracer. The relationship between the MOD and HA tracers is very consistent over most of the HNH, and the disagreement arises over fires with fuel consumption different from the mean and in the plumes traveling from those fires. The mean fuel consumption is strongly weighted

toward the early-season fires, so the locations where the MOD simulation deviates most from the HA tracer match the locations of late-season fires.

The comparison of simulated and observed CO does not provide information about the variability of fuel consumption unless the residual of fuel consumption variability is large relative to the precision of the observation. To determine the atmospheric signal of fuel consumption variability, the output from the HA simulation was scaled to the mean of each of the estimates MOD, NS and VAR. Subtraction of the scaled HA tracer from the simulated CO yielded a residual representing the difference in simulated total column CO relative to a source of identical magnitude with no variability in fuel consumption.

Figure 6-6a shows the distribution of absolute magnitude of this residual. The overwhelming majority of the retrievals have very small residuals. The vertical lines indicate the separation in the top 5% of the retrievals. The MOD and VAR appear to have similar distributions of the residuals, and both have considerably greater residuals than the NS estimate. However, the MOD has greater variability in fuel consumption, the VAR residuals are comparable in magnitude because the simulated CO from this estimate is greater.

Figure 6-6b shows how these differences measure up compared to the total column CO observed by MOPITT. This plot suggests that overall comparisons between simulated CO and observations will show only small differences, because the signal from fuel consumption variability is less than 10% in around 95% of cases. Figure 6-6c shows the residuals normalized to the estimated error in the MOPITT total column CO retrieval.

The top 5% of retrievals have residual signal from fuel consumption more than 1.5 times the retrieval error of the observation, for the MOD and VAR estimates. It is these retrievals that will drive the differences in agreement between estimates.

The next section will address the question of whether the comparison between simulated CO from the different estimates and observations can shed light on the accuracy of different representations of fuel consumption.

5.3. Comparison of simulated CO to observations

Figure 6-7 shows the time series of HNH CO burden calculated from the MOPITT data as well as from the simulations. Points on the time series shown are three-day averages, to reduce noise related to incomplete sampling by MOPITT. The large dip in CO burden near 10 May does appear to relate to incomplete MOPITT sampling, in spite of the averaging.

The MOPITT data show an overall downward trend during the study period. This downward trend is counter to the trend of the non-boreal sources, but simulations with the NS and VAR estimates for the boreal source show a trend closer to observations. The MOD estimate has a trend in the early part of the season that complements the trend in the BACK simulation, resulting in nearly constant total CO during May-July, and then increases sharply in August. The differences between the overall trend of the simulation and observations will affect the fit of the model over the whole study period.

Simulated CO from boreal fires was compared with observations by first subtracting the simulated CO from all other sources from the MOPITT observations. The residuals were then compared to simulated CO from boreal fires. Agreement between

observations and simulated CO from non-boreal sources was discussed in detail in Chapter 6. Overall, the simulation without the boreal source underestimates HNH CO by 25-30%, and overall agreement with observations is moderate (r=0.42-0.55).

Figure 6-8 shows correlation statistics for the HNH for each estimate compared to the MOPITT residuals, calculated over the entire study period as well as for individual months. In this case, the overall agreement between the model and observations reflects moderate performance of the simulation early in the study period and very poor performance in July and August. The three fuel model estimates, MOD, NS, and VAR, show similar performance in individual months, but the MOD does worse later in the season, and over the entire study period. This indicates that the change in fuel consumption of the MOD estimate between the early and late parts of the fire season is not reflected in the observations from this season. The late-season parameters of the MOD estimate were developed in an effort to account for very high levels of fuel consumption observed in extreme late-season fires [*Kasischke and Bruhwiler*, 2002; *Kasischke et al.*, 2005]. These fires, when they occur, dominate the total emissions from the boreal forest, and can significantly change the seasonal pattern of HNH CO [*Yurganov et al.*, 2004a; *Yurganov et al.*, 2005]. However, the results obtained in this study indicate that even though substantial areas burned during August 2000, the fuel consumption of these fires was not necessarily greater than for fires earlier in the season. This result is not quantitative, because the best agreement obtained between the model and measurements is still low, indicating that error in area burned or other model inputs is potentially large. The overall agreement between the simulation and observations

indicates some problem with the seasonal description of fuel consumption in the MOD estimate, but the performance of the other estimates is very similar, and only for May do the MOD, NS and VAR estimates perform much better than the HA simulation, which assumes fuel consumption is constant.

Since the input data are different for Asia and North America, evaluation of the model over these different regions may produce different results. Figure 6-9 shows the time series of estimated CO burden over North America (compare to Figure 6-7). Numerous features in the simulated CO during May-July appear to match well with MOPITT observations. Note that simulation results shown in this section are all sampled to match the MOPITT data. May features are related to CO from Russian fires transported east over North America. Canadian fires in mid-June and Alaskan fires in July appear to be captured similarly in the model output and MOPITT data. MOPITT data from August show numerous large features with no analogues in the simulation. These features are possibly related to biomass burning in the continental United States.

Figure 6-10 shows model fit statistics for retrievals over the North American land mass. In the individual months, the different estimates do not produce very different results. Overall, the NS and VAR estimates give similar results, with slightly better performance by the VAR estimate. This suggests that a high degree of confidence can be assigned to the fuel consumption parameterization in the VAR estimate, which is based on average values for different ecozones. This approach captures broad-scale variability between different forest types, but makes no attempt to capture fine-scale variability. The treatment of fine-scale variability in the MOD and NS estimates is subject to various

errors, which negate any improvement in agreement with observations relative to the simulation using a fixed fuel consumption.

Figure 6-11 shows the time series of CO burden over Asia, and Figure 6-12 shows model fit statistics for this region. The simulation results are mixed throughout May-July, with some features relatively close to MOPITT observations and others missed (10-15 June) or exaggerated (15-20 June, 20-25 July) by the simulation. The largest feature in the simulation, from fires in northeastern Russia during the second week in August, is conspicuously absent from the MOPITT data. This results in extremely poor agreement between model and measurements for August. The fires the simulation is responding to occurred in northeastern Yakutia and Magadan. Figure 6-13 shows the plume of elevated aerosol index detected by the Earth Probe TOMS instrument over this region during 5-11 August. This is the only significant aerosol event detected by TOMS over northern Asia during August. The timing of elevated aerosol observations agrees well with the model simulations. Figure 6-14 shows MOPITT sampling in this region during 4-11 August, indicating that while sampling is incomplete, some MOPITT retrievals should show the effects of the plume. Figure 6-15 shows the dates of MOPITT retrievals with total column CO greater than $3.0*10^{18}$ molecules cm^{-2}. This shows that the plume from the August events was sampled by MOPITT, but its contribution to the overall CO burden over Asia was much lower than that estimated by the model.

Overall, the differences between the three estimates showed that the seasonal patterns generated by the MOD estimate do not produce the best agreement with observations during the 2000 fire season. The two estimates without seasonal variation,

NS and VAR, gave similar results, both consistently better than the HA tracer with constant fuel consumption. The variable performance of the HA tracer indicates that variability in fuel consumption affects patterns of atmospheric CO, and that some of this variability is captured by the current models. Further investigation is required to determine if these results are consistent during both low and high years of fire activity, especially since the area burned in North America during the study period is well below the annual average.

6. Conclusions

Spatially resolved estimates of aboveground and ground-layer biomass were used to estimate carbon and trace gas emissions from forest fires in the boreal forest during 2000. Three different emissions estimation scenarios were evaluated, each with a different algorithm used to determine fuel consumption from the same source data. Comparison of the carbon emissions estimates showed that at the scale of a global emissions model (2° latitude by 2.5° longitude), area burned was by far the most important determinant of emissions per grid cell. The largest differences in fuel consumption per area burned came from the seasonal parameterization of fire type and severity in the algorithm used by *Kasischke et al.* [2005]. Spatial variability in fuel consumption was different depending on the model assumptions, but was a small contributor to variability at the atmospheric model scale.

CO emissions estimates were used in a CTM to simulate atmospheric patterns of CO from boreal forest fires. Comparison of these estimates with observations from the MOPITT instrument showed that the seasonal assumptions of *Kasischke et al.* [2005]

result in differences between early and late-season fires for 2000 that do not match observations. These seasonal patterns have been shown to effectively describe patterns of burning in cases with large, severe late-season fires [*Kasischke et al.*, 2005; *Yurganov et al.*, 2004a], but more research is needed to construct a more complete description of fire behavior and its seasonal trends.

The best results for spatial and temporal variability of fuel consumption in North American fires were obtained with aggregated estimates of fuel consumption based on broad ecosystem characteristics. In Russia, different treatments of spatial variability in fuel consumption performed very similarly, and all of the emissions scenarios performed better than the HA tracer for each individual month of the study period. None of the models tested improved agreement with observations over the entire study period relative to the HA tracer, indicating that temporal variability is a source of error in all of the emissions scenarios. The model scenarios capture some of the variability in fuel consumption, but substantial variability clearly goes uncaptured by current models. The conclusions of this study, especially relating to seasonal variability in fire behavior, should be evaluated for a different year, especially a year with above-average area burned in North America, to determine if its conclusions are robust.

7. Tables

		MOD	NS	VAR-RUS
Fraction of Crown Fires (RUS/NA)				
	early	0.1/0.7	0.4/0.8	0.2
	middle	0.4/0.8	0.4/0.8	0.6
	late	0.9/0.9	0.4/0.8	0.9
Aboveground Fuel Consumption				
	Surface Fires	0.0525-0.8[a]	0.0525-0.8	0.1
	Crown Fires	0.21-1	0.21-1	0.35
Ground-Layer Fuel Consumption				
Surface Fires	**early**	2 cm	4 cm	10%
	middle	4 cm	4 cm	10%
	late	8 cm	4 cm	10%
Crown Fires	**early**	3 cm	6 cm	15%
	middle	6 cm	6 cm	15%
	late	12 cm	6 cm	15%

a. This fraction varies with total above-ground biomass. 80% of above-ground fuel is consumed in areas with <10 tons per hectare, while only 5.25% is consumed in areas with >20 t ha-1.

Table 6-1. Fuel consumption parameters for scenarios used in this study. Crown fire fraction in the MOD and NS scenarios is different for North American and Russian fires. Fractional aboveground fuel consumption varies in the MOD and NS scenarios according to total aboveground biomass density. The VAR estimate uses a different algorithm in North America, see text for details (Section 4.1).

		Area burned (Mha)	Carbon Release (Tg)	CO Release (Tg)	Fuel Consumption (t C ha-1) mean	grid mean	grid s.d.	Effective EF g CO kg-1 fuel
MOD	**Alaska**	0.302	4.55	1.66	15.02	15.29	0.48	164.48
	Canada	0.624	12.1	4.66	19.31	22.04	7.79	173.88
	Russia	9.36	103.84	36.09	11.09	17.53[a]	11.90	156.40
NS	**Alaska**	0.302	4.48	1.63	14.78	15.03	0.45	163.84
	Canada	0.624	9.07	3.31	14.53	15.58	0.22	164.12
	Russia	9.36	125.70	43.67	13.43	13.39	2.41	156.33
VAR	**Alaska**	0.302	6.06	2.17	20.00	20.00	0.00	161.51
	Canada	0.617	6.14	2.00	9.96	10.53	1.61	146.38
	Russia	9.36	252.06	83.5	26.93	27.83	7.78	148.98

[a]RUS-EK2M: 60% of grid cells have <15 t C ha-1, average is driven by very high emissions (50-60 t C ha-1) in a few cells containing small isolated late-season fires.

Table 6-2. Total area and emissions for Alaska, Canada and Russia for each model. The effective emissions factor (EF) is calculated assuming 45% carbon content of fuels.

	MOD	NS	VAR
All Boreal	0.75	0.98	0.98
Alaska	1.00	1.00	1.00
Canada	0.90	1.00	0.98
Russia	0.74	0.98	0.98

Table 6-3. Correlation between estimated CO emission and area burned for gridded emissions model outputs (2.5° longitude by 2° latitude, daily).

	MOPITT	BACK	MOD	NS	VAR
May	23.82	17.35	1.05	2.51	4.85
June	21.18	15.58	1.15	2.04	3.82
July	19.18	14.75	1.13	1.40	2.38
August	19.38	15.44	1.38	1.04	1.59
May-August	20.73	15.73	1.20	1.68	3.02

Table 6-4. Mean total column CO from MOPITT and simulation. BACK includes all non-boreal CO sources. Units are molecules cm^{-2} * 1e17.

	May	June	July	August	MJJA
MOD	0.42	0.70	0.77	0.65	0.66
NS	0.74	0.69	0.85	0.67	0.77
VAR	0.79	0.77	0.86	0.61	0.70

Table 6-5. Correlation between CTM-simulated MOPITT TC CO from each estimate and HA tracer.

8. Figures

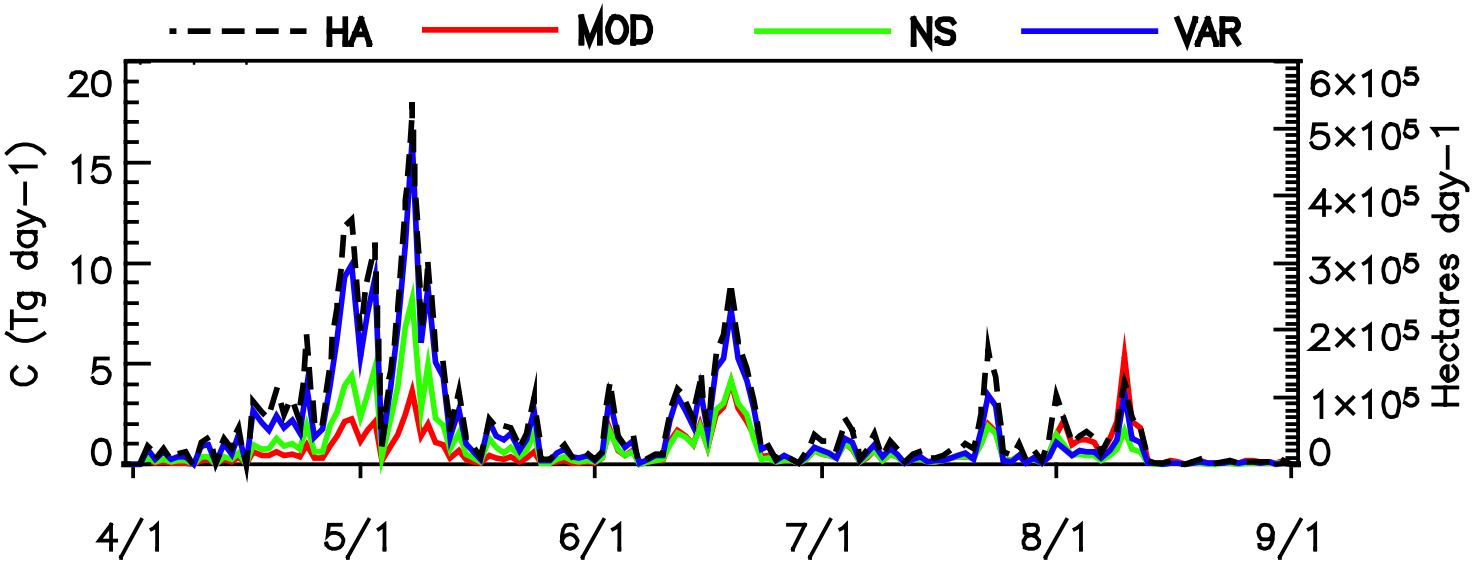

Figure 6-1. Time series of carbon emissions for each scenario in this study. Also shown (black line) is the time series of area burned.

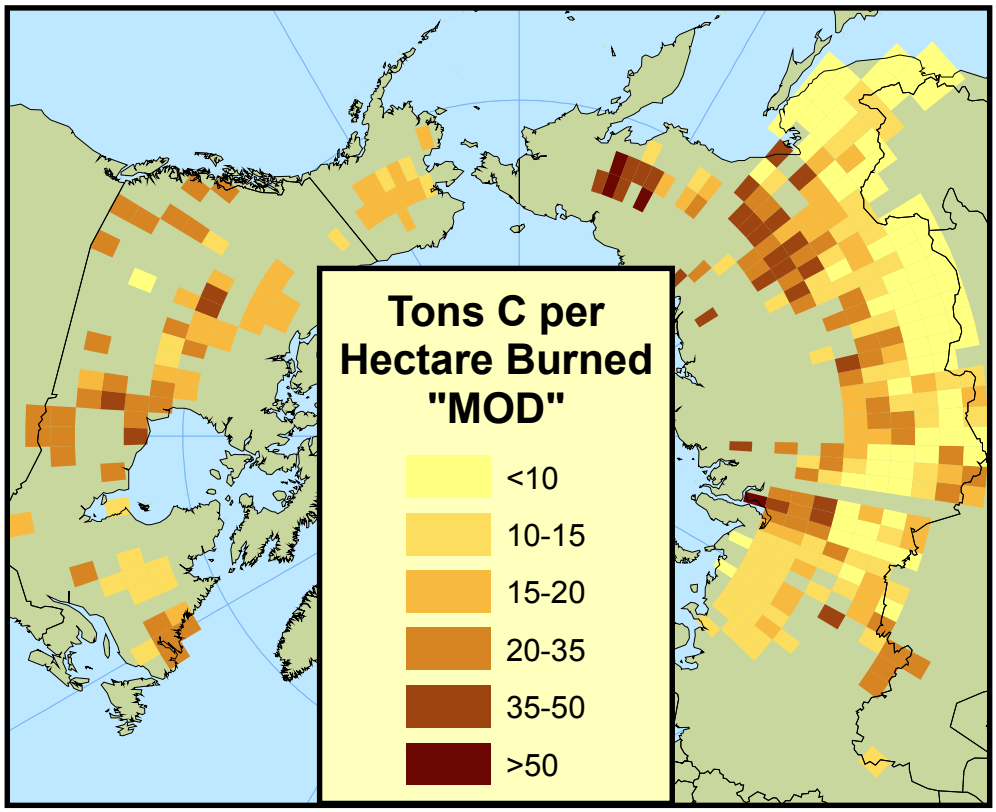

Figure 6-2. Tons of carbon released per hectare burned from the MOD estimate. Values shown are averages for each 2° latitude by 2.5° longitude grid cell. The MOD estimate corresponds to the "moderate" emissions scenario from *Kasischke et al.* [2005].

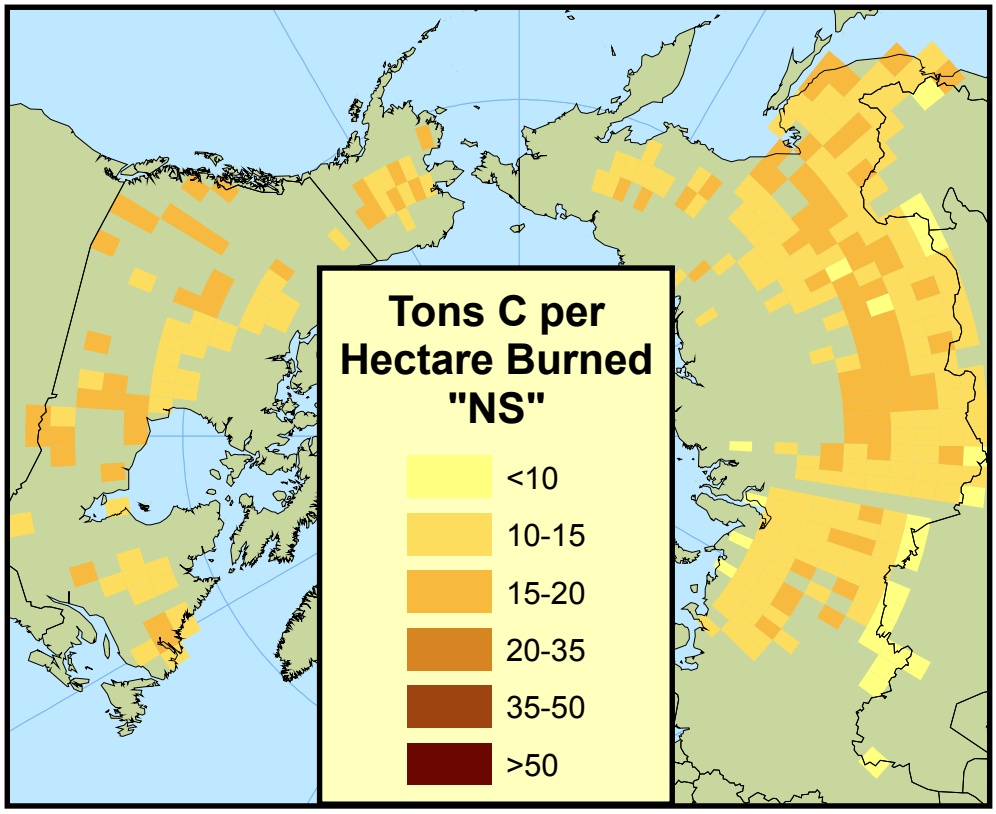

Figure 6-3. Carbon release per hectare burned from the non-seasonal (NS) estimate. This estimate is the same as the MOD estimate, with all seasonally variable parameters set at the mid-season values.

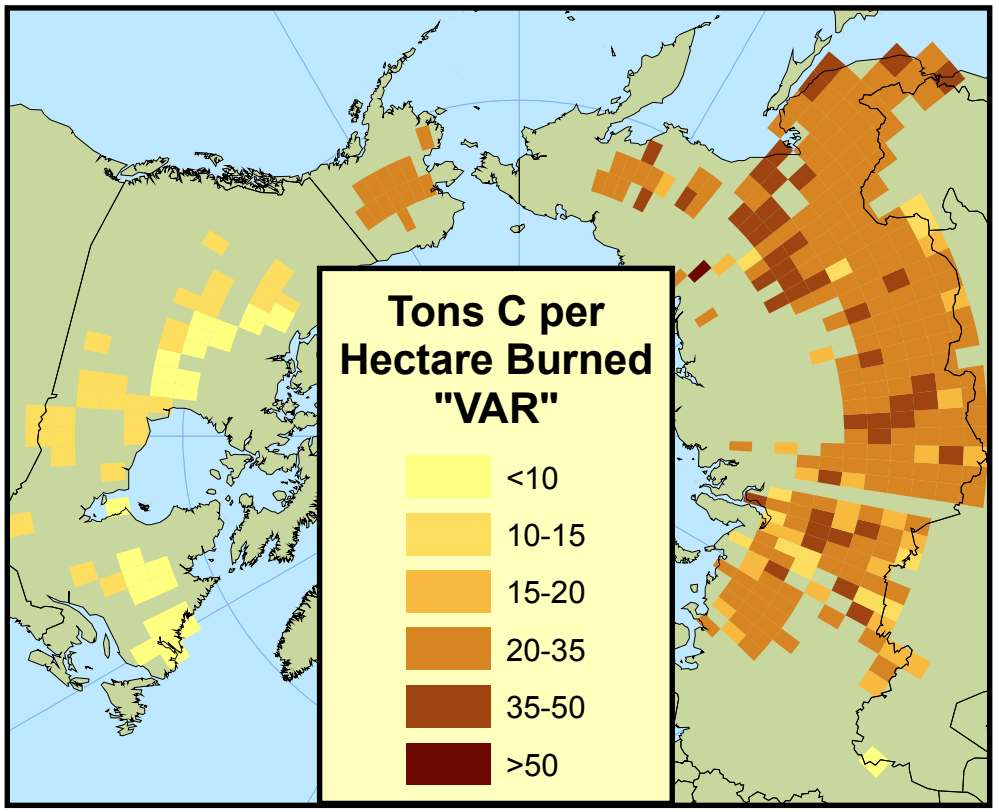

Figure 6-4. Carbon consumption per hectare burned from the VAR estimate. This estimate uses a different algorithm for fuel consumption, and was used for the studies in chapters 3-4 of this dissertation.

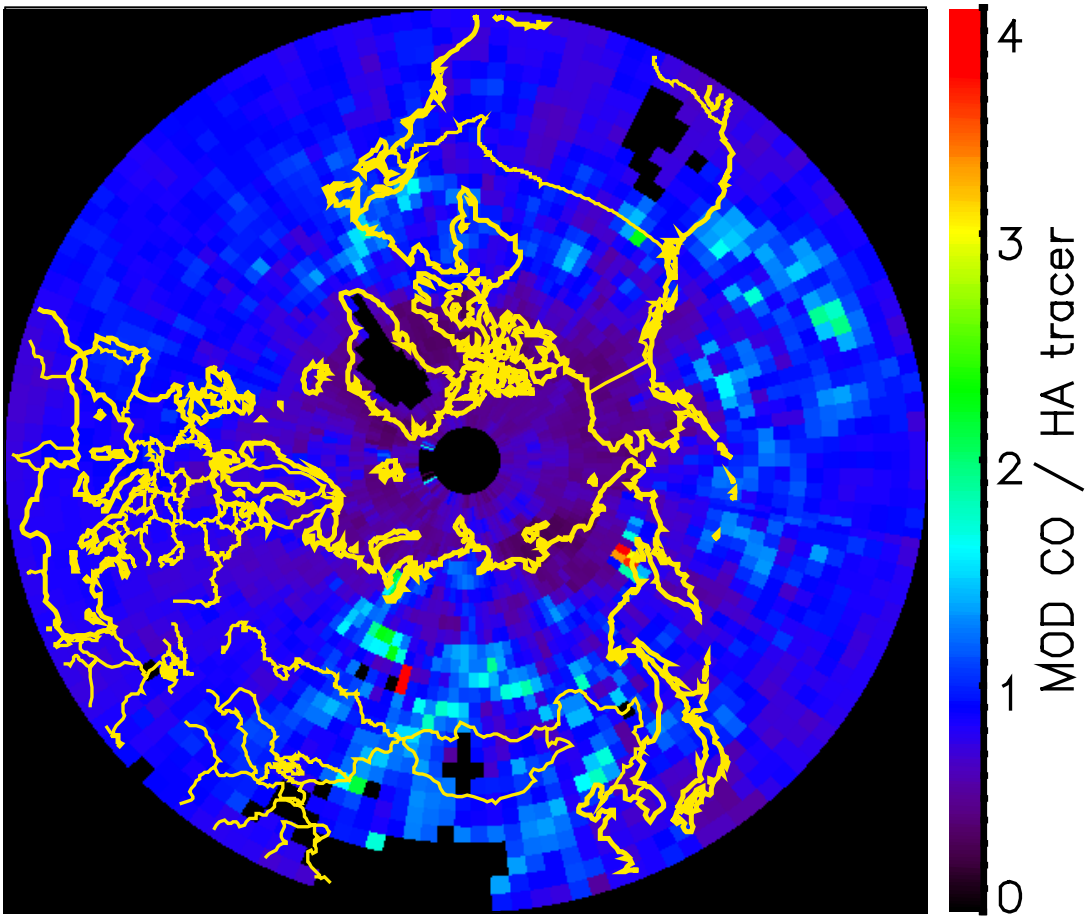

Figure 6-5. Ratio of MOD simulated CO to HA tracer. The tracer was scaled to have the same mean as the MOD simulated CO.

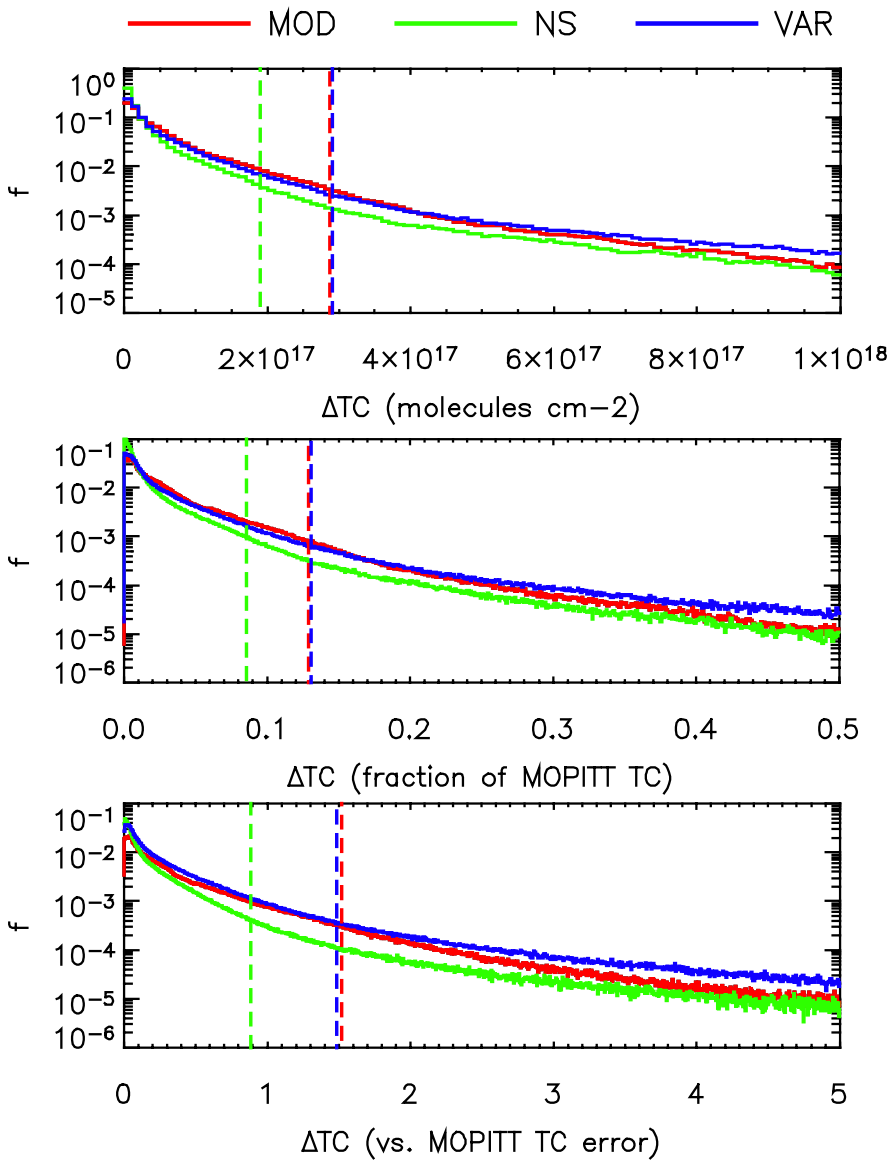

Figure 6-6. Influence of variability in fuel consumption on simulated MOPITT total column CO, shown here as a) absolute TC values, b) fraction of MOPITT TC, and c) proportion of error in MOPITT TC measurement. Vertical lines indicate 95% of values have differences equal or less. See text for details of calculations.

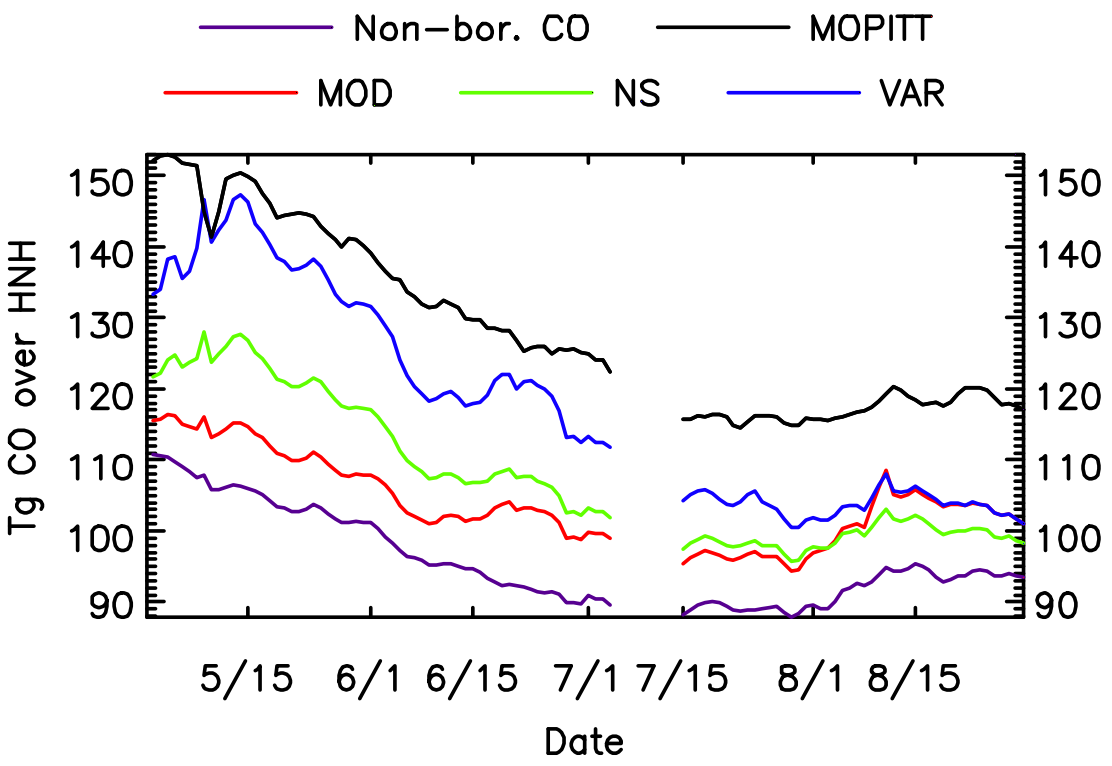

Figure 6-7. Time series of HNH CO burden calculated from MOPITT retrievals, as well as CTM simulation output. BACK simulation (purple line) includes all non-boreal CO sources. The other simulation results are total CO from all non-boreal sources plus boreal fire CO from the specified estimate.

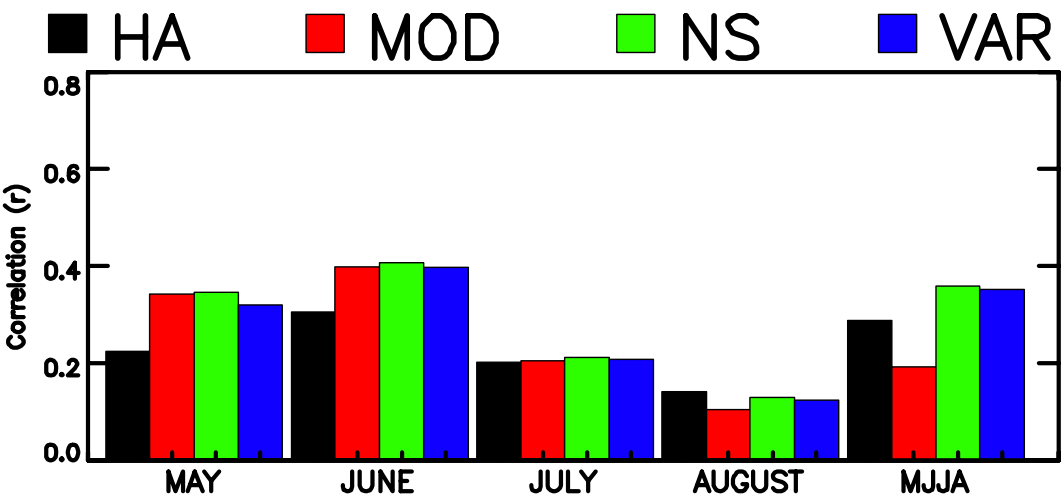

Figure 6-8. Correlation between simulation and observations for different scenarios. Correlation is calculated by comparing simulated CO from each boreal source scenario with residual CO obtained by subtracting the CO from non-boreal sources from the MOPITT observations.

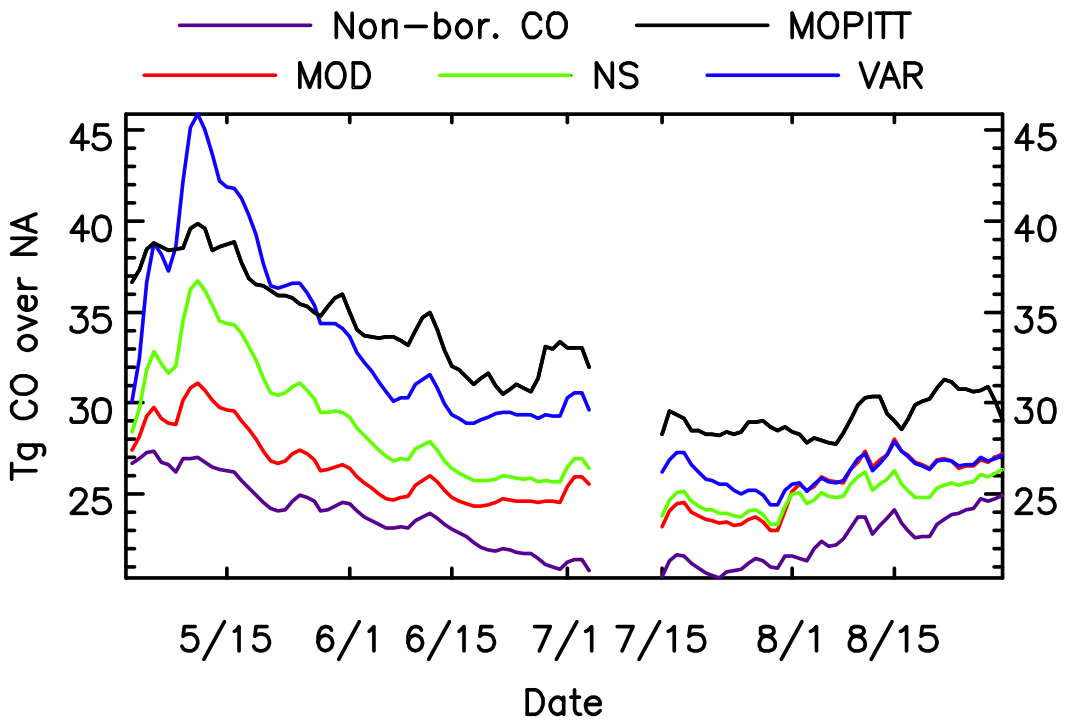

Figure 6-9. Time series of CO burden over North America calculated from MOPITT data and CTM simulation output.

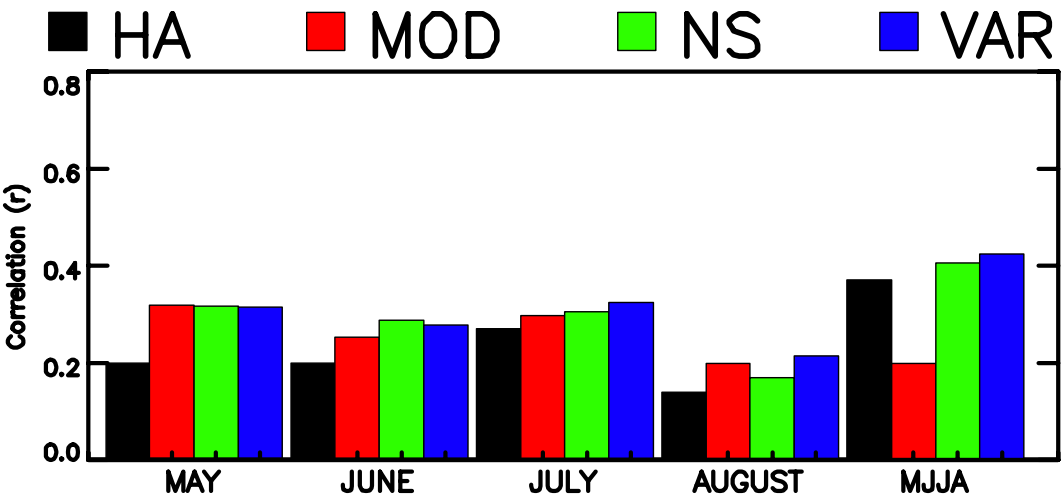

Figure 6-10. Model fit statistics for retrievals over North America.

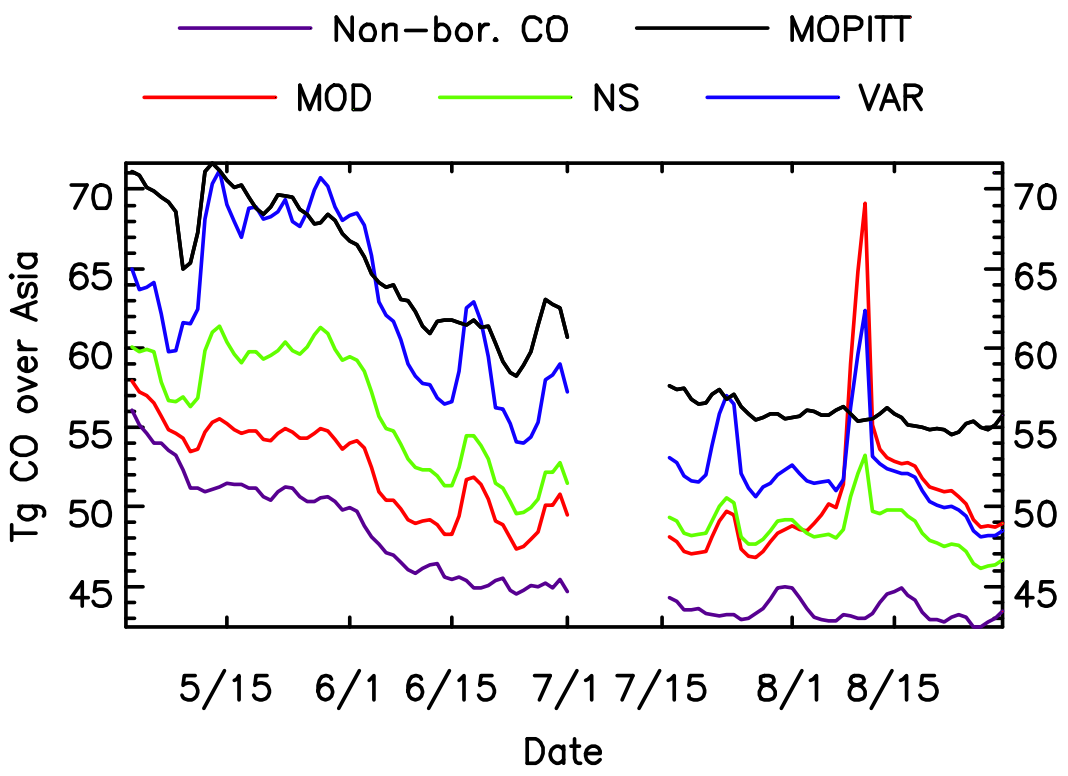

Figure 6-11. Time series of CO burden over Asia calculated from MOPITT data and simulation results.

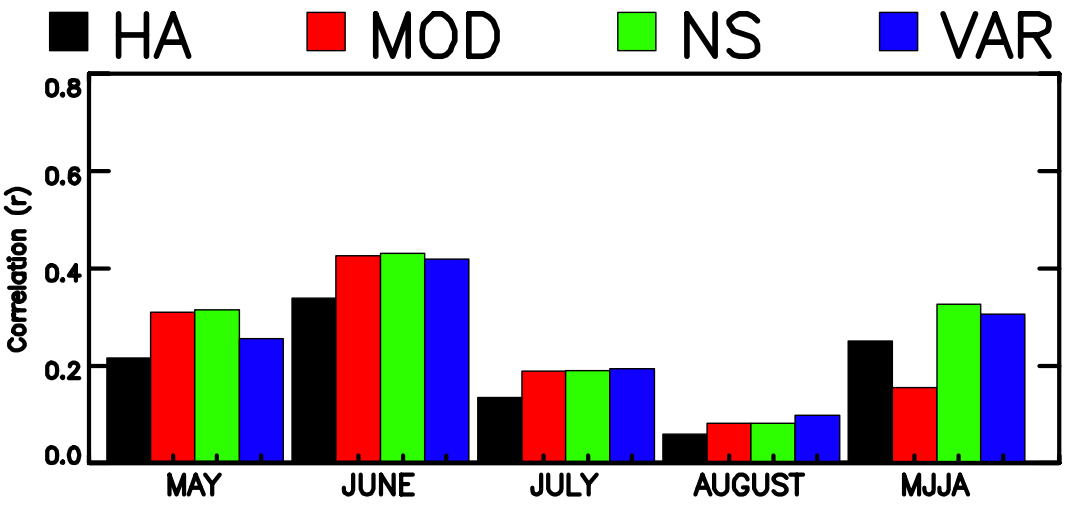

Figure 6-12. Correlations between model and observations for Asia.

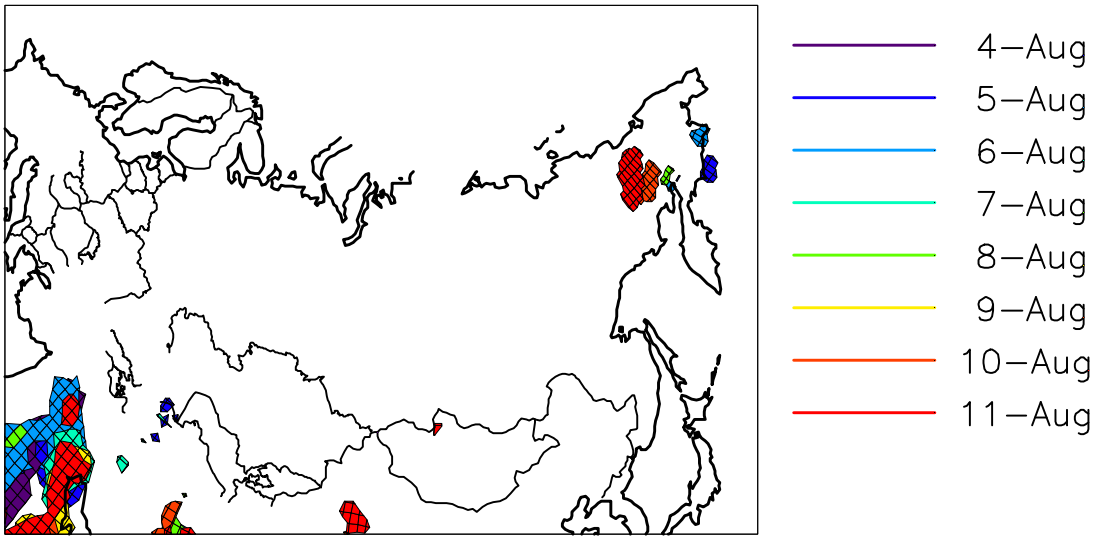

Figure 6-13. TOMS aerosol detections during 4-11 August. Regions shown are areas with a TOMS aerosol index greater than 1.5.

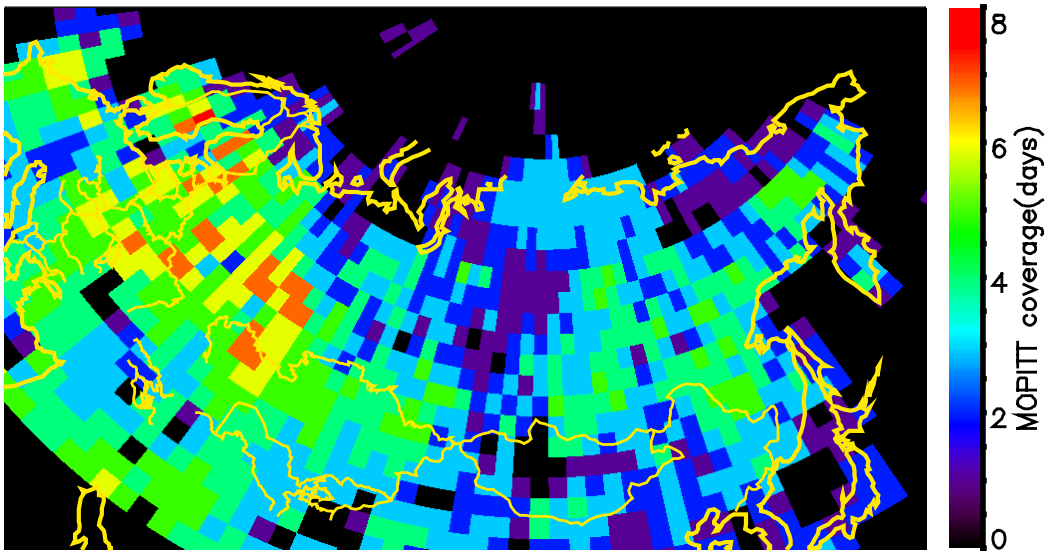

Figure 6-14. MOPITT coverage over Asia during 4-11 August. Color indicates the number of days with valid MOPITT retrievals for each 2° by 2.5° grid cell during 4-11 August.

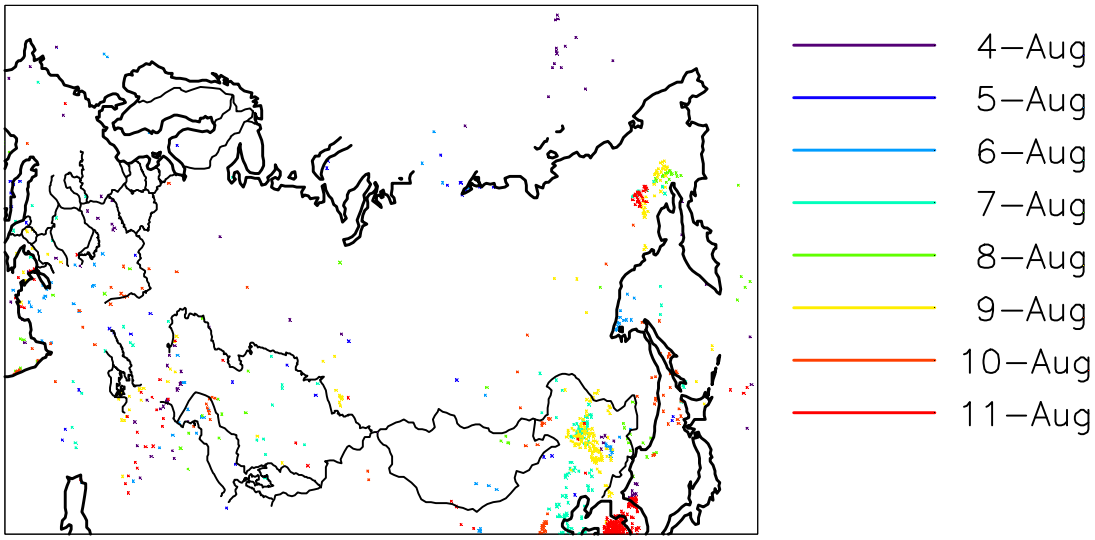

Figure 6-15. MOPITT detections with total column CO greater than 3.0e18 molecules cm-2 during 4-11 August.

Chapter 7. Conclusions

The studies presented in this dissertation demonstrate the power of an approach that integrates a spatially and temporally explicit emissions model with a chemistry and transport model (CTM) to achieve process-based examination of uncertainties in trace gas emissions from boreal forest fires. The innovation of the methodology used in these studies is that rather than evaluating the consequences of different input data sources and modeling assumptions for total trace gas emissions, this approach permits detailed examination of how uncertainties in process-based emissions models affect the spatial and temporal pattern of atmospheric CO. This integrated approach enables atmospheric data to be leveraged much more effectively. The goal of this approach is not merely to reduce uncertainty in estimated emissions, but to evaluate hypotheses to better understand the processes that drive the emissions model.

This approach was applied first to the problem of atmospheric injection height. It was demonstrated that injection height is a critical parameter for inverse modeling of boreal fire emissions. Different types of atmospheric measurement showed dramatically different sensitivity to injection height: surface measurements showed sensitivity to fire emissions injected at high altitude that was only a third of the simulated sensitivity of these measurements to surface emissions. The MOPITT data showed the opposite pattern of sensitivity, with high-altitude injection resulting in a 10% larger signal from biomass burning compared with surface injection. Beyond the theoretical implications for inverse estimation of source magnitude, this study examined injection height by comparison of observations to a CTM simulation of CO from boreal forest fires. The best agreement with observations was obtained with a pressure-weighted distribution of boreal fire

emissions through the tropospheric column, but examination of a case study in southern Russia showed that the injection properties of boreal forest fires have substantial fine-scale variability that will be a source of error in any fixed parameterization of injection height.

Temporal variability in boreal forest fire emissions was the subject of the investigation in Chapter Four. Using MOPITT data and continuous CO analyzer data from Mace Head, Ireland, it was demonstrated that temporal information in the boreal emissions model was sufficiently accurate that agreement with observations could be improved with 7-day aggregate data, compared to the monthly aggregation common in temporally resolved emissions estimates. Results from daily data were varied, and indicated that in the accuracy of the daily information could only be accurately evaluated with high-frequency, high-precision atmospheric measurements near the emissions source. The value of a high-resolution description of an emissions source as highly transient as boreal forest fires is intuitively obvious. However, the analysis in Chapter Four showed that atmospheric measurements have limited sensitivity to variability in emissions at scales finer than 7 days. Improved understanding of the observational requirements of specific problems is another benefit of the modeling approach used in these studies.

Burned area is still the largest uncertainty in emissions estimates, and the comparison of three different burned area products in Chapter Five revealed significant shortcomings in each of the products. The temporal patterns of fuel consumption in different products had an effect on simulated atmospheric CO as great as the spatial patterns. The GBA-2000 burned area and the burned area datasets from *Kasischke et al.*

[2005] gave similar agreement with atmospheric observations, despite dramatically different temporal patterns over the whole boreal forest and different spatial patterns over Russia, indicating that neither product is definitive. The GLOBSCAR product, while producing very poor agreement with observations over the entire study period, produced better results at the end of the study period, indicating that the most significant problem with this data set is the known, and correctable, problem of detection of burned areas from previous years.

Fuel consumption by boreal forest fires is one of the most critical factors in determining the carbon balance of boreal forest ecosystems, and may determine whether the boreal forest is a net source or sink of carbon on a decadal scale. Chapter Six compared emissions estimates using different treatments of fuel consumption from recently published literature, to evaluate the effects on spatial and temporal patterns of CO emissions. The largest source of variability in the estimates of fuel consumption evaluated was the seasonal parameterization of fire severity in the model of *Kasischke et al.* [2005]. Seasonal variability in fuel consumption was found to have a strong impact on trends in the CO burden in the High Northern Hemisphere. Spatial variability in fuel consumption was shown to have a small impact on CO measurements in well-mixed air masses, but the comparison of modeled CO to observations indicated this variability could be detected in MOPITT measurements.

Taken together, these studies represent substantial new knowledge about the boreal forest fire CO source and its effects on atmospheric patterns of CO. These studies demonstrate the power of an approach to inversion of atmospheric measurements which integrates process-based modeling of the emissions source.

The possibilities of this methodology extend far beyond the studies in this dissertation. In the time since this project was begun, several new instruments for remote sensing of atmospheric composition have come online, including AIRS, TES, and SCIAMACHY. The data from these instruments will make possible a wider range of studies to examine more complex questions about the behavior of land-surface processes. The problem of trace gas exchanges between the biosphere and atmosphere is inherently cross-disciplinary. This dissertation serves as a demonstration of the power of a cross-disciplinary approach.

References

Alexeyev, V.A., and R.A. Birdsey, General Technical Report NE-244: Carbon Storage in Forests and Peatlands of Russia, in *Northeast Research Station General Technical Reports*, edited by U.F. Service, pp. 141, USDA Forest Service, Delaware, OH, 1998.

Alexeyev, V.A., R.A. Birdsey, V.D. Stakanov, and I.A. Korotkov, Carbon Storage in the Asian Boreal Forests of Russia, in *Fire, Climate Change, and Carbon Cycling in the Boreal Forest*, edited by E.S. Kasischke, and B.J. Stocks, pp. 239-257, Springer, New York, 2000.

Allen, D., K. Pickering, and M. Fox-Rabinovitz, Evaluation of pollutant outflow and CO sources during TRACE-P using model-calculated, aircraft-based, and Measurements of Pollution in the Troposphere (MOPITT)-derived CO concentrations, *Journal of Geophysical Research-Atmospheres*, *109* (D15), D15S03, doi:10.1029/2003JD004250, 2004.

Allen, D.J., P. Kasibhatla, A.M. Thompson, R.B. Rood, B.G. Doddridge, K.E. Pickering, R.D. Hudson, and S.J. Lin, Transport-induced interannual variability of carbon monoxide determined using a chemistry and transport model, *Journal of Geophysical Research-Atmospheres*, *101* (D22), 28655-28669, 1996.

Allen, D.J., K.E. Pickering, and A. Molod, An evaluation of deep convective mixing in the Goddard Chemical Transport Model using International Satellite Cloud Climatology Project cloud parameters, *Journal of Geophysical Research-Atmospheres*, *102* (D21), 25467-25476, 1997.

Amiro, B.D., J.B. Todd, B.M. Wotton, K.A. Logan, M.D. Flannigan, B.J. Stocks, J.A. Mason, D.L. Martell, and K.G. Hirsch, Direct carbon emissions from Canadian forest fires, 1959-1999, *Canadian Journal of Forest Research-Revue Canadienne De Recherche Forestiere*, *31* (3), 512-525, 2001.

Andreae, M.O., and P. Merlet, Emission of trace gases and aerosols from biomass burning, *Global Biogeochemical Cycles*, *15* (4), 955-966, 2001.

Apps, M.J., W.A. Kurz, R.J. Luxmore, L.O. Nilsson, R.A. Sedjo, R. Schmidt, L.G. Simpson, and T.S. Vinson, Boreal Forests and Tundra, *Water Air and Soil Pollution*, *70*, 39-53, 1993.

Arellano, A.F., P.S. Kasibhatla, L. Giglio, G.R. van der Werf, and J.T. Randerson, Top-down estimates of global CO sources using MOPITT measurements, *Geophysical Research Letters*, *31* (1), doi:10.1029/2003GL018609, 2004.

Barbosa, P.M., D. Stroppiana, J.M. Gregoire, and J.M.C. Pereira, An assessment of vegetation fire in Africa (1981-1991): Burned areas, burned biomass, and atmospheric emissions, *Global Biogeochemical Cycles*, *13* (4), 933-950, 1999.

Bey, I., D.J. Jacob, R.M. Yantosca, J.A. Logan, B.D. Field, A.M. Fiore, Q.B. Li, H.G.Y. Liu, L.J. Mickley, and M.G. Schultz, Global modeling of tropospheric chemistry with assimilated meteorology: Model description and evaluation, *Journal of Geophysical Research-Atmospheres*, *106* (D19), 23073-23095, 2001.

Boles, S.H., and D.L. Verbyla, Comparison of three AVHRR-based fire detection algorithms for interior Alaska, *Remote Sensing of Environment*, *72* (1), 1-16, 2000.

Boschetti, L., H.D. Eva, P.A. Brivio, and J.M. Gregoire, Lessons to be learned from the comparison of three satellite-derived biomass burning products, *Geophysical Research Letters*, *31* (21), doi:10.1029/2004GL021229, 2004.

Bourgeau-Chavez, L.L., E.S. Kasischke, J.P. Mudd, and N.H.F. French, Characteristics of Forest Ecozones in the North American Boreal Region, in *Fire, Climate Change, and Carbon Cycling in the Boreal Forest*, edited by E.S. Kasischke, and B.J. Stocks, pp. 258-273, Springer, New York, 2000.

Byram, G.M., Combustion of Forest Fuels, in *Forest Fire: Control and Use*, edited by K.P. Davis, pp. 61-89, McGraw-Hill, New York, 1959.

Christopher, S.A., J. Chou, R.M. Welch, D.V. Kliche, and V.S. Connors, Satellite investigations of fire, smoke, and carbon monoxide during April 1994 MAPS mission: Case studies over tropical Asia, *Journal of Geophysical Research-Atmospheres*, *103* (D15), 19327-19336, 1998.

Ciais, P., P.P. Tans, M. Trolier, J.W.C. White, and R.J. Francey, A Large Northern-Hemisphere Terrestrial Co2 Sink Indicated By the C-13/C-12 Ratio of Atmospheric Co2, *Science*, *269* (5227), 1098-1102, 1995.

Cofer III, W.R., E.L. Winstead, B.J. Stocks, L.W. Overbay, J.G. Goldammer, D.R. Cahoon, and J.S. Levine, Emissions from Boreal Forest Fires: Are the Atmospheric Impacts Underestimated? in *Biomass Burning and Global Change*, edited by J.S. Levine, pp. 834-839, The MIT Press, Cambridge, Massachusetts, 1996.

Colarco, P.R., M.R. Schoeberl, B.G. Doddridge, L.T. Marufu, O. Torres, and E.J. Welton, Transport of smoke from Canadian forest fires to the surface near Washington, D. C.: Injection height, entrainment, and optical properties, *Journal of Geophysical Research-Atmospheres*, *109* (D6), D06203, doi:10.1029/2003JD004248, 2004.

Connellan, J.P., P. O'Brien, A.F. Roddy, D. Lowry, and E. Nisbet, A characterization of atmospheric methane in the North Atlantic from concentration and carbon isotope measurements made at Mace Head, in *EGS - AGU - EUG Joint Assembly*, EGU, Nice, 2003.

Deeter, M.N., Calculation and Application of MOPITT Averaging Kernels, NCAR, 2000.

Deeter, M.N., L.K. Emmons, G.L. Francis, D.P. Edwards, J.C. Gille, J.X. Warner, B. Khattatov, D. Ziskin, J.F. Lamarque, S.P. Ho, V. Yudin, J.L. Attie, D. Packman, J. Chen, D. Mao, and J.R. Drummond, Operational carbon monoxide retrieval algorithm and selected results for the MOPITT instrument, *Journal of Geophysical Research-Atmospheres*, *108* (D14), doi:10.1029/2002JD003186, 2003.

Derwent, R.G., D.B. Ryall, S.G. Jennings, T.G. Spain, and P.G. Simmonds, Black carbon aerosol and carbon monoxide in European regionally-polluted air masses at Mace Head, Ireland during 1995-1998, *Atmospheric Environment*, *35*, 6371-6378, 2001.

Dlugokencky, E.J., L.P. Steele, P.M. Lang, and K.A. Masarie, The growth rate and distribution of atmospheric methane, *Journal Of Geophysical Research-Atmospheres*, *99* (D8), 17021-17044, 1994.

Dlugokencky, E.J., B.P. Walter, K.A. Masarie, P.M. Lang, and E.S. Kasischke, Measurements of an anomalous global methane increase during 1998, *Geophysical Research Letters*, *28*, 499-502, 2001.

Drummond, J.R., and G.S. Mand, The measurements of pollution in the troposphere (MOPITT) instrument: Overall performance and calibration requirements, *Journal of Atmospheric and Oceanic Technology*, *13* (2), 314-320, 1996.

Duncan, B.N., R.V. Martin, A.C. Staudt, R. Yevich, and J.A. Logan, Interannual and seasonal variability of biomass burning emissions constrained by satellite observations, *Journal of Geophysical Research-Atmospheres*, *108* (D2), doi:10.1029/2002JD002378, 2003.

Emmons, L.K., M.N. Deeter, J.C. Gille, D.P. Edwards, J.L. Attie, J. Warner, D. Ziskin, G. Francis, B. Khattatov, V. Yudin, J.F. Lamarque, S.P. Ho, D. Mao, J.S. Chen, J. Drummond, P. Novelli, G. Sachse, M.T. Coffey, J.W. Hannigan, C. Gerbig, S. Kawakami, Y. Kondo, N. Takegawa, H. Schlager, J. Baehr, and H. Ziereis, Validation of Measurements of Pollution in the Troposphere (MOPITT) CO retrievals with aircraft in situ profiles, *Journal of Geophysical Research-Atmospheres*, *109* (D3), D03309, doi:10.1029/2003JD004101, 2004.

Falkowski, P., R.J. Scholes, E. Boyle, J. Canadell, D. Canfield, J. Elser, N. Gruber, K. Hibbard, P. Hogberg, S. Linder, F.T. Mackenzie, B.M. III, T. Pedersen, Y. Rosenthal, S. Seitzinger, V. Smetacek, and W. Steffen, The Global Carbon Cycle: A Test of Our Knowledge of Earth as a System, *Science*, *290* (13 October 2000), 291-296, 2000.

Faluvegi, G.S., K. Alapaty, H.G. Reichle, R. Mathur, S. Raman, and V.S. Connors, Simulation of carbon monoxide transport during April 1994, *Journal of Geophysical Research-Atmospheres*, *104* (D17), 21471-21485, 1999.

Fan, S., M. Gloor, J. Mahlman, S. Pacala, J. Sarmiento, T. Takahashi, and P. Tans, A large terrestrial carbon sink in North America implied by atmospheric and oceanic carbon dioxide data and models, *Science*, *282* (5388), 442-446, 1998.

Flannigan, M.D., Y. Bergeron, O. Engelmark, and B.M. Wotton, Future wildfire in circumboreal forests in relation to global warming, *Journal of Vegetation Science*, *9* (4), 469-476, 1998.

Flannigan, M.D., and J.B. Harrington, A study of the relation of meteorological variables to monthly provincial area burned by wildfire in Canada (1953-1980), *Journal of Applied Meteorology*, *27* (4), 441-452, 1988.

Forster, C., U. Wandinger, G. Wotawa, P. James, I. Mattis, D. Althausen, P. Simmonds, S. O'Doherty, S.G. Jennings, C. Kleefeld, J. Schneider, T. Trickl, S. Kreipl, H. Jager, and A. Stohl, Transport of boreal forest fire emissions from Canada to Europe, *Journal of Geophysical Research-Atmospheres*, *106* (D19), 22887-22906, 2001.

Fraser, R.H., R. Fernandes, and R. Latifovic, Multi-temporal mapping of burned forest over Canada using satellite-based change metrics, *Geocarto International*, *18* (1), 37-48, 2003.

Fraser, R.H., and Z. Li, Estimating fire-related parameters in boreal forest using SPOT VEGETATION, *Remote Sensing Of Environment*, *82* (1), 95-110, 2002.

Fraser, R.H., Z. Li, and J. Cihlar, Hotspot and NDVI differencing synergy (HANDS): A new technique for burned area mapping over boreal forest, *Remote Sensing Of Environment*, *74*, 362-376, 2000.

French, N.H.F., E.S. Kasischke, B.J. Stocks, J.P. Mudd, D.L. Martell, and B.S. Lee, Carbon release from fires in the North American boreal forest, in *Fire, Climate Change, and Carbon Cycling in the Boreal Forest*, edited by E.S. Kasischke, and B.J. Stocks, Springer, New York, 2000.

French, N.H.F., E.S. Kasischke, and D.G. Williams, Variability in the emission of carbon-based trace gases from wildfire in the Alaskan boreal forest, *Journal of Geophysical Research-Atmospheres*, *108* (D1), doi:10.1029/2001JD000480, 2002.

Fridland, V.M., Soil Map of the Russian Soviet Federative Socialist Republic at Scale 1:2.5 Million, edited by G.A.o.G.a. Cartography, All Union Academy of Agricultural Science, Moscow, 1988.

Fromm, M., J. Alfred, K. Hoppel, J. Hornstein, R. Bevilacqua, E. Shettle, R. Servranckx, Z.Q. Li, and B. Stocks, Observations of boreal forest fire smoke in the stratosphere by POAM III, SAGE II, and lidar in 1998, *Geophysical Research Letters*, *27* (9), 1407-1410, 2000.

Fromm, M.D., and R. Servranckx, Transport of forest fire smoke above the tropopause by supercell convection, *Geophysical Research Letters*, *30* (10), doi:10.1029/2002GL016820, 2003.

Fung, I.Y., J. John, J. Lerner, E. Matthews, M. Prather, L.P. Steele, and P.J. Fraser, 3-dimensional model synthesis of the global methane cycle, *Journal of Geophysical Research-- Atmospheres*, *96* (d7), 13033-13065, 1991.

Giglio, L., J.D. Kendall, and R. Mack, A multi-year active fire dataset for the tropics derived from the TRMM VIRS, *International Journal Of Remote Sensing*, *24* (22), 4505-4525, 2003.

Goode, J.G., R.J. Yokelson, D.E. Ward, R.A. Susott, R.E. Babbitt, M.A. Davies, and W.M. Hao, Measurements of excess O-3, CO2, CO, CH4, C2H4, C2H2, HCN, NO, NH3, HCOOH, CH3COOH, HCHO, and CH3OH in 1997 Alaskan biomass burning plumes by airborne fourier transform infrared spectroscopy (AFTIR), *Journal of Geophysical Research-Atmospheres*, *105* (D17), 22147-22166, 2000.

Hao, W.M., and M.H. Liu, Spatial distribution of tropical biomass burning in 1980 with 5° x 5° resolution, *Global Biogeochemical Cycles*, *8*, 495-503, 1994.

Harden, J.W., S.E. Trumbore, B.J. Stocks, A. Hirsch, S.T. Gower, K.P. O'Neill, and E.S. Kasischke, The role of fire in the boreal carbon budget, *Global Change Biology*, *6* (Suppl. 1), 174-184, 2000.

Heald, C.L., D.J. Jacob, D.B.A. Jones, P.I. Palmer, J.A. Logan, D.G. Streets, G.W. Sachse, J.C. Gille, R.N. Hoffman, and T. Nehrkorn, Comparative inverse analysis of satellite (MOPITT) and aircraft (TRACE-P) observations to estimate Asian sources of carbon monoxide, *Journal Of Geophysical Research-Atmospheres*, *109* (D23306), D23306, doi:10.1029/2004JD005185, 2004.

Heald, C.L., D.J. Jacob, P.I. Palmer, M.J. Evans, G.W. Sachse, H.B. Singh, and D.R. Blake, Biomass burning emission inventory with daily resolution: Application to aircraft observations of Asian outflow, *Journal of Geophysical Research-Atmospheres*, *108* (D21), doi:10.1029/2002JD003082, 2003.

Hely, C., P.R. Dowty, S. Alleaume, K.K. Caylor, S. Korontzi, R.J. Swap, H.H. Shugart, and C.O. Justice, Regional fuel load for two climatically contrasting years in southern Africa, *Journal Of Geophysical Research-Atmospheres*, *108* (D13), 8475, doi:10.1029/2002JD002341, 2003.

Hobbs, P.V., J.S. Reid, J.A. Herring, J.D. Nance, R.E. Weiss, J.L. Ross, D.A. Hegg, R.D. Ottmar, and C. Liousse, Particle and trace gas measurements in the smoke from prescribed burns of forest products in the Pacific Northwest, in *Biomass Burning and Global Change*, edited by J.S. Levine, pp. 697-715, MIT Press, Cambridge, MA, 1996.

Hoelzemann, J.J., M.G. Schultz, G.P. Brasseur, C. Granier, and M. Simon, Global Wildland Fire Emission Model (GWEM): Evaluating the use of global area burnt satellite data, *Journal Of Geophysical Research-Atmospheres*, *109* (D14), D14S04, doi:10.1029/2003JD003666, 2004.

Holloway, T., H. Levy, and P. Kasibhatla, Global distribution of carbon monoxide, *Journal of Geophysical Research-Atmospheres*, *105* (D10), 12123-12147, 2000.

Hou, A.Y., S.Q. Zhang, and O. Reale, Variational Continuous Assimilation on TMI and SSM/I Rain Rates: Impact on GEOS-3 hurricane analyses and forecasts, *Monthly Weather Review*, *submitted*, 2003.

Houghton, J.T., and Y. Ding, *Climate Change 2001: the Scientific Basis: Contribution of Working Group I to the Third Assessment Report of the Intergovernmental Panel on Climate Change (IPCC)*, 944 pp., Cambridge University Press, Cambridge, UK, 2001.

Hyer, E.J., Modelling Emissions of Trace Gases from Fires in the North American Boreal Forest 1980-1997, *Occasional Papers of the Department of Geography*, *http://www.geog.umd.edu/academic/occasional/wp2001/*, 2001.

Isaev, A.S., G.N. Korovin, S.A. Bartalev, D.V. Ershov, A. Janetos, E.S. Kasischke, H.H. Shugart, N.H.F. French, B.E. Orlick, and T.L. Murphy, Using remote sensing to assess Russian forest fire carbon emissions, *Climatic Change*, *55* (1-2), 235-249, 2002.

Ito, A., and J.E. Penner, Global estimates of biomass burning emissions based on satellite imagery for the year 2000, *Journal Of Geophysical Research-Atmospheres*, *109* (D14), D14S05, doi:10.1029/2003JD004423, 2004.

Johnson, E.A., *Fire and Vegetation Dynamics: Studies from the North American Boreal Forest*, 129 pp., Cambridge University Press, Cambridge, 1992.

Jost, H.J., K. Drdla, A. Stohl, L. Pfister, M. Loewenstein, J.P. Lopez, P.K. Hudson, D.M. Murphy, D.J. Cziczo, M. Fromm, T.P. Bui, J. Dean-Day, C. Gerbig, M.J. Mahoney, E.C. Richard, N. Spichtinger, J.V. Pittman, E.M. Weinstock, J.C. Wilson, and I. Xueref, In-situ observations of mid-latitude forest fire plumes deep in the stratosphere, *Geophysical Research Letters*, *31* (11), doi:10.1029/2003GL019253, 2004.

Justice, C.O., L. Giglio, S. Korontzi, J. Owens, J.T. Morrisette, D. Roy, J. Descloitres, S. Alleaume, F. Petitcolin, and Y. Kaufman, The MODIS Fire Products, *Remote Sensing Of Environment*, *83*, 244-262, 2002.

Kajii, Y., S. Kato, D.G. Streets, N.Y. Tsai, A. Shvidenko, S. Nilsson, I. McCallum, N.P. Minko, N. Abushenko, D. Altyntsev, and T.V. Khodzer, Boreal forest fires in Siberia in 1998: Estimation of area burned and emissions of pollutants by

advanced very high resolution radiometer satellite data, *Journal of Geophysical Research-Atmospheres*, *107* (D24), doi:10.1029/2001JD001078, 2002.

Kaminski, T., P.J. Rayner, M. Heimann, and I.G. Enting, On aggregation errors in atmospheric transport inversions, *Journal of Geophysical Research-Atmospheres*, *106* (D5), 4703-4715, 2001.

Kasischke, E.S., K. Bergen, R. Fennimore, F. Sotelo, G. Stephens, A. Janetos, and H.H. Shugart, Satellite imagery gives clear picture of Russia's boreal forest fires, *EOS*, *80* (13), 141, 147, 1999.

Kasischke, E.S., and L.P. Bruhwiler, Emissions of carbon dioxide, carbon monoxide, and methane from boreal forest fires in 1998, *Journal of Geophysical Research-Atmospheres*, *108* (D1), doi:10.1029/2001JD000461, 2002.

Kasischke, E.S., N.L. Christensen, and E. Haney, Modeling of geometric properties of loblolly pine tree and stand characteristics for use in rader backscatter models, *IEEE Transactions On Geoscience And Remote Sensing*, *32*, 800-822, 1994.

Kasischke, E.S., N.L. Christensen, and B.J. Stocks, Fire, Global Warming, and the Carbon Balance of Boreal Forests, *Ecological Applications*, *5* (2), 437-451, 1995a.

Kasischke, E.S., N.H.F. French, L.L. Bourgeauchavez, and N.L. Christensen, Estimating Release of Carbon From 1990 and 1991 Forest-Fires in Alaska, *Journal of Geophysical Research-Atmospheres*, *100* (D2), 2941-2951, 1995b.

Kasischke, E.S., J.H. Hewson, B. Stocks, G. van der Werf, and J. Randerson, The use of ATSR active fire counts for estimating relative patterns of biomass burning - a study from the boreal forest region, *Geophysical Research Letters*, *30* (18), doi:10.1029/2003GL017859, 2003.

Kasischke, E.S., E.J. Hyer, P.C. Novelli, L.P. Bruhwiler, N.H.F. French, A.I. Sukhinin, J.H. Hewson, and B.J. Stocks, Influences of boreal fire emissions on Northern Hemisphere atmospheric carbon and carbon monoxide, *Global Biogeochemical Cycles*, *19* (GB1012), doi:10.1029/2004GB002300, 2005.

Kasischke, E.S., K.P. O'Neill, N.H.F. French, and L.L. Bourgeau-Chavez, Controls on patterns of biomass burning in Alaskan boreal forests, in *Fire, Climate Change, and Carbon Cycling in the Boreal Forest*, edited by E.S. Kasischke, and B.J. Stocks, pp. 173-196, Springer, New York, 2000.

Kasischke, E.S., and J.E. Penner, Improving global estimates of atmospheric emissions from biomass burning, *Journal Of Geophysical Research-Atmospheres*, *109* (D14), D14S01, doi:10.1029/2004JD004972, 2004.

Kasischke, E.S., D. Williams, and D. Barry, Analysis of the patterns of large fires in the boreal forest region of Alaska, *International Journal Of Wildland Fire*, *11* (2), 131-144, 2002.

Kaufman, Y.J., C.O. Justice, L.P. Flynn, J.D. Kendall, E.M. Prins, L. Giglio, D.E. Ward, W.P. Menzel, and A.W. Setzer, Potential global fire monitoring from EOS-MODIS, *Journal of Geophysical Research-Atmospheres*, *103* (D24), 32215-32238, 1998.

Kim, J., S.H. Choi, D. Edwards, H.C. Lee, H.K. Cho, and S.H. Lee, Correlation between aerosol optical depth and CO in the atmospheric for forest fire events, *American Geophysical Union Fall Meeting*, AGU, San Francisco, CA, 2004.

Korontzi, S., C.O. Justice, and R.J. Scholes, Influence of timing and spatial extent of savanna fires in southern Africa on atmospheric emissions, *Journal Of Arid Environments*, *54* (2), 395-404, 2003a.

Korontzi, S., D.E. Ward, R.A. Susott, R.J. Yokelson, C.O. Justice, P.V. Hobbs, E.A.H. Smithwick, and W.M. Hao, Seasonal variation and ecosystem dependence of emission factors for selected trace gases and PM2.5 for southern African savanna fires, *Journal Of Geophysical Research-Atmospheres*, *108* (D24), 4758, doi:10.1029/2003JD003730, 2003b.

Kuhlbusch, T.A.J., R.G. Zepp, W.L. Miller, and R.A. Burke, Carbon monoxide fluxes of different soil layers in upland Canadian boreal forests, *Tellus Series B-Chemical and Physical Meteorology*, *50* (4), 353-365, 1998.

Lacelle, B., Canada's soil organic carbon data base, in *Soil Processes and the Carbon Cycle*, edited by R. Lal, J.M. Kimble, R.F. Follet, and B.A. Stewart, pp. 93-101, CRC Press, Boca Raton, 1997.

Lacelle, B., C. Tarnocai, S. Waltman, J. Kimble, F. Orozco-Chavez, and B. Jakobsen, North American Soil Carbon Map (provisional), Agriculture and Agri-food Canada, USDA, INEGI, Institute of Geography, University of Copenhagen, Copenhagen, 1997.

Lamarque, J.F., D.P. Edwards, L.K. Emmons, J.C. Gille, O. Wilhelmi, C. Gerbig, D. Prevedel, M.N. Deeter, J. Warner, D.C. Ziskin, B. Khattatov, G.L. Francis, V. Yudin, S. Ho, D. Mao, J. Chen, and J.R. Drummond, Identification of CO plumes from MOPITT data: Application to the August 2000 Idaho-Montana forest fires, *Geophysical Research Letters*, *30* (13), doi:10.1029/2003GL017503, 2003.

Laursen, K.K., P.V. Hobbs, L.F. Radke, and R.A. Rasmussen, Some Trace Gas Emissions From North-American Biomass Fires With an Assessment of Regional and Global Fluxes From Biomass Burning, *Journal of Geophysical Research-Atmospheres*, *97* (D18), 20687-20701, 1992.

Lavoue, D., C. Liousse, H. Cachier, B.J. Stocks, and J.G. Goldammer, Modeling of carbonaceous particles emitted by boreal and temperate wildfires at northern latitudes, *Journal of Geophysical Research-Atmospheres*, *105* (D22), 26871-26890, 2000.

Li, Z.Q., J. Cihlar, L. Moreau, F.T. Huang, and B. Lee, Monitoring fire activities in the boreal ecosystem, *Journal of Geophysical Research-Atmospheres*, *102* (D24), 29611-29624, 1997.

Liu, J., J.R. Drummond, Q. Li, J.C. Gille, and D.C. Ziskin, Satellite mapping of CO emission from forest fires in Northwest America using MOPITT observations, *Remote Sensing of Environment*, *95*, 502-516, 2005.

Livesey, N.J., M.D. Fromm, J.W. Waters, G.L. Manney, M.L. Santee, and W.G. Read, Enhancements in lower stratospheric CH3CN observed by the upper atmosphere research satellite microwave limb sounder following boreal forest fires, *Journal of Geophysical Research-Atmospheres*, *109* (D6), D06308, doi:10.1029/2003JD004055, 2004.

Logan, J.A., M.J. Prather, S.C. Wofsy, and M.B. McElroy, tropospheric chemistry: a global perspective, *Journal of Geophysical Research*, *86* (C8), 7210-7254, 1981.

Lowe, J.J., K. Power, and M.W. Marsan, Canada's Forest Inventory 1991: Summary by Terrestrial Ecozones and Ecoregions, Canadian Forest Service Pacific Forestry Center, Edmonton, 1996.

Malingreau, J.P., and J.-M. Grégoire, Developing a Global Vegetation Fire Monitoring System for Global Change Studies: a Framework, in *Biomass Burning and Global Change*, edited by J.S. Levine, pp. 14-24, The MIT Press, Cambridge, MA, 1996.

Newell, R.E., J. Henry G. Reichle, and W. Seiler, Carbon Monoxide and the Burning Earth, *Scientific American* (October 1989), 82-88, 1989.

Novelli, P.C., J.W. Elkins, and L.P. Steele, The development and evaluation of a gravimetric reference scale for measurements of atmospheric carbon monoxide, *Journal of Geophysical Research*, *96*, 13109-13121, 1991.

Novelli, P.C., K.A. Masarie, and P.M. Lang, Distributions and recent changes of carbon monoxide in the lower troposphere, *Journal Of Geophysical Research-Atmospheres*, *103* (D15), 19015-19033, 1998.

Novelli, P.C., K.A. Masarie, P.M. Lang, B.D. Hall, R.C. Myers, and J.W. Elkins, Reanalysis of tropospheric CO trends: Effects of the 1997-1998 wildfires, *Journal of Geophysical Research-Atmospheres*, *108* (D15), doi:10.1029/2002JD003031, 2003.

Novelli, P.C., and L.P. Steele, Mixing Ratios of Carbon Monoxide in the Troposphere, *Journal of Geophysical Research*, *97* (D18), 20731-20750, 1992.

Palmer, P.I., D.J. Jacob, D.B.A. Jones, C.L. Heald, R.M. Yantosca, J.A. Logan, G.W. Sachse, and D.G. Streets, Inverting for emissions of carbon monoxide from Asia using aircraft observations over the western Pacific, *Journal of Geophysical Research-Atmospheres*, *108* (D21), doi:10.1029/2003JD003397, 2003.

Park, R.J., K.E. Pickering, D.J. Allen, G.L. Stenchikov, and M.S. Fox-Rabinovitz, Global simulation of tropospheric ozone using the University of Maryland Chemical Transport Model (UMD-CTM): 1. Model description and evaluation, *Journal of Geophysical Research-Atmospheres*, *109* (D9), D09303, doi:10.1029/2003JD004269, 2004.

Penner, M., K. Power, C. Muhairwe, R. Tellier, and Y. Wang, Canada's Forest Biomass Resources: Deriving Estimates from Canada's Forest Inventory., edited by C.F. Service, Canadian Forest Service, Victoria, BC, 1997.

Petron, G., C. Granier, B. Khattatov, V. Yudin, J.F. Lamarque, L. Emmons, J. Gille, and D.P. Edwards, Monthly CO surface sources inventory based on the 2000-2001 MOPITT satellite data, *Geophysical Research Letters*, *31* (21), 2004.

Potter, C.S., J.T. Randerson, C.B. Field, P.A. Matson, P.M. Vitousek, H.A. Mooney, and S.A. Klooster, Terrestrial ecosystem production: A process model based on global satellite and surface data, *Global Biogeochemical Cycles*, *7* (4), 811-842, 1993.

Prinn, R.G., R.F. Weiss, P.J. Fraser, P.G. Simmonds, D.M. Cunnold, F.N. Alyea, S. O'Doherty, P. Salameh, B.R. Miller, J. Huang, R.H.J. Wang, D.E. Hartley, C. Harth, L.P. Steele, G. Sturrock, P.M. Midgley, and A. McCulloch, A History of Chemically and Radiatively Important Gases in Air deduced from ALE/GAGE/AGAGE, *Journal Of Geophysical Research-Atmospheres*, *105*, 17,751-17,792, 2000.

Reichle Jr., H.G., S.M. Beck, R.E. Haynes, W.E. Hesketh, J.A. Holland, W.D. Hypes, H.D. Orr III, R.T. Sherrill, H.A. Wallio, J.C. Casas, M.S. Saylor, and B.B. Gormsen, Carbon Monoxide Measurements in the Troposphere, *Science*, *218*, 1024-1026, 1982.

Reid, J.S., E.M. Prins, D.L. Westphal, C.C. Schmidt, K.A. Richardson, S.A. Christopher, T.F. Eck, E.A. Reid, C.A. Curtis, and J.P. Hoffman, Real-time monitoring of South American smoke particle emissions and transport using a coupled remote sensing/box-model approach, *Geophysical Research Letters*, *31* (6), doi:10.1029/2003GL018845, 2004.

Sarmiento, J.L., and S.C. Wofsy, A U.S. Carbon Cycle Science Plan, pp. 69, U.S Global Change Research Program, Carbon and Climate Working Group, Washington, D.C., 1999.

Schlesinger, P., and T. Stone, Forest and Landcover Data of Russia and the Former Soviet Union, Woods Hole Research Center, Woods Hole, MA, 2001.

Scholes, R.J., J. Kendall, and C.O. Justice, The quantity of biomass burned in southern Africa, *Journal of Geophysical Research-Atmospheres*, *101* (D19), 23667-23676, 1996.

Seiler, W., and P.J. Crutzen, Estimates of gross and net fluxes of carbon between the biosphere and atmosphere from biomass burning, *Climatic Change*, *2*, 207-247, 1980.

Shvidenko, A., and S. Nilsson, A synthesis of the impact of Russian forests on the global carbon budget for 1961-1998, *Tellus Series B-Chemical And Physical Meteorology*, *55* (2), 391-415, 2003.

Silva, J.M.N., J. Cadima, J.M.C. Pereira, and J.M. Gregoire, Assessing the feasibility of a global model for multi-temporal burned area mapping using SPOT-VEGETATION data, *International Journal Of Remote Sensing*, *25* (22), 4889-4913, 2004.

Simmonds, P.G., R.G. Derwent, A. McCulloch, S. O'Doherty, and A. Gaudry, Long-term trends in concentrations of halocarbons and radiatively active trace gases in Atlantic and European air masses monitored at Mace Head, Ireland from 1987-1994, *Atmospheric Environment*, *30* (23), 4041-4063, 1996.

Simon, M., S. Plummer, F. Fierens, J.J. Hoelzemann, and O. Arino, Burnt area detection at global scale using ATSR-2: The GLOBSCAR products and their qualification, *Journal Of Geophysical Research-Atmospheres*, *109* (D14), D14S02, doi:10.1029/2003JD003622, 2004.

Skinner, W.R., B.J. Stocks, D.L. Martell, B. Bonsal, and A. Shabbar, The association between circulation anomalies in the mid- troposphere and area burned by wildland fire in Canada, *Theoretical and Applied Climatology*, *63* (1-2), 89-105, 1999.

Soja, A.J., A.I. Sukhinin, D.R. Cahoon, H.H. Shugart, and P.W. Stackhouse, AVHRR-derived fire frequency, distribution and area burned in Siberia, *International Journal of Remote Sensing*, *25* (10), 1939-1960, 2004.

Spichtinger, N., M. Wenig, P. James, T. Wagner, U. Platt, and A. Stohl, Satellite detection of a continental-scale plume of nitrogen oxides from boreal forest fires, *Geophysical Research Letters*, *28* (24), 4579-4582, 2001.

Spivakovsky, C.M., J.A. Logan, S.A. Montzka, Y.J. Balkanski, M. Foreman-Fowler, D.B.A. Jones, L.W. Horowitz, A.C. Fusco, C.A.M. Brenninkmeijer, M.J. Prather, S.C. Wofsy, and M.B. McElroy, Three-dimensional climatological distribution of tropospheric OH: Update and evaluation, *Journal Of Geophysical Research-Atmospheres*, *105* (D7), doi:101.1029/1999JD901006 (8931-8980), 2000.

Stocks, B.J., Fire behavior in immature jack pine, *canadian journal of forest research*, *17* (1), 80-86, 1987.

Stocks, B.J., B.D. Amiro, and B.D. Wotton, Large Forest Fires in Canada 1959-1997, *Journal of Geophysical Research*, *108* (D1), doi:10.1029/2001JD000484, 2002.

Stocks, B.J., M.A. Fosberg, T.J. Lynham, L. Mearns, B.M. Wotton, Q. Yang, J.Z. Jin, K. Lawrence, G.R. Hartley, J.A. Mason, and D.W. McKenney, Climate change and forest fire potential in Russian and Canadian boreal forests, *Climatic Change*, *38* (1), 1-13, 1998.

Stocks, B.J., and J.B. Kauffman, Biomass consumption and behavior of wildland fires in boreal, temperate, and tropical ecosystems: parameters necessary to interpret historic fire regimes and future fire scenarios, in *Sediment Records of Biomass Burning and Global Change*, edited by J.S. Clark, H. Cachier, J.G. Goldammer, and B.J. Stocks, Springer-Verlag, Berlin, 1997.

Stocks, B.J., b.d. lawson, m.e.alexander, c.e.v. wagner, r.s. mcalpine, t.j. lynham, and d.e. dube, The Canadian Forest Fire Danger Rating System-- an overview, *Forestry Chronicle*, *65* (6), 450-457, 1989.

Stolbovoi, V., and I. McCallum, Land Resources of Russia, International Institute for Applied Systems Analysis, Laxenburg, 2002.

Streets, D.G., T.C. Bond, G.R. Carmichael, S.D. Fernandes, Q. Fu, D. He, Z. Klimont, S.M. Nelson, N.Y. Tsai, M.Q. Wang, J.H. Woo, and K.F. Yarber, An inventory of gaseous and primary aerosol emissions in Asia in the year 2000, *Journal of Geophysical Research-Atmospheres*, *108* (D21), doi:10.1029/2002JD003093, 2003a.

Streets, D.G., K.F. Yarber, J.H. Woo, and G.R. Carmichael, Biomass burning in Asia: Annual and seasonal estimates and atmospheric emissions, *Global Biogeochemical Cycles*, *17* (4), 2003b.

Stroppiana, D., S. Pinnock, and J.M. Gregoire, The Global Fire Product: daily fire occurrence from April 1992 to December 1993 derived from NOAA AVHRR data, *International Journal Of Remote Sensing*, *21* (6-7), 1279-1288, 2000.

Sukhinin, A.I., N.H.F. French, E.S. Kasischke, J.H. Hewson, A.J. Soja, I.A. Csiszar, E.J. Hyer, T. Loboda, S.G. Conard, V.I. Romasko, E.A. Pavlichenko, S.I. Miskiv, and O.A. Slinkina, Satellite-Based Mapping of Fires in Russia: New Products for Fire Management and Carbon Cycle Studies, *Remote Sensing of Environment*, *in press*, 2004.

Tans, P.P., P.S. Bakwin, and D.W. Guenther, A feasible Global Carbon Cycle Observing System: a plan to decipher today's carbon cycle based on observations, *Global Change Biology*, *2*, 309-318, 1996.

Tansey, K., J.M. Gregoire, E. Binaghi, L. Boschetti, P.A. Brivio, D. Ershov, S. Flasse, R. Fraser, D. Graetz, M. Maggi, P. Peduzzi, J. Pereira, J. Silva, A. Sousa, and D. Stroppiana, A global inventory of burned areas at 1km resolution for the year

2000 derived from SPOT VEGETATION data, *Climatic Change*, *67* (2-3), 345-377, 2004a.

Tansey, K., J.M. Gregoire, D. Stroppiana, A. Sousa, J. Silva, J.M.C. Pereira, L. Boschetti, M. Maggi, P.A. Brivio, R. Fraser, S. Flasse, D. Ershov, E. Binaghi, D. Graetz, and P. Peduzzi, Vegetation burning in the year 2000: Global burned area estimates from SPOT VEGETATION data, *Journal Of Geophysical Research-Atmospheres*, *109* (D14), D14S03, doi:10.1029/2003JD003598, 2004b.

Trentmann, J., M.O. Andreae, H.F. Graf, P.V. Hobbs, R.D. Ottmar, and T. Trautmann, Simulation of a biomass-burning plume: Comparison of model results with observations, *Journal of Geophysical Research-Atmospheres*, *107* (D1-D2), doi:10.1029/2001JD000410, 2002.

van der Werf, G.R., J.T. Randerson, G.J. Collatz, and L. Giglio, Carbon emissions from fires in tropical and subtropical ecosystems, *Global Change Biology*, *9* (4), 547, 2003.

Waldrop, M.M., An Inquiry Into the State of the Earth, *Science*, *226* (4670), 33-35, 1984.

Warner, J.X., J.C. Gille, D.P. Edwards, D.C. Ziskin, M.W. Smith, P.L. Bailey, and L. Rokke, Cloud detection and clearing for the Earth Observing System Terra satellite Measurements of Pollution in the Troposphere (MOPITT) experiment, *Applied Optics*, *40* (8), 1269-1284, 2001.

Watson, R.T., H. Rodhe, H. Oeschger, and U. Siegenthaler, Greenhouse Gases and Aerosols, in *Climate Change, the Intergovernmental Panel on Climate Change Scientific Assessment*, edited by J.T. Houghton, G.J. Jenkins, and J.J. Ephraums, pp. 1-40, Cambridge University Press, Cambridge, 1990.

Wotawa, G., P.C. Novelli, M. Trainer, and C. Granier, Inter-annual variability of summertime CO concentrations in the Northern Hemisphere explained by boreal forest fires in North America and Russia, *Geophysical Research Letters*, *28* (24), 4575-4578, 2001.

Yevich, R., and J.A. Logan, An assessment of biofuel use and burning of agricultural waste in the developing world, *Global Biogeochemical Cycles*, *17* (4), 1095, 2003.

Yokelson, R.J., R. Susott, D.E. Ward, J. Reardon, and D.W.T. Griffith, Emissions from smoldering combustion of biomass measured by open-path Fourier transform infrared spectroscopy, *Journal of Geophysical Research-Atmospheres*, *102* (D15), 18865-18877, 1997.

Yurganov, L.N., T. Blumenstock, E.I. Grechko, F. Hase, E.J. Hyer, E.S. Kasischke, M. Koike, Y. Kondo, I. Kramer, F.-Y. Leung, E. Mahieu, J. Mellqvist, J. Notholt, P.C. Novelli, C.P. Rinsland, H.E. Scheel, A. Schulz, A. Strandberg, R. Sussman, H. Tanimoto, V. Velazco, R. Zander, and Y. Zhao, A quantitative assessment of

the 1998 carbon monoxide emission anomaly in the the Northern Hemisphere based on total column and surface concentration measurements, *Journal of Geophysical Research*, *109* (D15305), doi:10.1029/2004JD004559, 2004a.

Yurganov, L.N., P. Duchatelet, A.V. Dzhola, D.P. Edwards, F. Hase, I. Kramer, E. Mahieu, J. Mellqvist, J. Notholt, P.C. Novelli, A. Rockmann, H.E. Scheel, M. Schneider, A. Schulz, A. Strandberg, R. Sussmann, H. Tanimoto, V. Velazco, J.R. Drummond, and J.C. Gille, Increased Northern Hemispheric carbon monoxide burden in the troposphere in 2002 and 2003 detected from the ground and from space, *Atmospheric Chemistry And Physics*, *5*, 563-573, 2005.

Zepp, R.G., W.L. Miller, M.A. Tarr, R.A. Burke, and B.J. Stocks, Soil-atmosphere fluxes of carbon monoxide during early stages of postfire succession in upland Canadian boreal forests, *Journal of Geophysical Research-Atmospheres*, *102* (D24), 29301-29311, 1997.